

DTIC FILE COPY
AD-A230 325

1

GL-TR-90-0333(A)
ENVIRONMENTAL RESEARCH PAPERS, NO. 1074

Proceedings of the 8th Annual DARPA/AFGL Seismic
Research Symposium, 6-8 May 1986
ADDENDUM

Editors:

JAMES F. LEWKOWICZ
JEANNE M. McPHETRES

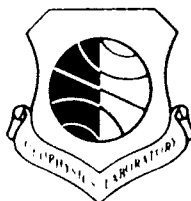
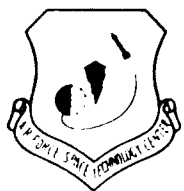
DTIC
ELECTE
DEC 27 1990
S B D
Ca



13 December 1990



Approved for public release; distribution unlimited.




EARTH SCIENCES DIVISION PROJECT 2309
GEOPHYSICS LABORATORY
HANSCOM AFB, MA 01731-5000


90 12 26 012

"This technical report has been reviewed and is approved for publication."

FOR THE COMMANDER



JAMES F. LEWKOWICZ
Branch Chief
Solid Earth Geophysics Branch
Earth Sciences Division



DONALD H. ECKHARDT
Director
Earth Sciences Division

This report has been reviewed by the ESD Public Affairs Office (PA) and is releasable to the National Technical Information Service (NTIS).

Qualified requestors may obtain additional copies from the Defense Technical Information Center. All others should apply to the National Technical Information Service.

If your address has changed, or if you wish to be removed from the mailing list, or if the addressee is no longer employed by your organization, please notify GL/IMA, Hanscom AFB, MA 01731-5000. This will assist us in maintaining a current mailing list.

Do not return copies of this report unless contractual obligations or notices on a specific document requires that it be returned.

13 December 1990

Scientific, Interim

Proceedings of the 8th Annual DARPA/AFGL Seismic
Research Symposium, 6-8 May 1986
ADDENDUM

PE 61102F
PR 2309
TA G2
WU 06

Editors: James F. Lewkowicz
Jeanne M. McPhetres

Air Force Geophysics Laboratory, AFSC
AFGL/LWH
Hanscom AFB, MA 01731-5000

GL-TR-90-0333(A)
ERP, No. 1074

DARPA/GSD
1400 Wilson Boulevard
Arlington, VA 22209-2308

This research was supported by DARPA under PE 61101E and 62714E.

Approved for Public Release; distribution unlimited

This volume contains papers that were received too late for inclusion in the
initial Proceedings.

underground nuclear explosion; seismic waves; regional
seismology arrays; yield estimation; source coupling

112

UNCLASSIFIED

UNCLASSIFIED

UNCLASSIFIED

UL

•

•

•

•

•

•

•

•

•

•

•

•

•

•

•

•

•

•

•

•

•

•

•

•

•

•

•

•

•

•



DEPARTMENT OF THE AIR FORCE
AIR FORCE GEOPHYSICS LABORATORY (AFSC)
HANSCOM AIR FORCE BASE, MASSACHUSETTS 01731-5000

AUG 1 1986

Dear Meeting Participants

This volume contains papers that were received too late for inclusion in the initial Proceedings.

The first paper in this volume is by Dr. Ralph Alewine III, Director, Geophysical Sciences Division, Defense Advanced Research Projects Agency (DARPA). In this paper Dr. Alewine III outlines two research areas in seismology of major importance to DARPA: verification of the unratified Threshold Test Ban Treaty (TTBT) and a yet to be negotiated Comprehensive Test Ban Treaty (CTBT). Research in the recent past has focussed on verifying compliance with the TTBT. However, present and future research efforts will be directed toward verifying a CTBT. This second area emphasizes regional wave propagation and provides an abundance of research opportunities. I realize it represents a shift away from the past DARPA supported research and it is difficult to change research directions, especially for universities. However, I encourage you to consider the technical problems one must solve to effectively monitor a CTBT and factor these into your research plans. And at the expense of being redundant, suggest you consider using NORESS data to study these problems. It is providing high quality data that is available to all scientists in the Program.

I thank Mr. William J. Best for attending and providing the meeting summary and Brian Stump for submitting written comments.

Finally, the overwhelming majority of papers presented at the meeting were excellent and I want to thank everyone for their efforts. I believe the presentations were much improved from last year's meeting.

Thank you again for your efforts.

Sincerely

James F. Lewkowicz
JAMES F. LEWKOWICZ

Accession For	
NTIS GRA&I	<input checked="checked" type="checkbox"/>
DTIC TAB	<input type="checkbox"/>
Unannounced	<input type="checkbox"/>
Justification	
By	
Distribution/	
Availability Codes	
Dist	Avail and/or Special
A-1	

<u>CONTENTS</u>	<u>PAGE</u>
Nuclear Test Verification Ralph Alewine	1
The Curious Case of the Missing Explosion Eugene Herrin	12
Analysis of Teleseismic P Wave Coda Using Multichannel Deconvolution Methods and Comparison to Finite Difference Calculations Zoltan A. Der, Keith L. McLaughlin, Alison C. Lees, and Rong-Song Jih	32
Salt Dome-Related Seismicity near Kulyab, Tadjikistan, USSR; David W. Simpson and William Leith	40
Focal Depths of Shallow Local Earthquakes From Comparison of Polarization Filtered Data With Synthetics N. L. Barstow, J. A. Carter and A. Suteau-Henson	51
Observations of First-Order Mantle Reverberations Justin S. Revenaugh and Thomas H. Jordan	59
Yield Estimates from Vertical- and Transverse-Component Lg Spectra and Polarization Filtering to Enhance Regional Phases Shelton S. Alexander	67
A Numerical Investigation of Topographic Effects on 2-D Explosive Line Sources K. L. McLaughlin, R. S. Jih, and Z. Der	82
Estimates of Seismic Coupling and Nuclear Explosion Yields Using Seismic Magnitude and Moment Data Charles B. Archambeau	90
Comments received from B. Stump	109

Handwritten notes:
 The above list of contents is a preliminary one and is subject to change.
 The order of the papers is not necessarily the order in which they were received.
 The order of the papers is not necessarily the order in which they were received.



NUCLEAR TEST VERIFICATION

GEOPHYSICAL SCIENCES DIVISION

DEFENSE SCIENCES OFFICE



OBJECTIVE

Improve U.S. capability to detect and characterize nuclear explosions in all environments

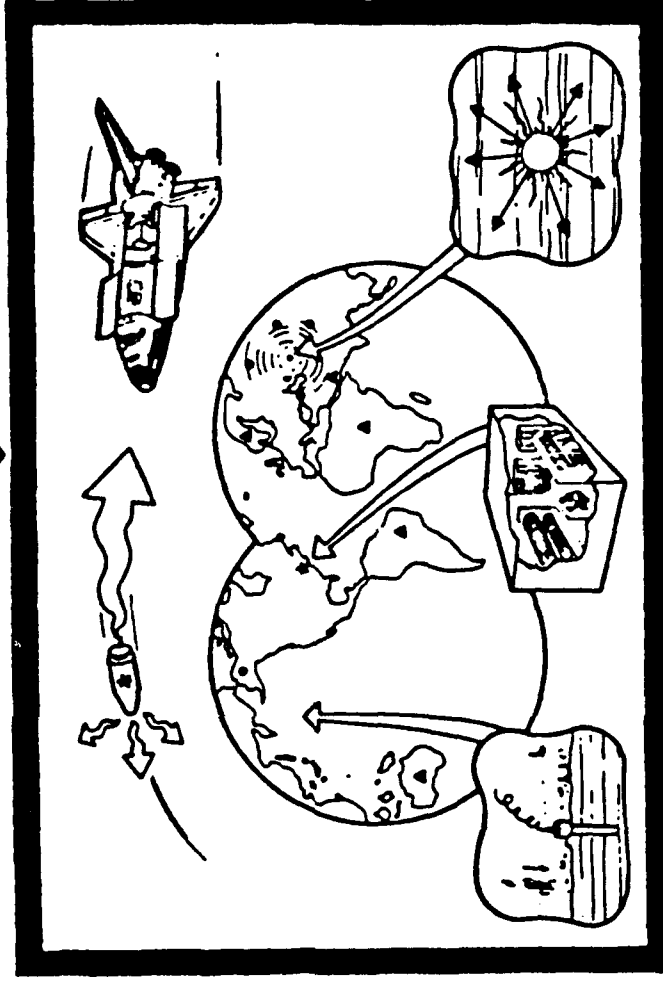
SEISMIC MONITORING

- ▶ Improve yield estimation for Threshold Test Ban Treaty monitoring
- ▶ Improve event detection and identification
 - In global non-proliferation
 - Using in-country stations in USSR
- ▶ Technical support for U.S. treaty policy and international test ban treaty activities

NON SEISMIC MONITORING

- ▶ Develop techniques for remote detection and characterization of nuclear materials
- ▶ Fundamental geophysics research for DoD requirements

RADIATION SENSOR DEVELOPMENT



ADVANCED
SEISMIC
DETECTORS



DATA
INTERPRETATION



YIELD
ESTIMATION

NUCLEAR MONITORING RESEARCH OBJECTIVES

COMPREHENSIVE TEST BAN TREATY

- DEVELOP AND DEMONSTRATE TECHNOLOGIES TO REDUCE DETECTION AND IDENTIFICATION LEVELS FOR MONITORING UNDERGROUND EXPLOSIONS TO AS LOW A LEVEL AS POSSIBLE

FOR RESEARCH PURPOSES AIM AT MONITORING AT
A 1 KILOTON LEVEL

- ASSESS THE THREAT OF CHEATING (EVASION) AND DEVELOP COUNTER-MEASURES
- PROVIDE STUDIES AND ASSESSMENTS OF PRESENT AND POTENTIAL CAPABILITIES FOR MONITORING

STUDIES AND METHODS SHOULD BE APPLICABLE FIRST TO
USSR AND SECOND TO GLOBAL MONITORING

THRESHOLD TEST BAN TREATY MONITORING

- DEVELOP AND DEMONSTRATE METHODOLOGIES FOR ACCURATE YIELD ESTIMATION AT THE 150 KILOTON LEVEL FOR USE AGAINST SOVIET TESTS
- PROVIDE STUDIES AND ASSESSMENTS OF CURRENT AND POTENTIAL CAPABILITIES
- PROVIDE TECHNICAL ANALYSES ON CAPABILITIES AT LOWER THRESHOLDS

ASPECTS OF CTBT MONITORING RESEARCH

- * DEVELOPMENT AND DEMONSTRATION OF DATA COLLECTION FACILITIES
 - ADVANCED ARRAYS
 - ULTRA-SENSITIVE INSTRUMENTATION
 - DATA COLLECTION FOR SPECIAL RESEARCH TOPICS
- * DEVELOPMENT OF TECHNOLOGIES AND METHODS TO ANALYZE DATA
 - INTELLIGENT ARRAY PROCESSING SYSTEM
 - AUTOMATED SIGNAL PROCESSING TECHNIQUES
 - EVENT IDENTIFICATION METHODS
- * UPGRADE OF INTERNATIONAL MONITORING SYSTEM
 - UPGRADED EQUIPMENT IN SELECTED COUNTRIES
 - IMPROVED DATA HANDLING/PROCESSING PROCEDURES

SEISMIC DETECTION METHODS

- REGIONAL ARRAY DEVELOPMENT
- HIGH FREQUENCY SIGNAL DETECTION
- CHINA SEISMIC NETWORK
- ADVANCED SEISMOMETER DEVELOPMENT
- SUPPORT TO GLOBAL DIGITAL SEISMIC NETWORK

SIGNAL ANALYSIS AND EVENT IDENTIFICATION

- INTELLIGENT ARRAY PROCESSING SYSTEM
- DISCRIMINATION METHODS USING REGIONAL ARRAY DATA
- LOCATION OF EVENTS USING REGIONAL ARRAY DATA
- CHEMICAL EXPLOSION IDENTIFICATION
- SEISMIC WORKSTATION DEVELOPMENT
- USE OF EXPERT SYSTEMS TECHNOLOGY IN AEDS MISSION

SEISMIC YIELD ESTIMATION METHODS

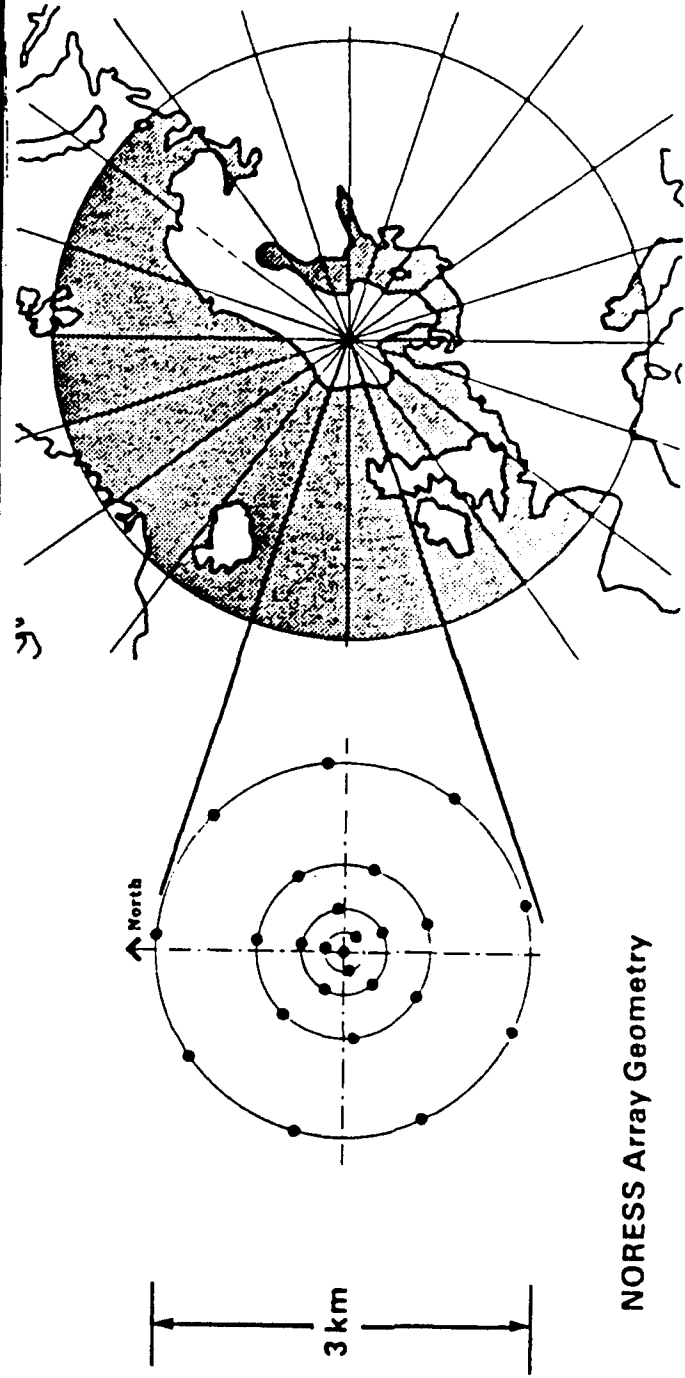
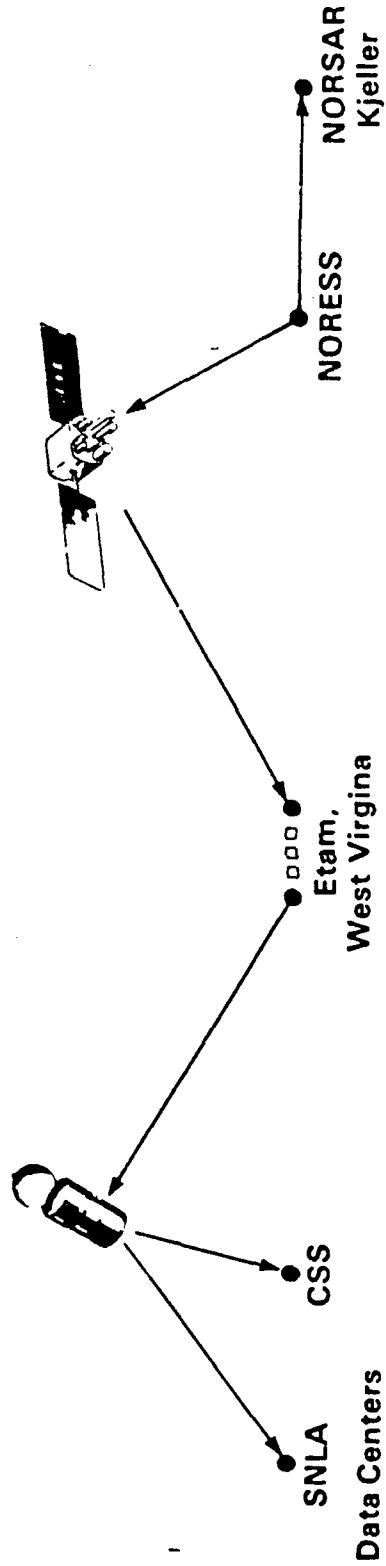
- MOMENT TENSOR DEVELOPMENT AND TRANSFER
- L6 YIELD DEVELOPMENT
- UNIFIED SEISMIC YIELD METHODS
- YIELDS OF NOVAYA ZEMLYA EVENTS
- TTBT OPTIONS

NUCLEAR MATERIALS DETECTION

- GAMMA RAY SPECTROMETER/IMAGER (ANGAS)
- NEUTRON SPECTROMETER/IMAGER (ANGAS)
- WINKER DEVELOPMENT - TEST FLIGHTS
- TRITIUM DETECTION
- GAMMA RAY IMAGING METHODS



NORWEGIAN REGIONAL SEISMIC ARRAY (NORESS)



SIGNAL PROCESSING

OBJECTIVE: DEMONSTRATE THE TECHNOLOGIES TO RECEIVE, PROCESS
AND STORE DATA FROM MONITORING FACILITIES IN THE
USSR

NEW PROJECT UNDERWAY: INTELLIGENT ARRAY PROCESSING SYSTEM

WILL PROVIDE FRAMEWORK FOR SYSTEM

NEEDED: ADVANCED SIGNAL/PHASE DETECTION AND RECOGNITION
METHODS

IMPROVED INFORMATION FROM ARRAYS AND SINGLE
STATIONS EG. 3-COMPONENT ARRAY PROCESSING,
POLARIZATION PROCESSING FOR AZIMUTH AND
PHASE IDENTIFICATION

IMPROVED METHODS FOR DEPTH DETERMINATION USING
REGIONAL PHASES

IMPROVED METHODS FOR RECOGNIZING CHEMICAL SHOTS

IMPROVED METHODS FOR DISCRIMINATION

SITE SPECIFIC "EXPERTISE"

METHODS FOR COMBINING INFORMATION FROM ARRAYS
AND SINGLE STATIONS

NOTE: MUCH OF THE DEVELOPMENT FOR THE NEW SYSTEM WILL ALSO
HAVE APPLICATION IN THE GSE SPECIFICATIONS IF THEY ARE
"PACKAGED" PROPERLY

EVASION

LISTED IN INCREASING ORDER OF IMPORTANCE

THREAT OF CHEATING

COUNTER-MEASURE

MULTIPLE SHOT

HIGH FREQUENCY DATA ANALYSIS
(NEEDS TO BE TESTED)

HIDE-IN-EARTHQUAKE

MULTIPLE-STATION, HIGH DYNAMIC
RANGE RECORDING

CHEMICAL EXPLOSIONS

SPECTRAL DISCRIMINANT?
(NEEDS TO BE DEVELOPED)

CAVITY DECOUPLING

LOW DETECTION THRESHOLDS
HIGH FREQUENCY SIGNAL ANALYSIS

KEY QUESTIONS FOR CAVITY DECOUPLING

HOW SOLID ARE THE OBSERVATIONS OF DECREASING DECOUPLING FACTORS
AT HIGH FREQUENCY? ARE THESE OBSERVATIONS RELEVANT TO
POTENTIAL SOVIET TESTS?

FOR FULL DECOUPLING, WHAT DO WE EXPECT?

WHAT FREQUENCIES CAN BE OBSERVED AT WHAT DISTANCES ALONG WHAT
PATHS

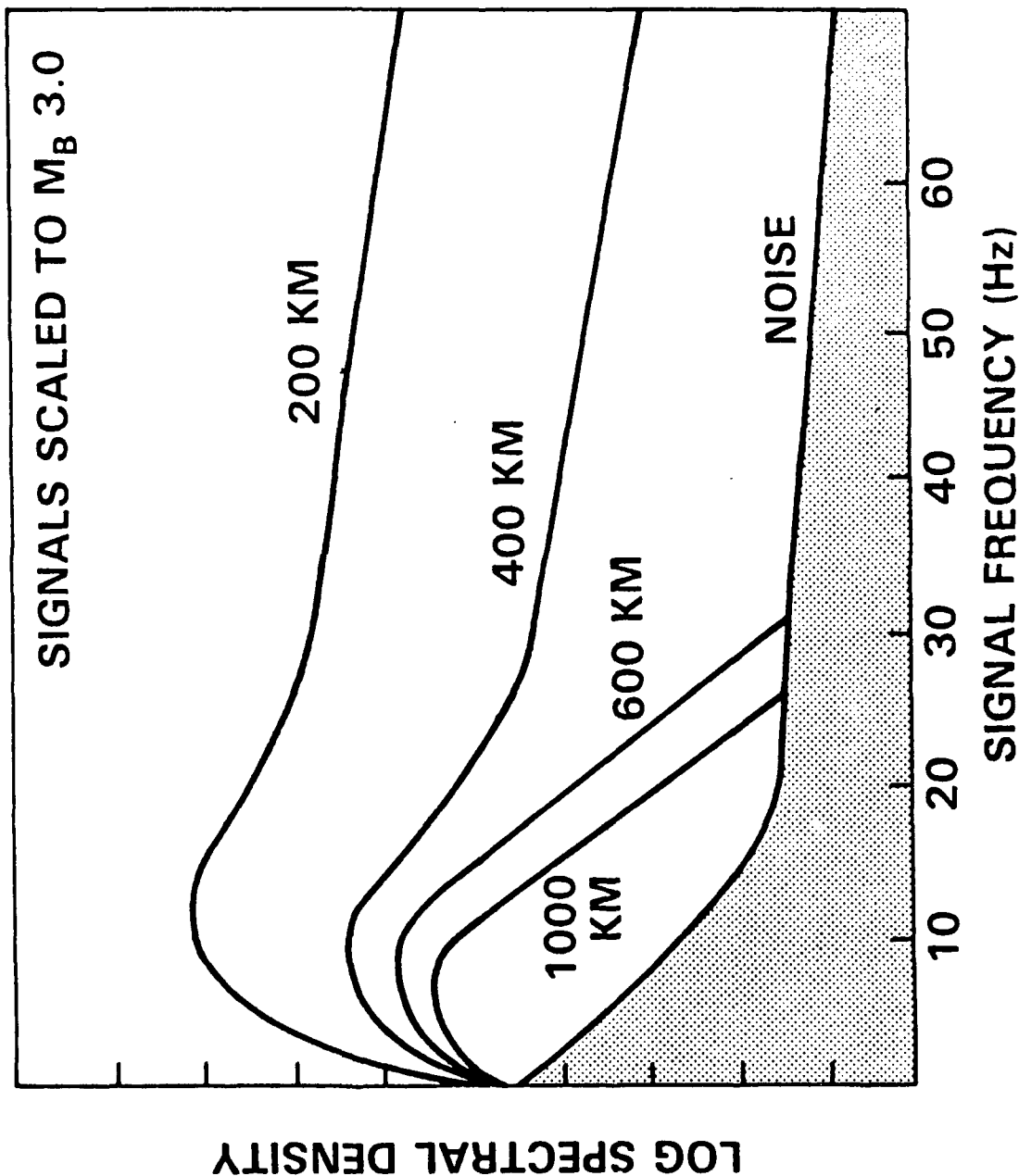
WHERE ARE THE THREATS IN THE SOVIET UNION? WHAT PROPAGATION
EFFECTS DO WE EXPECT IN THE VICINITY OF THESE THREATS?

HOW CAN AN EVASION ATTEMPT BE RECOGNIZED? WHAT IS THE
"FALSE ALARM PROBLEM"?

WHAT COUNTER-MEASURES ARE NEEDED TO COPE WITH THE THREAT?
(ASSUME MONITORING OF VARIOUS THRESHOLDS)



SPECTRA FOR EVENTS RECORDED AT NORESS



NEW DATA SOURCES

DIGITAL DATA

NORESS	25 ELEMENT SP VERTICAL ARRAY 4 ELEMENT 3-COMPONENT 1 3-COMPONENT "HIGH FREQUENCY" SITE 125 S/S, 24 BIT A/D
CHINESE NETWORK	9 STATION 3-COMPONENT NETWORK
LAJITAS, TX	VARIOUS SP CONFIGURATIONS
MSS	LIMITED DATA FROM THE PACIFIC
RSTN, SRO, ASRO, DWWSSN	

ALPHANUMERIC DATA BASES

BULLETINS	NORESS, GSETT, FINNISH NETWORK, SOVIET NETWORK
EVENT PARAMETERS	GSETT, SOVIET EXPLOSIONS, US EXPLOSIONS, FRENCH EXPLOSIONS

THE CURIOUS CASE OF THE MISSING EXPLOSION

Eugene Herrin
Geophysical Laboratory
Southern Methodist University

"Is there any point to which you would wish to draw my attention?"

"To the curious incident of the dog in the night-time."

"The dog did nothing in the night-time."

"That was the curious incident," remarked Sherlock Holmes.
("Silver Blaze", A. Conan Doyle)

This narrative could properly be classified as historical fiction. Most of what is reported here actually happened, but some of the events occurred only in the imagination of the writer. We begin by considering the capabilities of a regional network designed to monitor an area of thick salt deposits in the western portion of the Permian Basin of Texas and New Mexico. The stations in the network are at Lajitas, Texas; Hobart, Oklahoma; and Winnemucca, Nevada (see Figure 3). Noise levels at the three stations are based upon actual noise observed at these sites and at similar sites. The minimum background noise at Lajitas is the lowest ever observed in the frequency band of 5 to 40 Hz. This minimum noise level is shown in Figure 1. The minimum levels reported for NORSAR (NORESS site) are somewhat higher, by about 10 dB or more. Measurements at Hobart in the frequency band 1 to 4 Hz show noise levels similar to NORSAR. The background level at Winnemucca based on early measurements is between the Lajitas and the Hobart values. The Lajitas and Winnemucca stations have state-of-the-art, three-component, short

MINIMUM AMBIENT NOISE LEVELS
NIGHTTIME, NO WIND
50 FT BORE HOLE

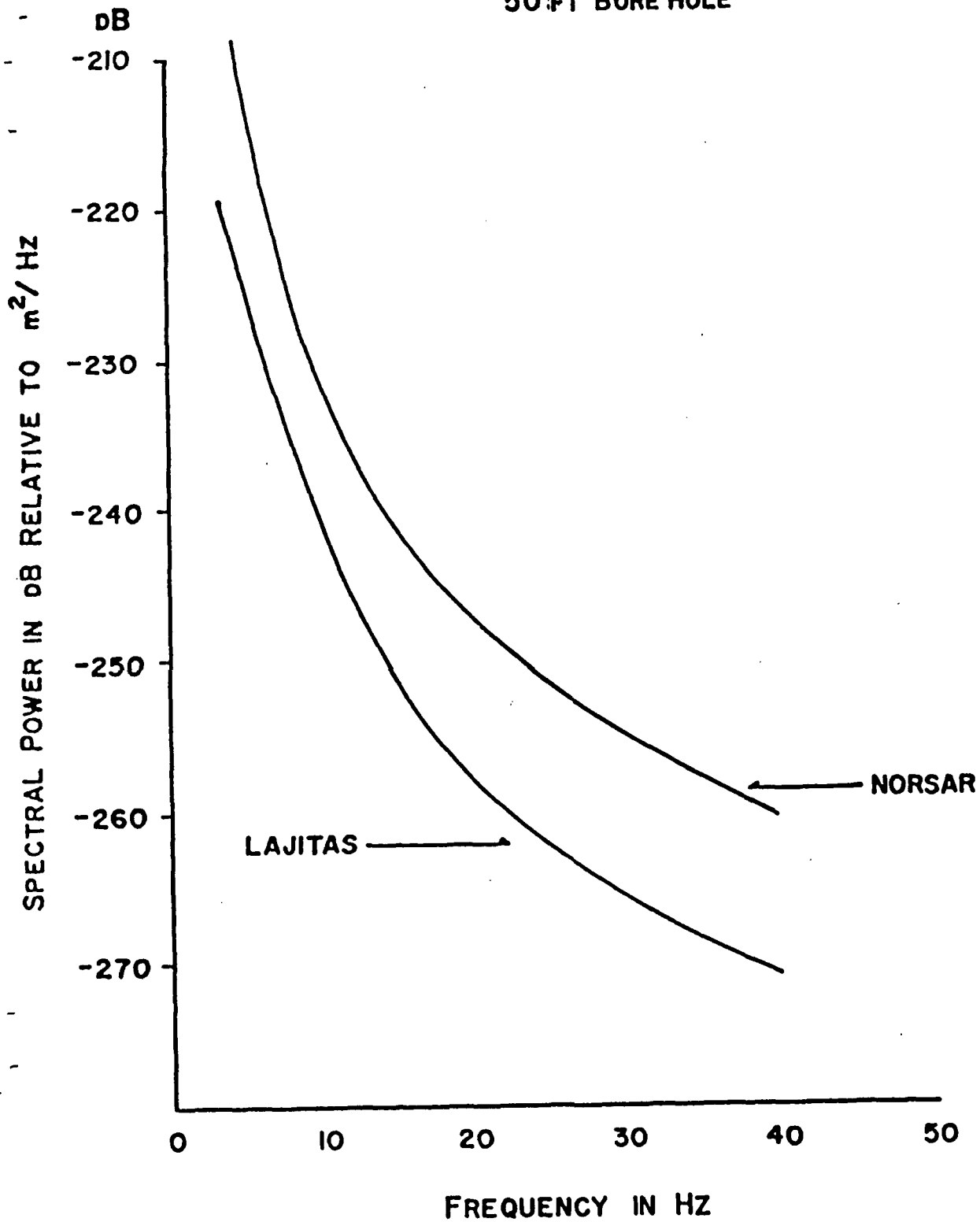


Figure 1. Minimum Seismic Noise Levels at Lajitas and Norsar.

period instruments in 50 ft. boreholes. At Hobart, a 15 element, short period array of surface instruments is located on basement rock. This array is identical to the NORESS array without the outer ring.

Background levels shown in Figure 1 are the minimum noise levels under ideal conditions which exist only a small fraction of the time. The major source of background noise is the effect of wind at the site as is shown in Figure 2. NORSAR has noise levels similar to those at Lajitas under high-wind conditions. We expect to observe the same effect at the Hobart array.

Figure 3 shows the location of a number of events as well as the locations of the stations. GNOME was a 3 kt explosion tamped in salt which was actually observed at Lajitas, Hobart and Winnemucca. SLEUTH is a planned 3 kt decoupled shot in the Salado formation in the same general area as the GNOME event. Figure 4 shows the stratigraphic units in the area. The Salado salt provides the depth and thickness needed to decouple a 3 kt nuclear explosion.

The southeastern corner of New Mexico is an area dotted with potash mines as shown in Figure 5. Mining potassium bearing minerals from the salt and anhydrite units is accomplished using the room-and-pillar method with the separation of the ore being done on the surface near the working shafts. The area is almost a wasteland covered with mounds of discarded evaporites and dessication ponds. Once the mining has proceeded as far away from the working shaft as is practical, the pillars are systematically removed allowing the mine to subside. This

LAJITAS SEISMIC BACKGROUND NOISE

vs

WIND SPEED
50 ft. Bore-Hole

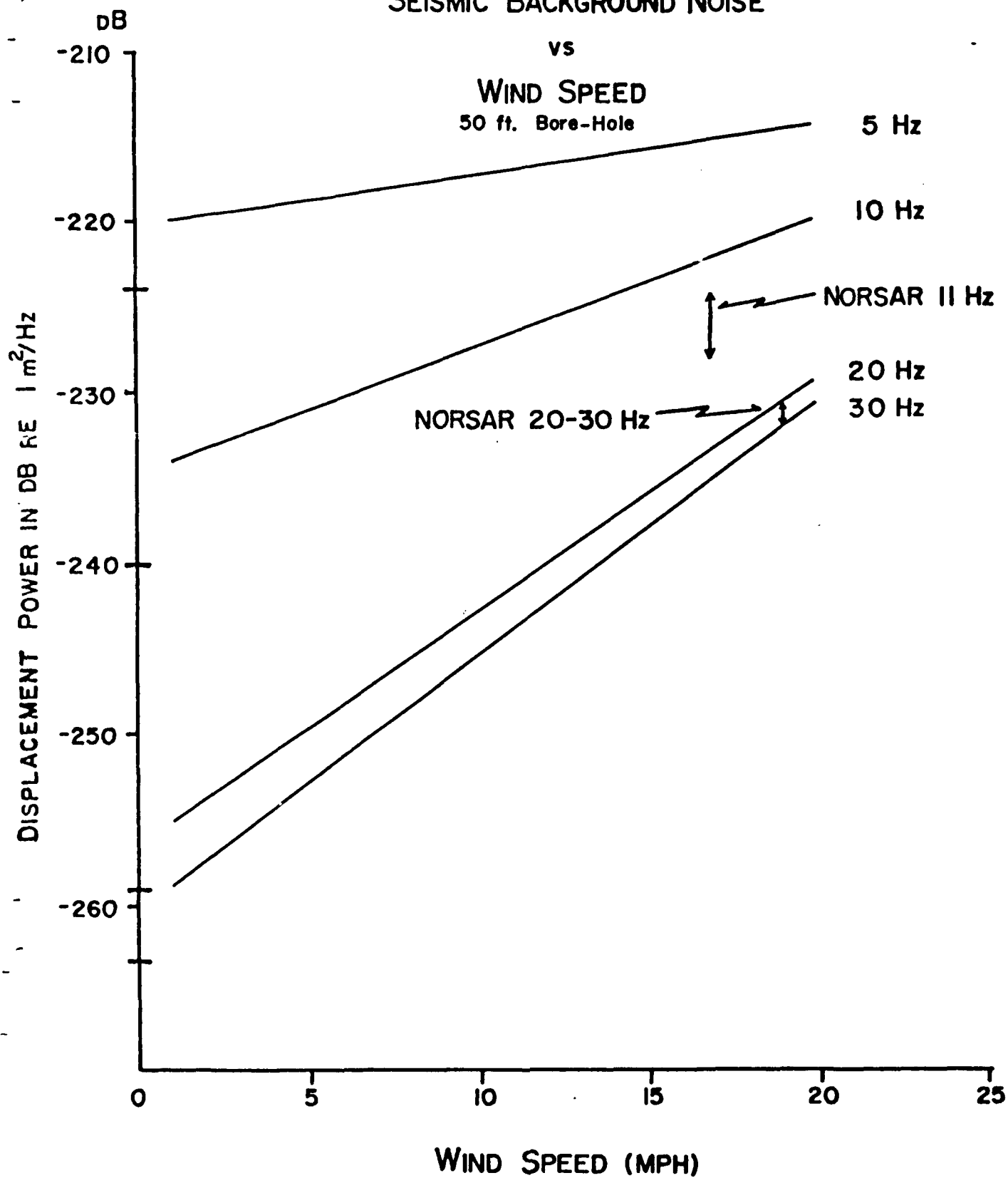


Figure 2. Seismic background versus wind speed at Lajitas.

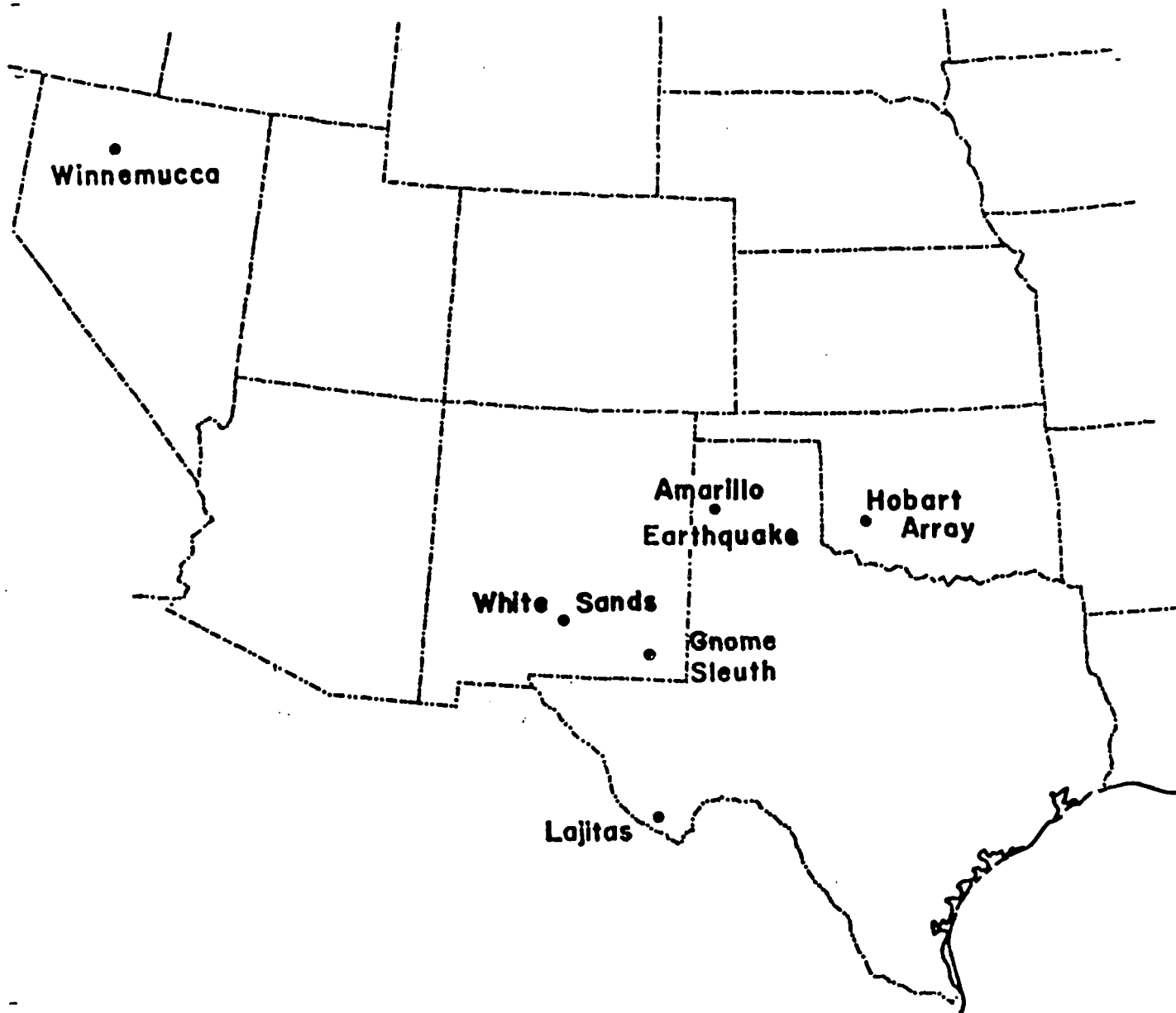


Figure 3. Map showing locations of seismic stations and events.

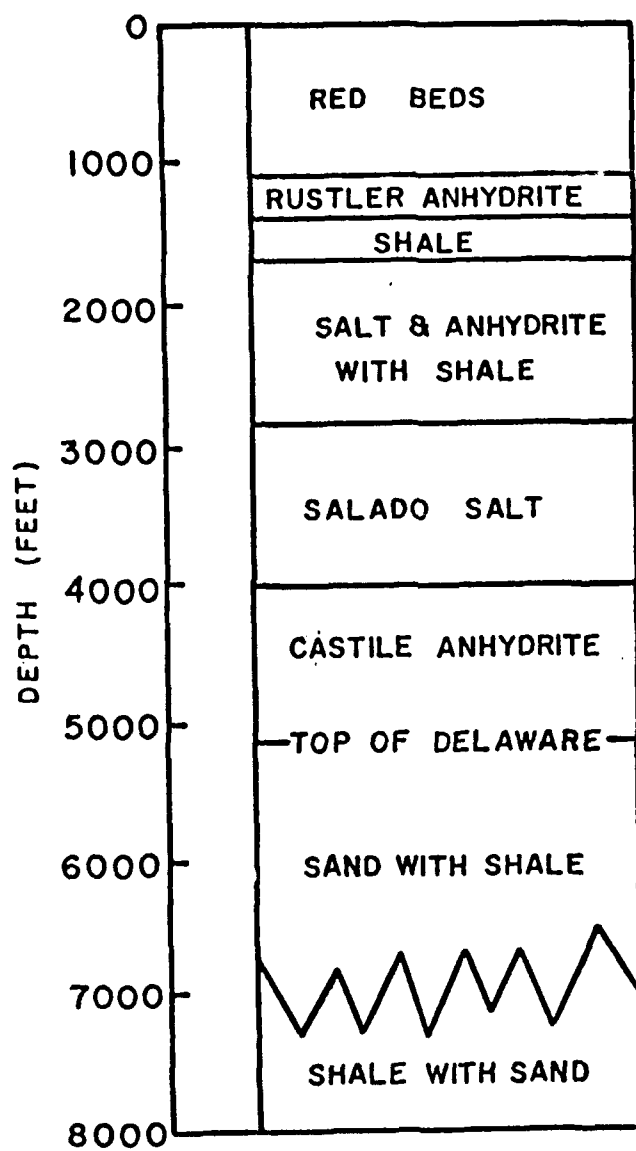


Figure 4. Stratigraphic section of GNOME/SLEUTH site.



Figure 5. Map showing potash mining activity in the GNOME/SLEUTH vicinity. Dots indicate location of potash mines.

collapse leads to obvious surface effects over the area which has been mined. After this procedure is completed, a new shaft is dug and the operation is repeated. Travellers crossing this region must beware of dangerous scarps which develop in the highways above collapsing mines.

In the midst of this region under one of the mined areas a cavity with a 40 meter radius has been constructed at a depth of 1000 meters in the Salado salt. The salt removed in this process represents only a small addition to the wastes already present on the surface. A 3 kt nuclear device is placed in the cavity ready for the decoupled test which has been code-named SLEUTH.

The F_n signal levels from a 3 kt shot fully tamped in salt (GNOME) observed at the three stations in the monitoring network are given in Table 1, along with the distances to the stations. The very low signal level at Winnemucca resulted from the high attenuation of F_n across the Basin and Range province. Propagation to Lajitas and Hobart, however, is as expected in the mid-continent. We assume a decoupling ratio of 100 at 1 to 2 Hz for SLEUTH compared to GNOME, thus we can accurately predict the F_n amplitude levels (1-2 Hz) at the three stations for the decoupled shot.

On Tuesday, 25 June 1985, preparations were being made for a 4 kt HE shot (MINOR SCALE) at the White Sands test site (see Figure 3). A cold front was crossing Colorado and Utah at that time as shown in Figure 6. The pattern of fronts moving west to east shown in this map is typical of the weather pattern in this region in the spring and early summer and again in the fall. The frontal movements and wind patterns are highly predictable. On

Table 1.

SIGNAL LEVELS

<u>Station</u>	(km) <u>Distance</u>	<u>Pn Amplitudes (millimcrons)</u>	
		<u>GNOME</u>	<u>SLEUTH</u>
Lajitas	378	42	0.4
Hobart	561	35	0.3
Winnemucca	1574	1	0.01

GNOME	3 kt	tamped in salt
SLEUTH	3 kt	in salt cavity, radius 40 meters depth 1000 meters in Salado formation.

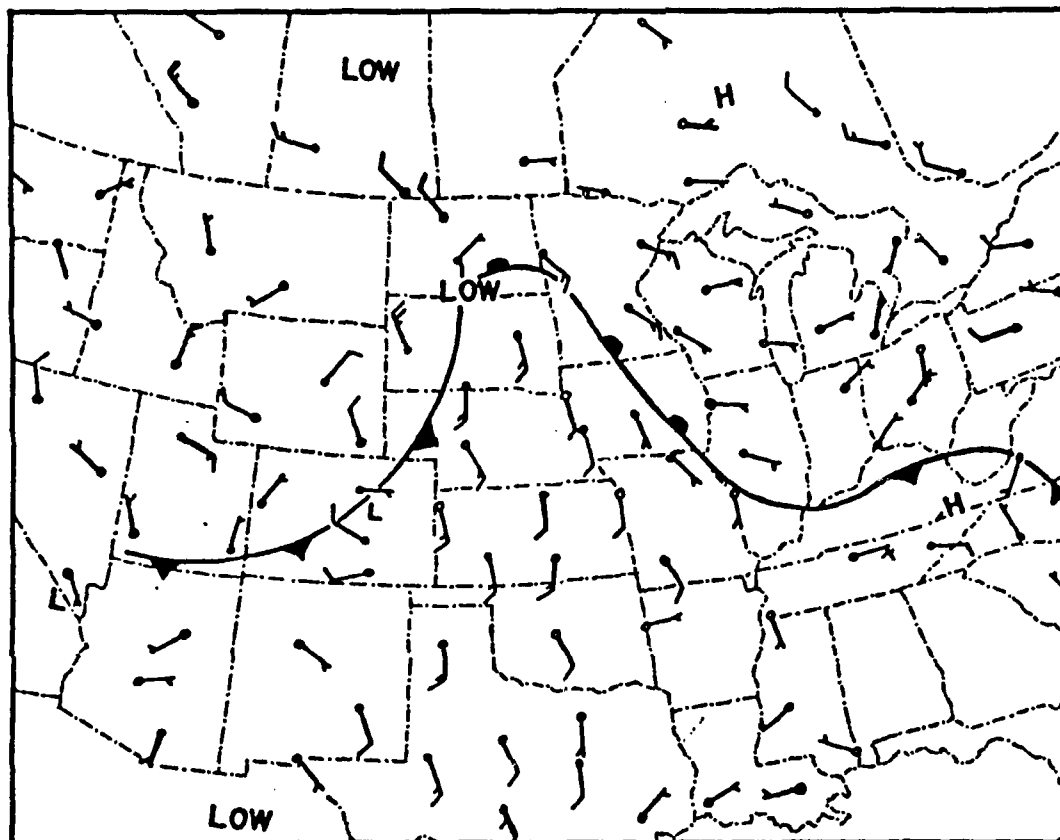


Figure 6. Weather map for Tuesday, 25 June 1985.

Wednesday, 26 June (Julian day 177), the cold front had passed into New Mexico, but had not yet begun to affect the wind patterns at Lajitas. That afternoon an earthquake of about magnitude 3 occurred west of Amarillo, Texas, and was recorded on the high-frequency (sample rate 250 per sec) system operating at the Lajitas station. The distance to Lajitas from the epicenter is 670 km. Figure 8 shows the signal and the signal-to-noise spectrum for this event. There is good signal-to-noise-ratio to frequencies greater than 15 Hz. This event was located within the 16-element seismic network operated by Stone and Webster Engineering as part of the nuclear waste disposal survey in the Texas Panhandle; therefore, we were able to compute an accurate epicenter for the event using the network records. Digital data were available for a station 48 km from the epicenter so that a good displacement spectrum could be computed. This spectrum showed a clear corner at 6 Hz, a constant level at lower frequencies and a roll-off above the corner frequency of 60 dB/decade (f^{-3}). Using this spectrum and the digital record at Lajitas, we were able to produce a good estimate of the apparent Q for P_n along this path. The value of Q was 246 which is consistent with $Q(P_n)$ reported from northeast of Moscow along a line from the Volga River to Vorkuta (Yegorkin and Kun, Izvestiya, 1978, Vol. 14, No. 4, 262-269).

On Thursday, 27 June (Day 178) 1985, the cold front had moved through Oklahoma and much of Texas (Figure 9). Winds at Hobart and Lajitas were 20 to 30 mph from the north. That morning MINOR SCALE was fired at White Sands, and thirty seconds

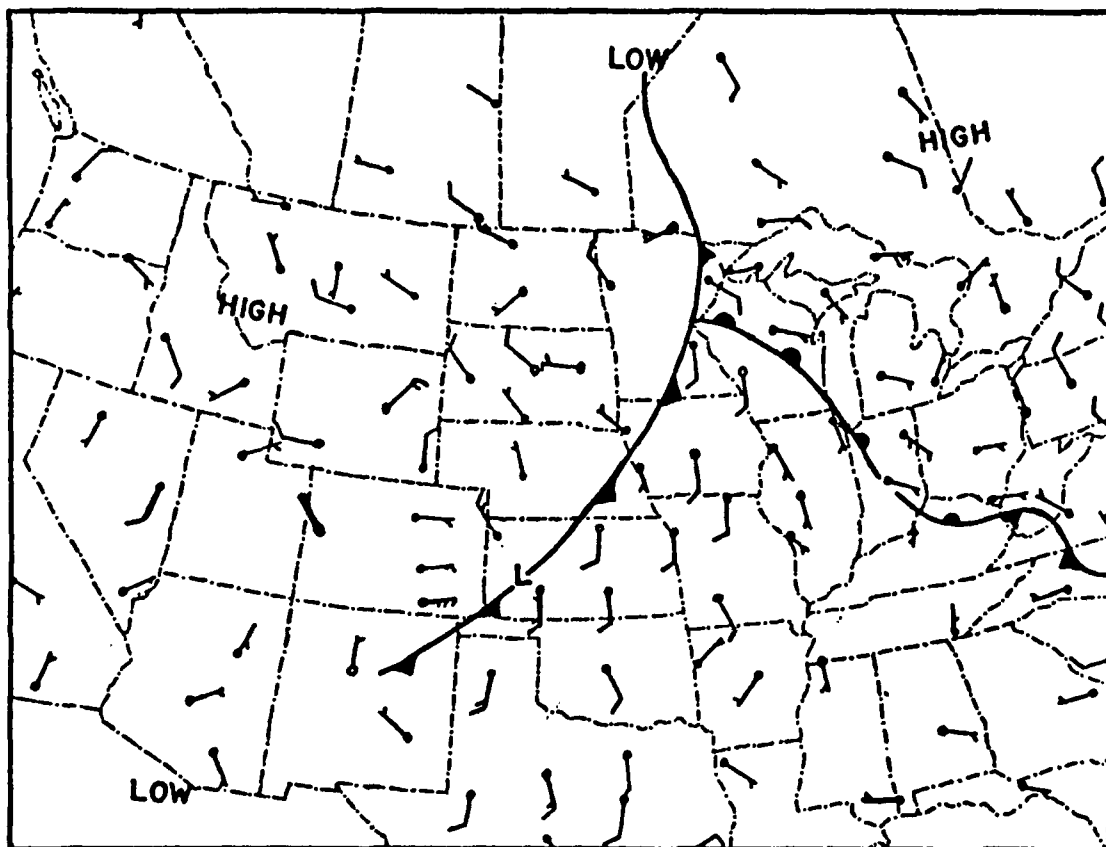


Figure 7. Weather map for Wednesday, 26 June 1985.

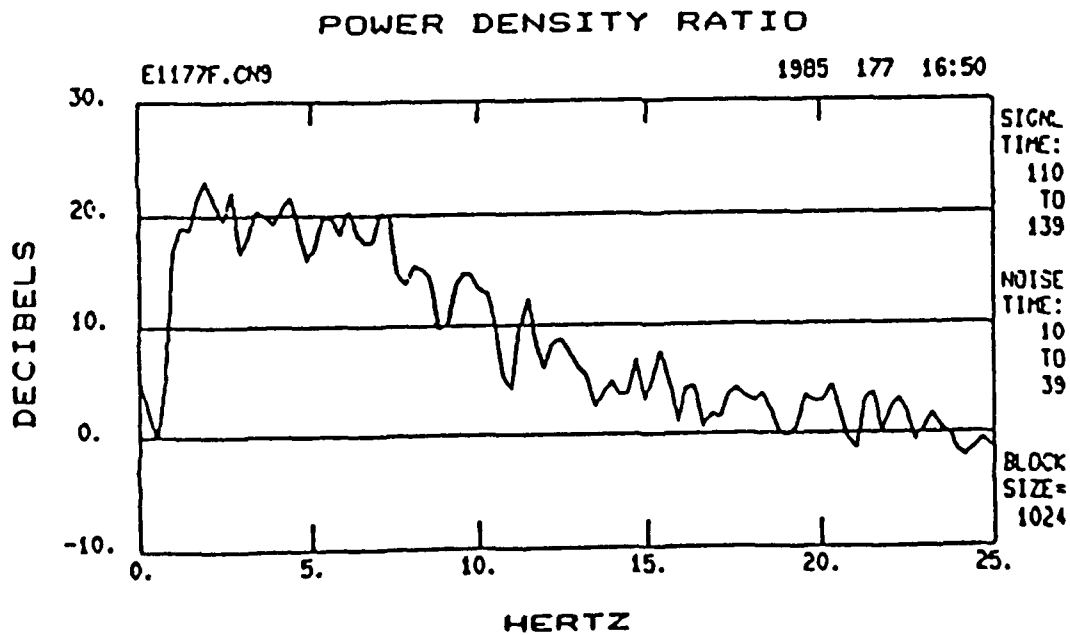
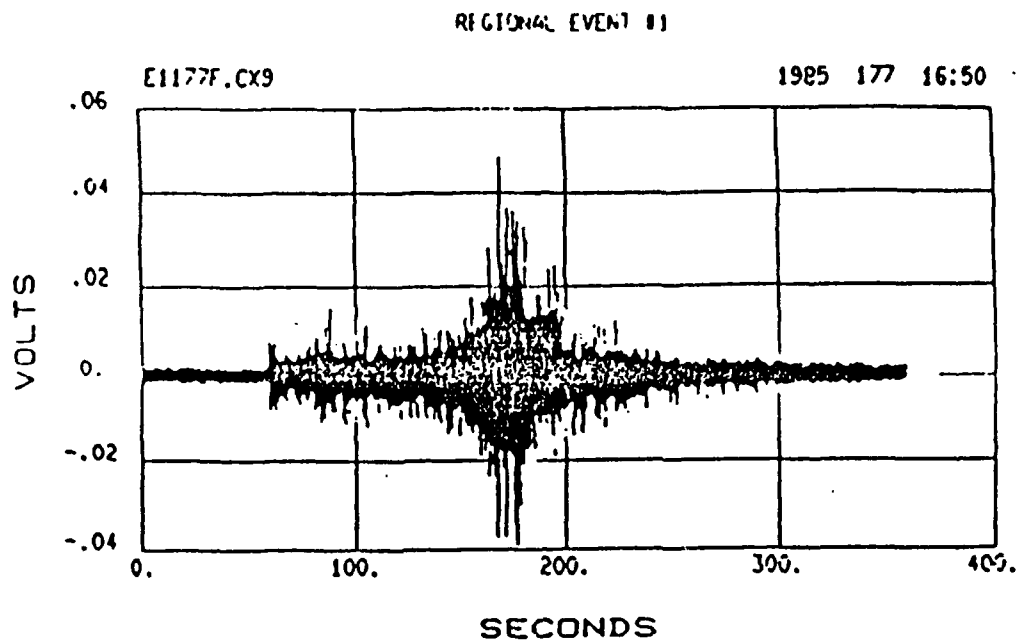


Figure 8. Amarillo earthquake, High-frequency recording (250 samples per second) from 330 ft. Z component at Lajitas and signal-to-noise spectrum for this record.

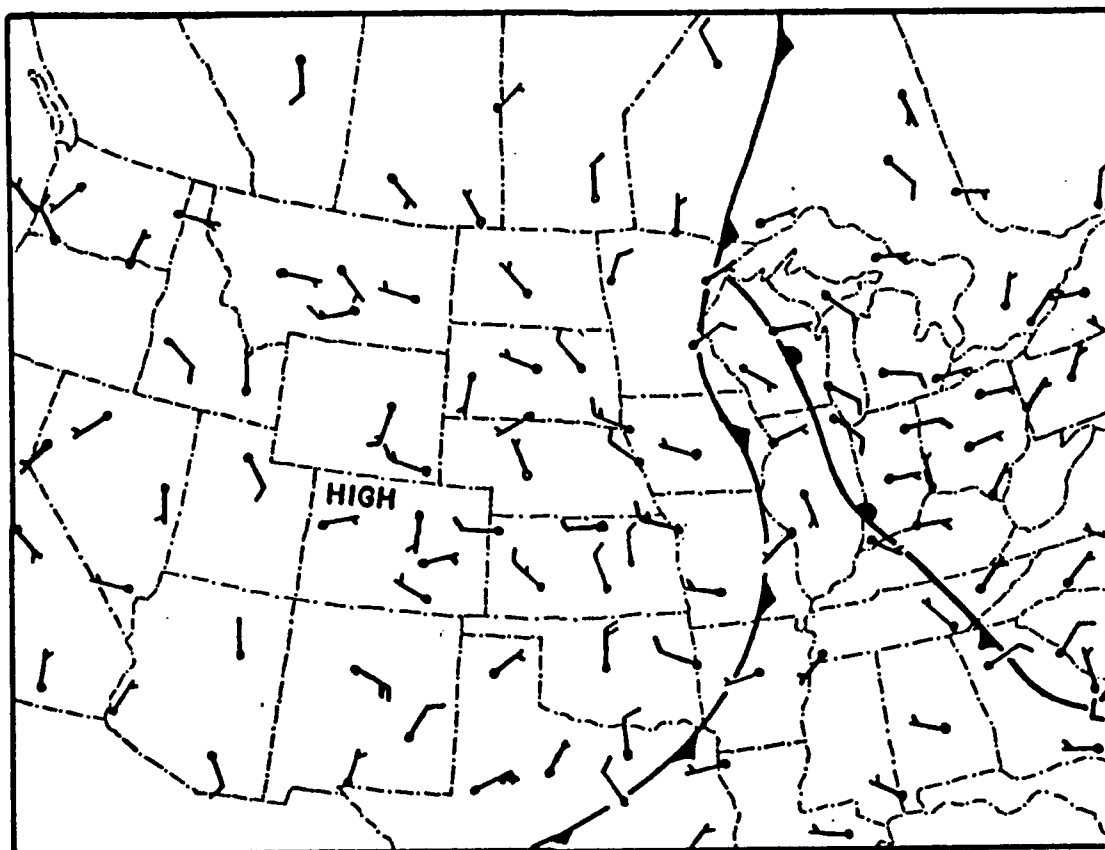


Figure 9. Weather map for Thursday, 27 June 1985.

later the decoupled nuclear shot, SLEUTH, was fired. Figure 10 shows the signal from MINOR SCALE. The amplitude of Pn from this event was about 4 times as large as from the Amarillo earthquake the previous day, as would be expected based on the yield of MINOR SCALE. The wind at Lajitas was 20-30 mph at the time of the event (Figure 10), whereas conditions had been nearly calm during the recording of the Amarillo earthquake on the previous day. Even though the vertical instrument was located at a depth of 100 meters, wind-noise was a major problem on day 178. This effect is clearly seen in Figure 11, where the signal-to-noise spectrum falls to zero dB at 6 Hz for MINOR SCALE. This result can be contrasted with the effective bandwidth of 16 Hz seen for the more distant, significantly smaller event recorded on the previous day when the wind was nearly calm.

SLEUTH was not detected at Lajitas. Pn was below the noise level and the Lg wave train was swamped by the Lg signal from MINOR SCALE. Figure 12 shows the predicted displacement spectra for GNOME and SLEUTH based on the corner frequencies for 3 kt tamped and decoupled events given by Archambeau and the Q-value obtained from the Amarillo earthquake. The displacement spectra of the background noise on days 177 and 178 are also shown. From this figure we see that if SLEUTH had been fired on day 177, Pn would have been detected at Lajitas, in agreement with Archambeau's predictions. By picking the right time to fire SLEUTH, based on the weather patterns and the known time of MINOR SCALE, the most sensitive high-frequency station in the network was made incapable of detecting the event. At Hobart, Oklahoma, the wind was 15 to 20 knots (around 25 mph) from the north

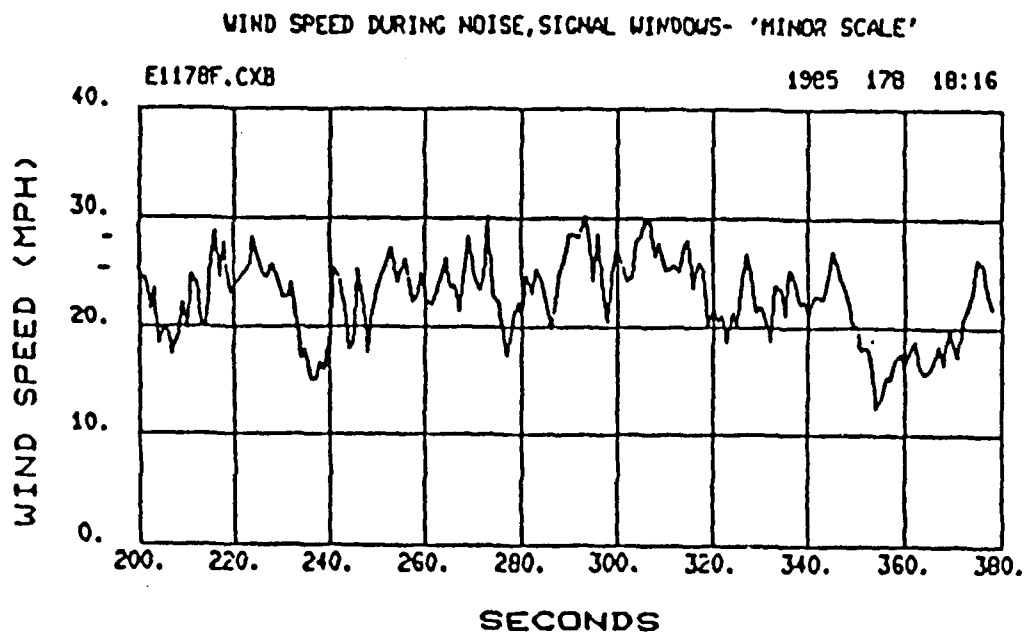
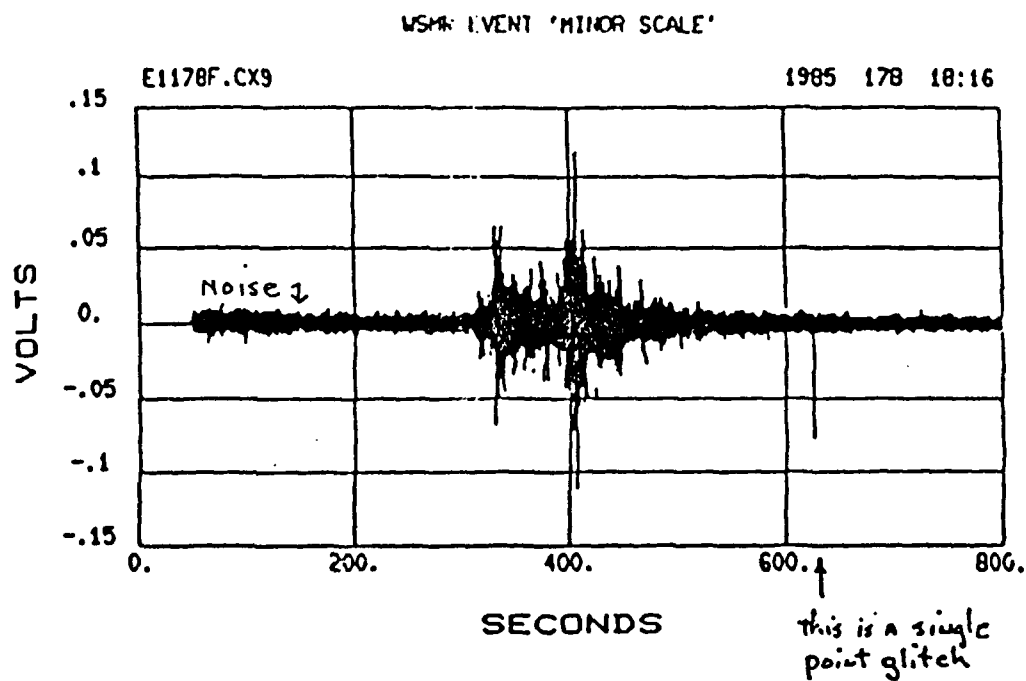


Figure 10. Minor Scale: Record from 330 ft. borehole instrument and plot of wind speed during P-wave arrival time.

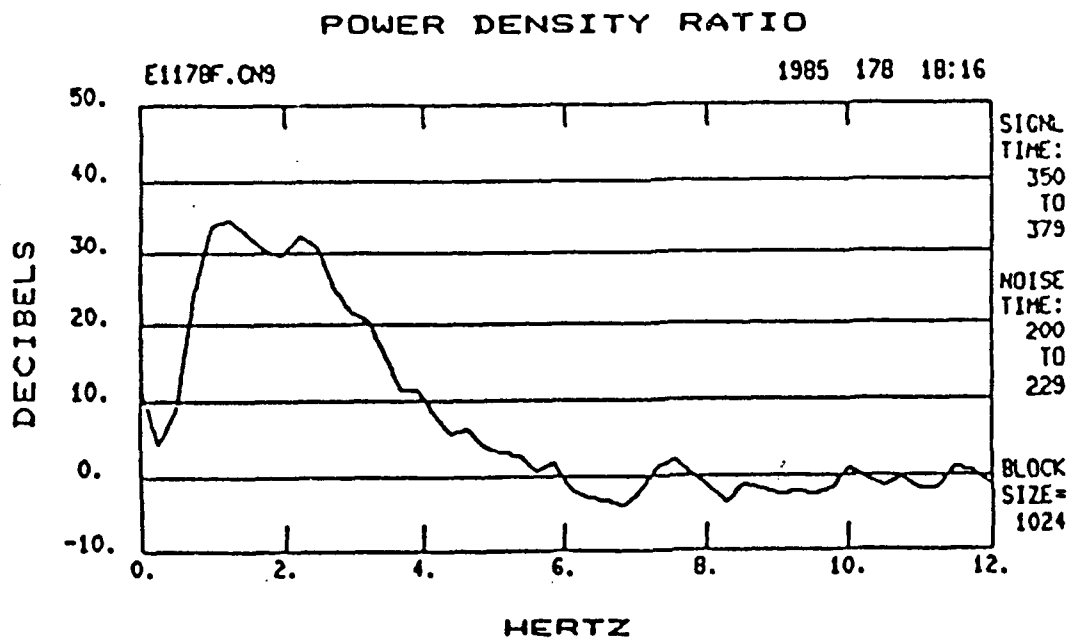


Figure 11. Minor Scale: Signal-to-noise spectrum
from P-wave, 330 ft. borehole instrument.

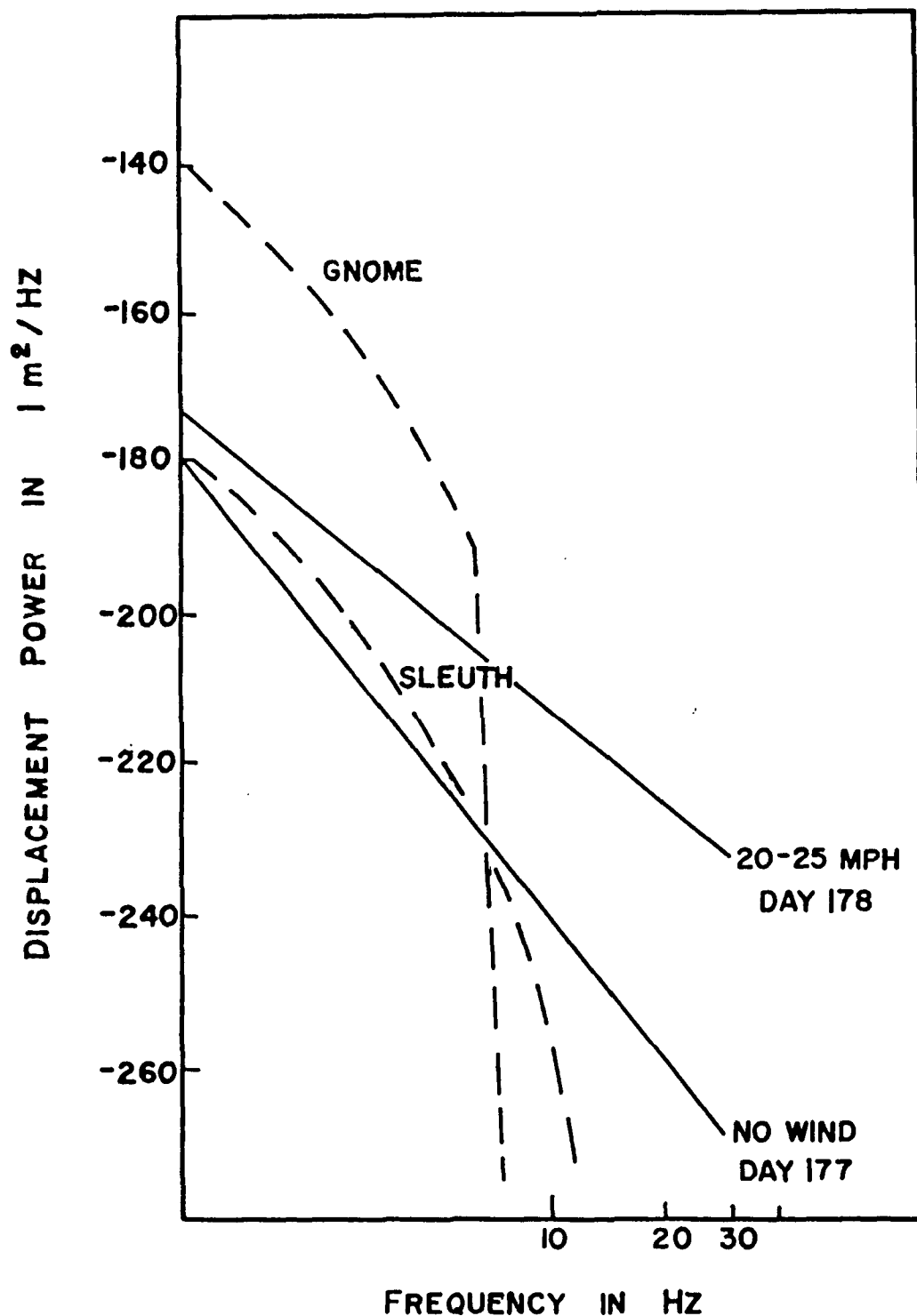


Figure 12. Displacement spectra for GNOME and SLEUTH at Lajitas and the background noise at Lajitas.

(Figure 9). The surface array there could be expected to produce signal-to-noise improvement over a single surface instrument of about 3.5 at 1 to 2 Hz and about 2 at 10 Hz. The background noise; however, could be expected to be higher by at least a factor of 5 because of the high winds. Thus the Hobart array would fail to detect Pn from SLEUTH. Again, Lg would be lost in the coda of MINOR SCALE, and could not be pulled out by array processing because of the similarity of azimuths for the two events relative to the array. Because of poor propagation across the Basin and Range Province, Pn from SLEUTH could not be detected at Winnemucca no matter what the noise conditions were at that station. Thus we see that an excellent regional network designed to monitor an area with salt deposits failed to detect a 3 kt decoupled shot.

"The dog did nothing in the night-time."

The failure of the network occurred because the evader could pick the most advantageous time to fire the clandestine test. SLEUTH is not one-of-a-kind. Predictable weather conditions similar to those on 27 June 1985, occur in West Texas and Oklahoma several times each year. Shots of 1/2 kt of HE or larger are not uncommon at White Sands Test Site. Cavity mining could go on year after year in southeastern New Mexico completely masked by the potash mining in the area. By waiting for the

same sequence of events that occurred on 27 June, several decoupled nuclear tests a year could be carried out with virtually no chance of detection.

Two factors are required for a successful clandestine test of the kind described in this paper. The first is a degradation of detection capability at the critical stations because of high wind. The second is a legitimate HE test under the control of the evader which can be used to mask the decoupled shot. The second factor must be regulated by legal means. Control of the first factor depends upon our ability to protect instruments from the effect of wind-induced seismic noise. Until these problems are solved, a clever evader can pick the right time to fire a decoupled shot with little risk of detection.

Acknowledgements. Dick Cromer (Sandia) and Paul Golden (SMU) computed the spectra used in this paper. Stone and Webster Engineering provided digital data from their network in the Texas Panhandle. This work was supported by DARPA/AFGL under contract No. F19628-85-K-0032 and by Sandia National Laboratories. John W. Harrington suggested the use of the quotation from A. Conan Doyle.

ANALYSIS OF TELESEISMIC P WAVE CODA USING MULTICHANNEL DECONVOLUTION METHODS AND COMPARISON TO FINITE DIFFERENCE CALCULATIONS

Zoltan A. Der, Keith L. McLaughlin, Alison C. Lees, and Rong-Song Jih
Teledyne-Geotech, 314 Montgomery Street, Alexandria, VA 22314

INTRODUCTION

A fundamental problem in nuclear explosion seismology is the determination of the nature of the P wavetrain observed at teleseismic distances. In order to derive source diagnostics from P waves one must know what features of the seismogram are due to the source region and which are related to the receiver structure. If we have recordings of multiple events in a limited source region available at a seismic array, this kind of decomposition of the P wave seismograms is possible utilizing the factorability of P wave spectra as first shown by Filson and Frasier (1972). In this report we first discuss the utilization of this P wave factorability in a multichannel deconvolution scheme, and then present the results of a number of deconvolutions in the context of elucidating the nature of the initial source generated P wavetrain and of understanding the P wave coda in terms of scattering generated in both the source and receiver regions. Finally, we show a way by which we may interpret such deconvolution results in the future in light of finite difference simulations of wave propagation in random heterogeneous media.

MULTICHANNEL DECONVOLUTION

As mentioned above, Filson and Frasier (1972) were the first to note the factorability of P wave spectra such that

$$Y_{ij}(\omega) = R_i(\omega) S_j(\omega)$$

where the i 's and j 's correspond to sources and receivers, respectively, $Y_{ij}(\omega)$ are the P wave spectra, $R_i(\omega)$ are the receiver factor spectra, and $S_j(\omega)$ are the source factor spectra. Shumway and Der (1985) utilized this idea to develop a maximum likelihood multichannel deconvolution method for decomposing P wave seismograms into source and site spike sequences assuming that the combination of the instrument and attenuation operators are known (optionally also including the explosion source wavelet). This approach is essentially a multichannel equivalent to the method given by Oldenburg (1981). Figure 1 is a flow diagram of the multichannel deconvolution scheme, the mathematical details of which can be found in Shumway and Der (1985).

At the beginning of the process, both the source and site spike sequences are initialized to delta functions and we obtain an estimate of the source spike sequences first. Then the site functions are estimated. In each step the combinations of the instrument and the t^* operators are factored out (explosion source spectral estimates may also be included at this step). Subsequent iterations refine the separation of the spectra into source and site sequences (and terms which are common to neither). We have used four iterations in our calculations. As a final step, we reconstruct the original seismograms to verify the results. The first iterative step in this scheme is a close equivalent of the method used recently by Douglas *et al* (1986) for deconvolving P wave seismograms at the AWRE arrays. In Douglas *et al*'s deconvolutions only the instrument and the t^* operators were factored out and the resulting waveforms were interpreted in terms of rise times and overshoots of the explosion sources as

well as in terms of pP and spall arrivals.

The purpose of any deconvolution is, of course, to facilitate the interpretation of the seismograms, i.e. to transform the wavelets into a spike-like form. Since the method is noncausal and the bandwidths over which we may flatten the spectrum by deconvolution are limited, we usually do not obtain exact delta functions but rather some approximations to them with spiked appearance. The side lobes of these approximations to the delta functions are, unfortunately, not entirely avoidable, especially for signals of narrow bandwidth along highly attenuating paths. Nevertheless, the results of the deconvolutions allow us to recognize the P and pP arrivals, but it may not be possible always to resolve them if the delays of pP relative to P are small.

RESULTS OF DECONVOLUTIONS OF SEVERAL DATA SETS

One of the first applications of the multichannel deconvolution technique was to a set of Kazakh events recorded at EKA, the deconvolved source time functions of which are shown in Figure 2. Only the event corresponding to the bottom trace, the presumed cratering event, was not contained, and its source time function is clearly different than those of the other events with no clear pP arrival and a much more complex initial P wavetrain. However, analyses of additional Kazakh events recorded at NORSAR also show some non-cratering events with no clear pP. We are in the process of attempting to find the reasons why some of these events look different from the rest. Most of the Kazakh events show a downswing interpretable as pP, in agreement with the findings of the AWRE group.

A test of the factorability of the spectra is the degree of success in reconstructing the complete set of $N \times M$ seismograms from only $N + M$ site and source factors. Figure 3 is an example of some original (top) and reconstructed (bottom) seismograms for the presumed Kazakh cratering event recorded at EKA. For each trace there is excellent agreement between the original and reconstructed traces, including detailed matches of fine details late in the coda and waveforms with high dominant frequencies near 2 Hz. The examples shown are representative of the quality of all our reconstructions.

We have also obtained interesting results from deconvolutions of other data sets. Pahute Mesa explosions showed complex source functions, often with no clear pP and numerous secondary pulses. The deconvolved source functions from teleseismic recordings of Yucca Flats events did not show significant improvement from the original traces because of the narrow band spectra of the recordings and the lack of high frequency content in the signals due to noise and the high levels of attenuation under NTS. The contrast between the Yucca Flats events and Piledriver was found to be particularly striking; Piledriver was detonated in granite north of Yucca Valley, and its deconvolved source time function is much more similar to those of the Kazakh events than to those of the Yucca Flats events. Deconvolutions of several Azgir events showed a late (1.5 sec after P) negative pulse that may be pP.

The site factors are complex and different for different test sites, in accordance with the known azimuth-slowness sensitivity of receiver effects. If we filter the site factors into the dominant frequency bands of the observed signals (Figure 4) we find, by comparing to similarly filtered deconvolved source factors, that the P wave coda is made up about equally of near source and receiver scattering contributions. We can identify features in the P wave coda corresponding to either the source or the receiver scattering contributions simply by inspection of the seismograms and by comparing them to the deconvolved source or site factors. By decomposing the P wave seismograms this way we may begin to interpret the coda and the scattering contributions to the P waves from near source or receiver scattering and may be able to locate and identify near source and receiver scatterers. A convenient method to model the scattering process is provided by the finite difference approximations to

the elastic wave equation. In the second part of this report we describe some ongoing work along these lines.

RESULTS OF FINITE DIFFERENCE SIMULATIONS

Our computer programs use the 2D second order finite difference approximation to the inhomogeneous wave equation (Kelly et al 1976) together with an array of subroutines that allow us to introduce various types of sources, transparent boundary conditions, and topography, and to sense various types of diagnostic quantities (displacements, dilatations, rotations etc) at arbitrary points within the grids (Jih et al 1985). The most restricting limitation is imposed by the 2D nature of the code, and adjustments must be made to the results so that they correspond to the real world which is characterized by a 3D structure. For instance, in three dimensions, Rayleigh waves have 2D spreading, while in 2D finite difference simulations, there is no spreading along the top of the grid.

The factorability of the spectrum demonstrated above must be due to the fact that there are two major regions of scattering along the ray path. These are in the lithosphere near each of the sources and the receivers. We plan therefore, to model the scattering process in each region separately. Near source scattering may be modeled by using the reciprocity principle, using an incident P wave and monitoring the dilatations at selected points corresponding to the locations of sources. This is equivalent to the determination of the P waveforms generated teleseismically by compressional line sources at the same locations. This was done to simulate the effects of the laterally varying structure at Yucca Flats.

Near receiver scattering can be modeled simply by making a body wave incident on a random model of the lithosphere and recording the motion at the surface or at some depth. Figure 5 shows a contour plot of velocities for one of the random media used; it has heterogeneity scale lengths between 250 and 700 meters and the grid size is 5 km by 3.75 km. The RMS velocity variation is 5%. The synthetic seismograms generated using such models have been used in this study for F-K analysis. F-K diagrams such as those shown in Figure 6 were computed by a double Fourier transform of a horizontal array of synthetic seismograms due to incident P or S waves on a random media. Using such F-K diagrams, we are able to distinguish among the various types of scattered waves by their apparent velocities.

Figure 6 shows examples of F-K diagrams obtained for the case of a random medium in Figure 5. The F-K power for the horizontal displacement is contoured on the left of this figure and that for the vertical displacement on the right. The vertical lines of high power in this figure correspond to the incident P wave and the slanting stripes of the high amplitudes correspond to the converted Rayleigh and S waves propagating horizontally along the surface.

Moving the sensor array to the depth of 1 km made the Rayleigh motion disappear as expected because of the diminution of the Rayleigh amplitudes with depth thus identifying the surface wave nature of these waves. Comparing the amplitude levels of the scattered Rayleigh waves to that of the incident wave on the vertical components we find that it amounted to 60-70% for this severe case of scattering. In the 3D case we would expect these levels to decrease rapidly as the inverse square root of time after the first arrival because of the geometrical spreading of the scattered Rayleigh waves. Nevertheless, the contribution of P-to-Rayleigh scattering to the seismogram would still be considerable.

PRELIMINARY CONCLUSIONS

Multichannel deconvolution of numerous events observed at the same array enables us to separate the contributions to the P wave train from near-receiver and near-source scattered waves. The source related wavetrains are generally complex, containing direct P, pP, and other later arrivals. Receiver and source scattering contribute about equally to the P wave codas. Most Kazakh events show identifiable pP arrivals, while Pahute Mesa events are complex, mostly without clear pP pulses. We were unable to obtain good results for Yucca Flats explosions because of the extremely limited bandwidth of these events.

Once the source and receiver factors are separated by deconvolution these can be modeled by finite difference simulations using various plausible models of the source and receiver regions. In this paper we show results for 2D P wave scattering in a heterogeneous lithosphere for perpendicularly incident waves. Upon the arrival of the P wave, scattered P and Rayleigh waves of considerable amplitude can be identified in the wavefield by F-K analyses. The amplitudes of scattered Rayleigh waves may be as large as 60-70% of the initially incident P.

REFERENCES

- Douglas, A., Marshall, P.D. and J.B. Young (1986), The P waves from the Amchitka Island explosions. (Manuscript)
- Filson, J. and C.W. Frasier (1972), Multisite estimation of explosive source parameters. *J. Geophys. Res.*, 77, 2045-2061.
- Jih, Rong-Song, McLaughlin, K.L. and Z.A. Der (1985), Boundary conditions of arbitrary polygonal topography in finite difference scheme for seismogram generation. (Manuscript) Teledyne-Geotech, Alexandria, VA.
- Kelley, K.R., Ward, R.W., Treitel, S., and R.M. Alford (1976), Synthetic seismograms: a finite difference approach. *Geophysics*, 41, 2-27.
- Oldenburg, D.W. (1981), A comprehensive solution of the deconvolution problem, *Geophys. J. R. astr. Soc.*, 65, 331-358.
- Shumway, R.H. and Z.A. Der (1985), Deconvolution of multiple time series. *Technometrics*, 27, 385-393.
- von Seggern, D.H. and R.R. Blandford (1972). Source time functions and spectra from underground nuclear explosions, *Geophys. J. Roy. Astr. Soc.*, 31, 83-97.

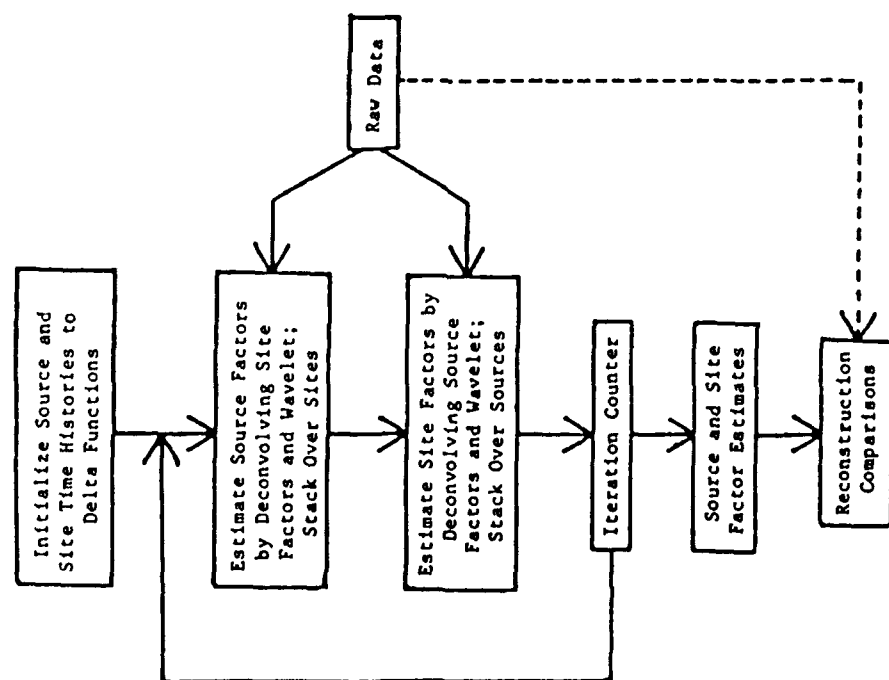


Figure 1. Flow diagram for the iterative multichannel deconvolution method.

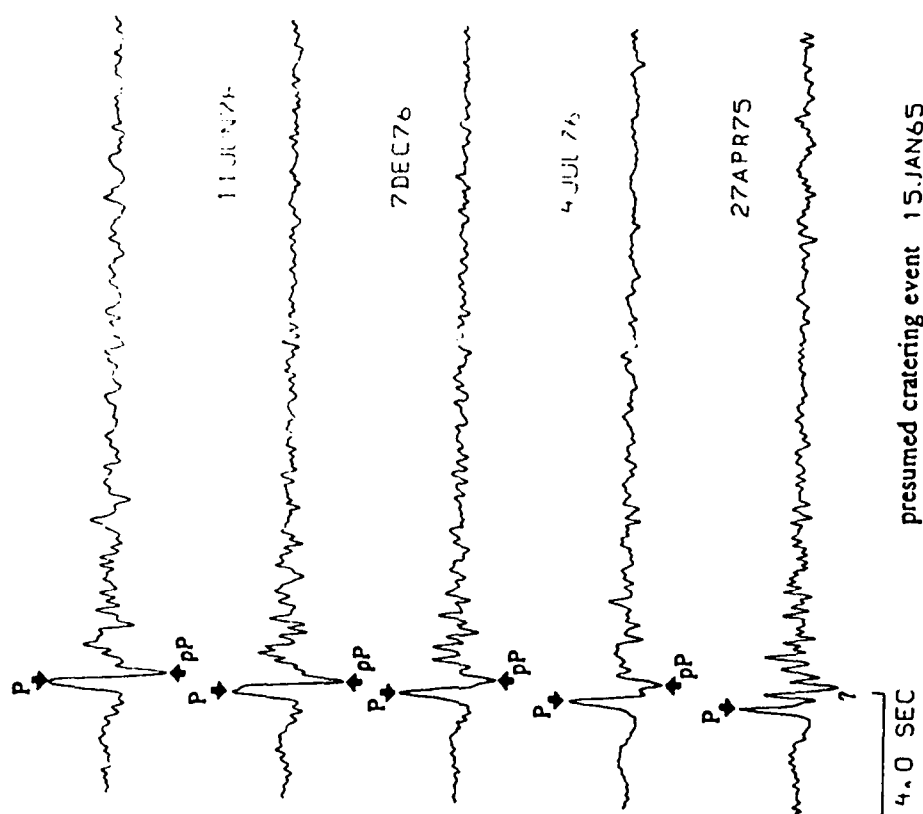


Figure 2. Results of source deconvolutions for a set of Kazakh nuclear explosions recorded at EKA. The bottom trace is the source function estimate for the presumed Kazakh cratering explosion.

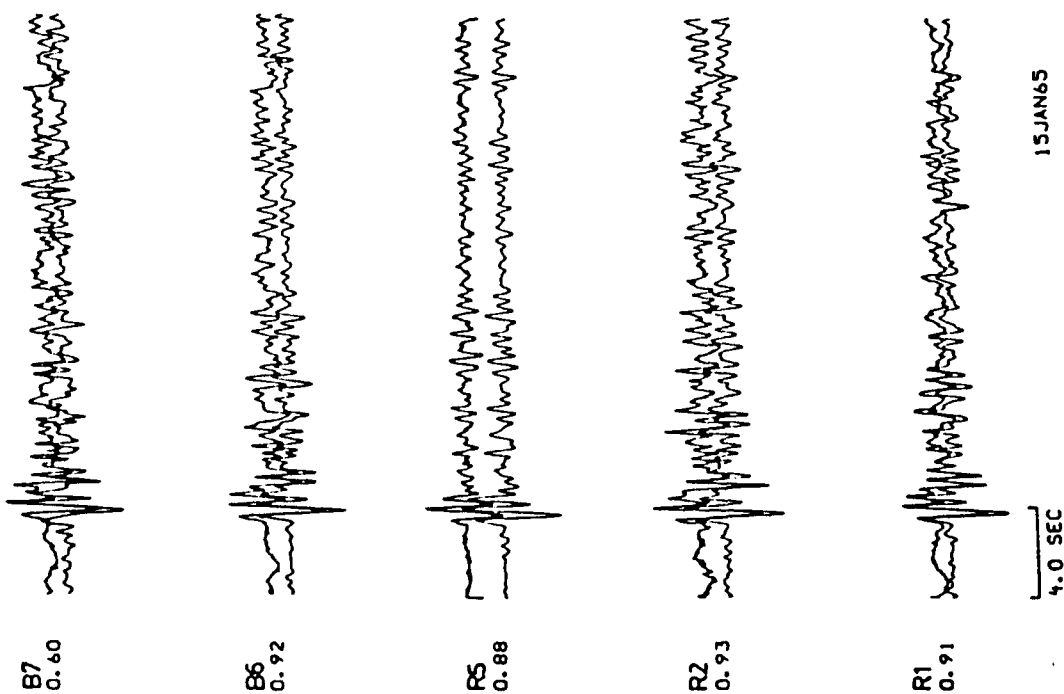


Figure 3. Original (top of each pair) and reconstructed (bottom) traces at EKA for the presumed Kazakh cratering event of 15 January 1965. To the left of each pair of traces is the designation for the station at EKA and the correlation coefficient between the original trace and its reconstruction. Note that even details late in the coda are reconstructed well.

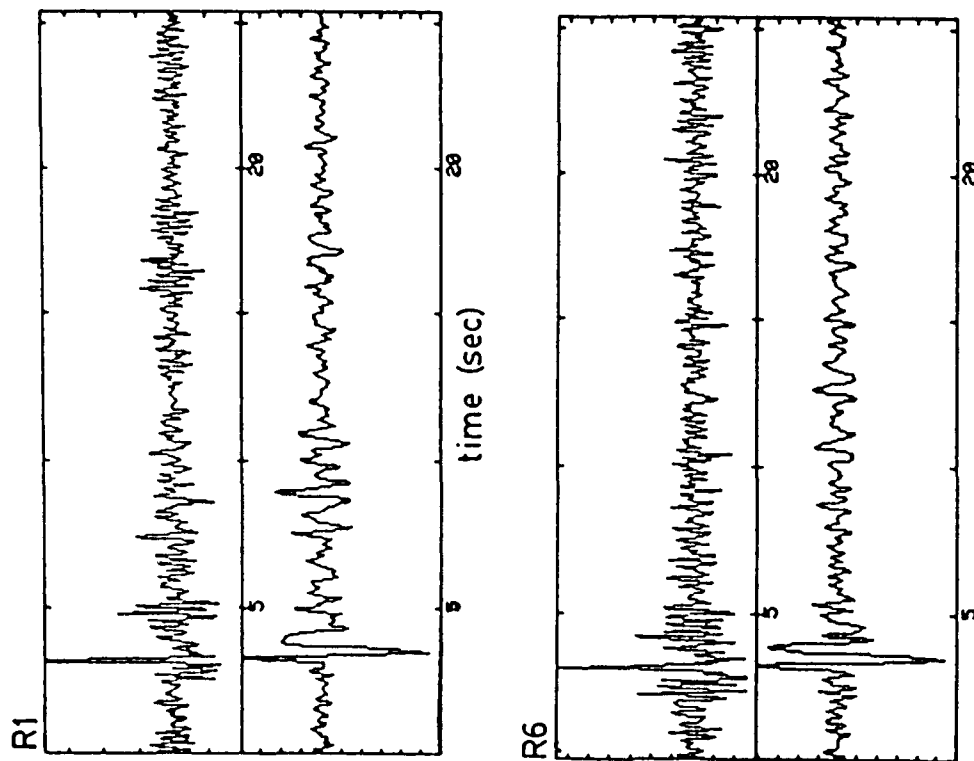


Figure 4. Examples of filtered site terms for the set of Kazakh data recorded at EKA. In each pair, the top trace is the deconvolved site term, which has been filtered in the bottom trace with a von Seggern and Blandford wavelet assuming a yield of 130 kt, $t^* = 0.15$ sec, and an EKA instrument response. Note the considerable power in the site-related coda as seen in the filtered trace of sensor R1.

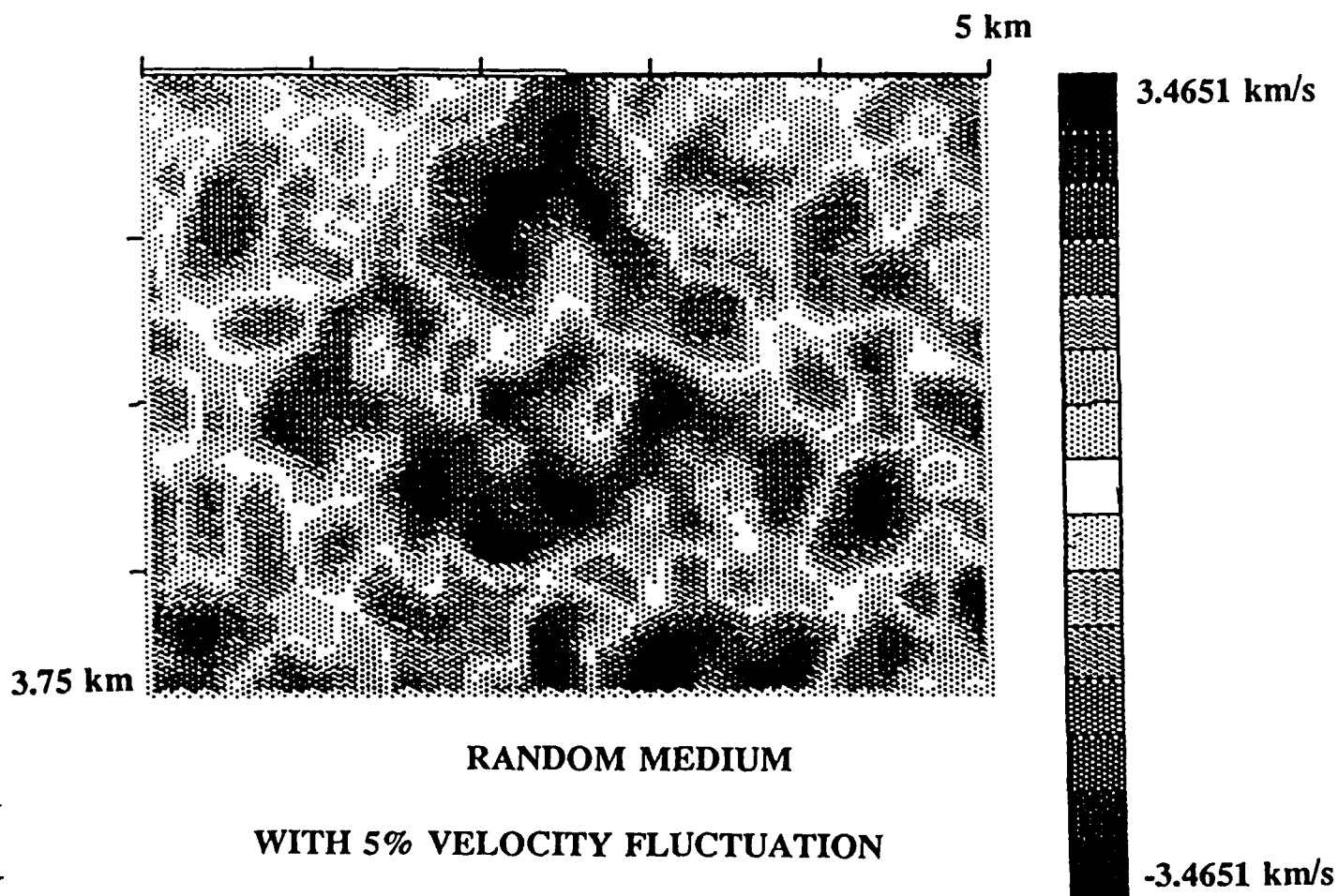
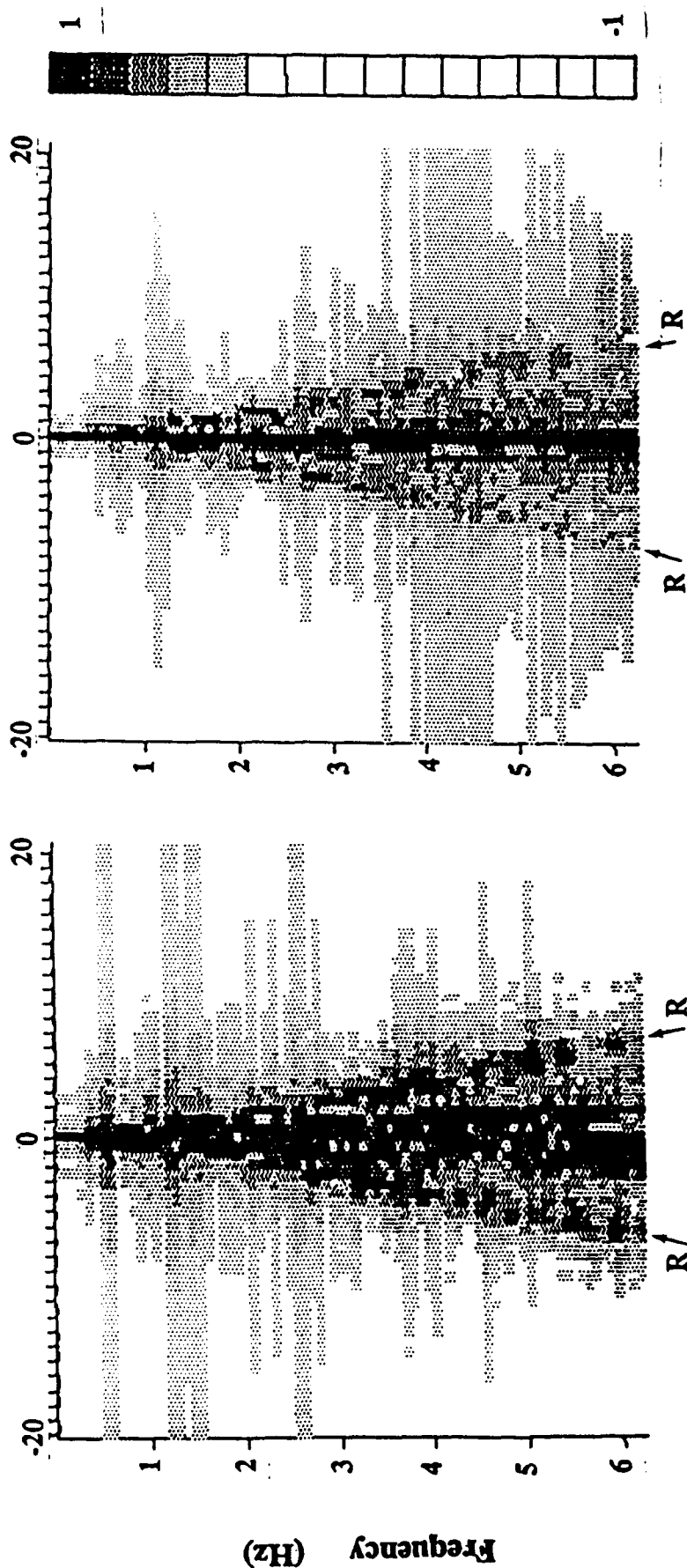


Figure 5. Contour plot of the velocities in the random medium used. The grid has the dimensions of 5 km by 3.75 km, the velocities have a 5% RMS variation.

Wave number (cycles/km)



F-K plot, Vertical Component

F-K plot, Horizontal Component

Figure 6. F-K spectrum of near surface horizontal (left) and vertical (right) motion excited by a P wave perpendicularly incident on the surface of a random medium. The sloping lines correspond to the velocities of horizontally traveling scattered Rayleigh waves. The amplitudes of scattered Rayleigh waves are 60-70% of the incident P on the vertical component.

Salt Dome-Related Seismicity near Kulyab, Tadjikistan, USSR

David W. Simpson and William Leith
Lamont-Doherty Geological Observatory
Columbia University, Palisades, NY 10964

Abstract

In the region near Kulyab, Tadjikistan, hundreds of shallow earthquakes with magnitudes greater than 2 1/2 have been reported in Soviet yearly catalogs since 1964. This area appears as a well-defined cluster of activity, well off the line of epicenters that defines the Gissar-Kokshal seismic zone, to the north of the Pamir ranges. The geology of the region is not strongly deformed as it is elsewhere along the Gissar-Kokshal zone. Instead, it is dominated by the presence of numerous salt domes surrounded by Neogene and Quaternary continental deposits. The spatial association of these earthquakes with the salt domes suggests that the two phenomena may be related. Moderate earthquakes ($M > 5$) occurred in 1972 and 1973, and intensities of surface shaking greater than $MM=6$ were reported from earthquakes in 1937, 1952, 1969, 1972, 1973 and 1978. The earthquake on 2 April 1973 and its aftershocks were located in a region where no salt domes have been mapped at the surface. However, a buried salt diapir has been mapped at depth by geophysical means. We have suggested the possibility that these earthquakes may have resulted from active salt diapirism at depth. The mechanism for producing this seismicity could be either by the active fracturing of the cap rock by the rising diapir, or by the concentration of tectonic stresses in the thinned section above the diapir. The salt-related earthquakes may have low b -values and produce lower frequency radiation than other events of the same size.

Introduction

Salt deposits, and specifically salt domes, are currently of special interest as possible sites for decoupling of underground nuclear explosions [Hannon, 1985] or for the underground storage of radioactive nuclear waste [Cohen, 1977]. The relatively structureless, homogeneous nature of salt formations, combined with the high solubility of rock salt, lend these formations to the mining of the large stable cavities that would be necessary to decouple a large underground nuclear explosion [Cohen, *op cit*]. In contrast with bedded salt deposits, salt domes are considered ideal cavity sites because of their large vertical dimensions and relatively

pure salt content.

Earthquakes associated with salt domes present two important problems: First, in terms of explosion decoupling and the detection of clandestine nuclear weapons tests, their spatial association with the cavity poses the obvious problem of discrimination. This may be compounded by the possibility that salt-related earthquakes have different source characteristics than "normal" earthquakes, as discussed below. Also, in terms of any engineering activities on the surface or within the salt dome, they represent a hazard to the stability of any cavity constructed. As potential sites for hazardous waste storage, earthquakes may possibly affect the short-term permeability of the cavity walls.

There is an extensive literature on salt diapirism [see summaries and bibliographies in: Braunstein and O'Brien, 1968; Jackson and Talbot, 1986; Lerche, 1986; Schreiber, 1986]. Salt domes form by the post-depositional flow of bedded salt upward through the overlying rock formations because of the gravity (density) instability inherent in buried salt. It is generally considered necessary for salt dome regions to have undergone some degree of tectonism (associated with sedimentary loading) in order for diapirs to develop. Therefore, the process of salt dome formation is unstable and episodic and the rates of salt dome uplift are highly variable, depending on both the tectonics of the region and the state of maturity of the diapir [Jackson and Talbot, 1985].

Salt itself is an extremely weak rock and deforms ductilely at geological strainrates [Carter, 1983]. Salt areas are generally not associated with earthquakes, and until this time there is no literature associating earthquakes with active salt doming. Where studies have been made of the seismicity of salt dome areas in East Texas and the Gulf Coast [Dorman and others, 1975; Racine and Klouda, 1979; Pennington, 1985], no definitive correlations between salt structures and earthquakes have been made.

Nevertheless, sounds of salt movement have been detected [Kent, 1979] in salt dome regions in Iran, and rock bursts have occurred in underground salt mines [see Baar, 1977]. Those salt dome areas where detailed seismicity studies have been made (east Texas, Louisiana, Oklahoma) are also areas where the domes are essentially inactive [mature, see Jackson and Talbot, 1985]. Our study therefore provides the first documentation of earthquakes related to active salt doming. This paper describes the geological and seismological attributes of the Kulyab salt dome area, and suggests a hypothesis for the mechanism of these salt dome earthquakes. This work is an outgrowth of our research on the seismicity and tectonics of Soviet Central Asia, where we have operated two telemetered seismic networks since 1975.

Geology

The Soviet republic of Tadjikistan is marked by an active tectonics and a high rate of natural seismicity.

As part of the India-Asia collision, the Jurassic and younger sediments that fill the sedimentary basin of the Tadjik Depression, a relatively low region that forms most of southwest Tadjikistan (Figure 1), have been deformed by folding and thrusting in the zone between the Pamir and Tien Shan ranges. Stratigraphic analysis of Cretaceous and younger sediments [Leith, 1985] suggests that the lithosphere beneath the Tadjik Depression is mechanically depressed adjacent to the Pamir, where sediments thicknesses reach more than 12 km. Throughout the Depression, Jurassic evaporites form the base of the sections exposed along thrust faults at the surface, and the overall structure of the Depression suggests that these basal evaporites form the decollement across which the thrusts are displaced [Leith and Alvarez, 1986]. Basin formation here, in (probably) middle Jurassic time, was followed by the deposition of large thicknesses of evaporites. Since the end of the Jurassic, shallow-water marine sedimentation in the Depression proceeded at a relatively slow rate as the basin subsided following the rifting event [Leith, 1985]. In the Kulyab synclinorium, a trough of thick, gently folded rocks that borders the Pamir range, this was followed by the deposition of more than 8 km of Neogene molasse since about middle Oligocene time. The rapid loading of the Jurassic-Paleogene section has provided the drive for the salt migration.

The Kulyab area, along the western limb of the Kulyab synclinorium, is marked by the outcrop of several large bodies of Jurassic-Lower Cretaceous salt [Luchnikov, 1982]. Several of these are obvious domes (Figure 3), while others mark the traces of mapped thrust faults. Several of the domes have prominent topographic relief. The Khodzhamumin dome, south of Kulyab (see Figures 3, 4) is comparable with the Kuk-e-Namak dome of Iran, rising more than 1500 m above the surrounding plain. There, a central stock feeds an oblate glacial flow (*namakier*) above folded and faulted upper Tertiary strata.

Geophysical studies and exploratory drilling have accompanied the search for oil and gas in the Kulyab area, which has helped both to delineate the distribution of salt at depth [Luchnikov, 1982; Azimov and others, 1982], and has enabled the mapping of a zone of overpressured formations to the west of Kulyab [Kissin, 1971]. A well drilled in the northern dome in Figure 3 ("Sartis") encountered pressures of 1.6 and 1.8 times hydrostatic in Turonian age strata at depths of 2642 and 2695 m, respectively [Kalomazov and Vakhtikov, 1975]. In general, the westernmost (up-structure) fields are overpressured (up to twice hydrostatic) while those to the east are not.

Seismicity

Tadjikistan experiences an average of six earthquakes a day, most of them concentrated along the Gissar-Kokshal seismic zone, 50-100 km north of Kulyab [Leith and Simpson, 1986]. Most of these earthquakes reflect the intense deformation that occurs at the leading edge of the Vakhsh fold-and-thrust belt

Figure 1. Location map: Generalized crustal structure and geology of the northern Tadjik Depression, including the Vakhsh fold-and-thrust belt (cross-ruled). Salt domes are located near Kulyab in the southeastern Tadjik Depression, 20-50 km from the Soviet-Afghan border (along the Pyandzh river, dashed line).

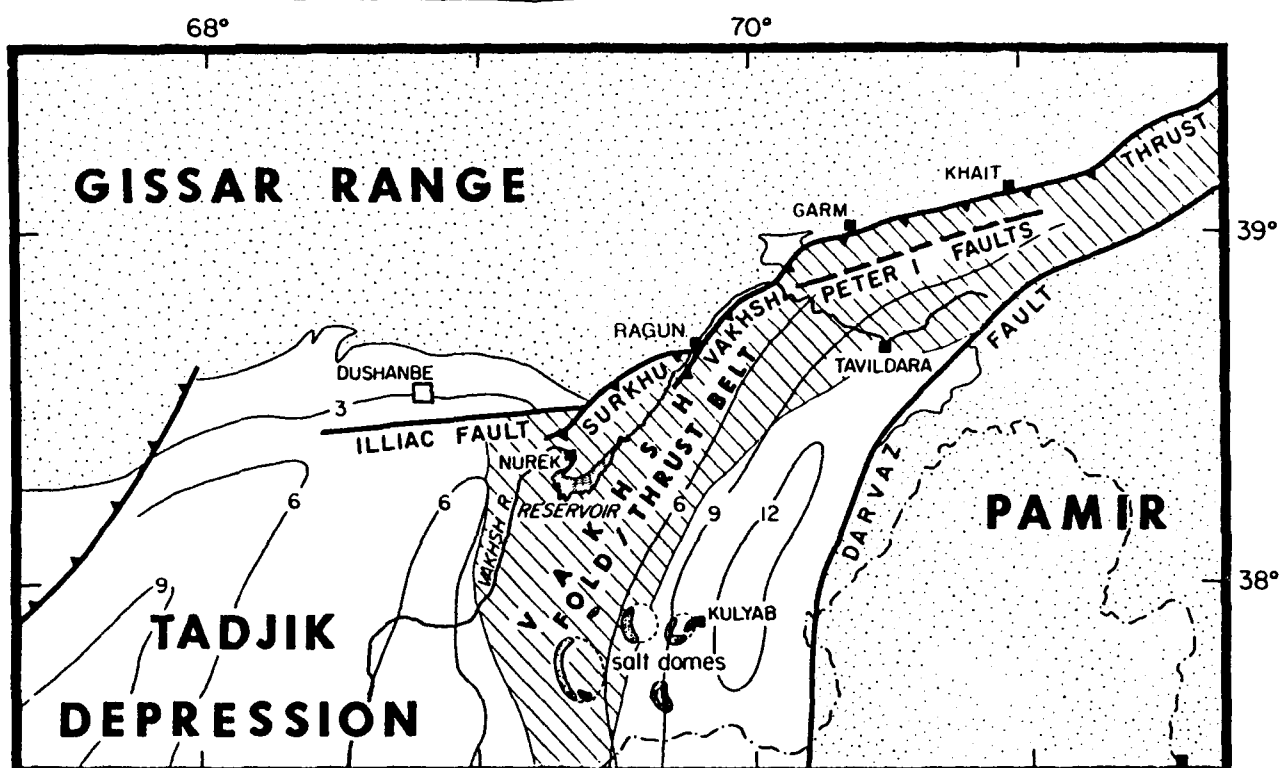
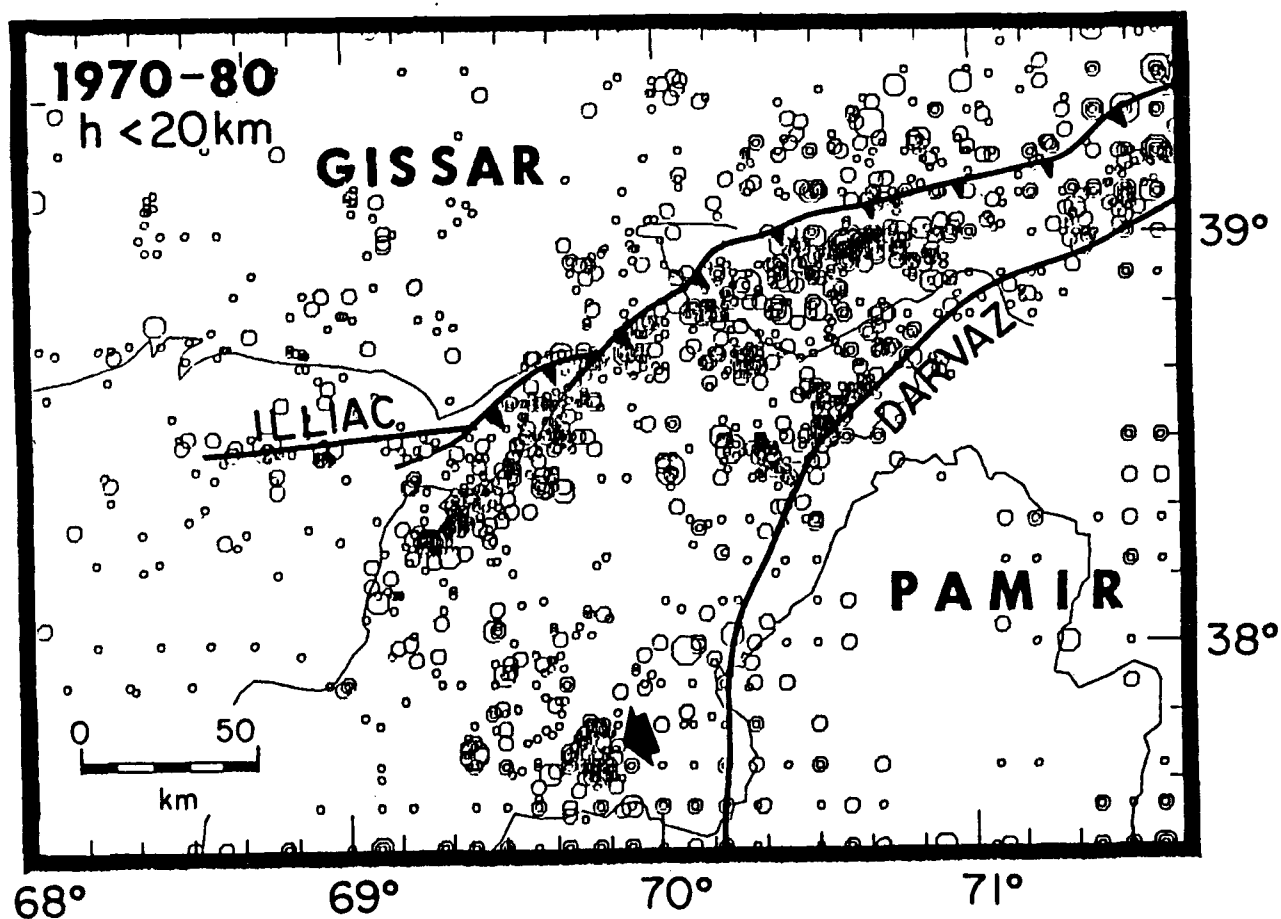


Figure 2. Shallow earthquakes for the area of Figure 1 from 1970-1980. Note that seismicity is most intense to the east and north of Nurek, within the frontal portions of the Vakhsh fold-and-thrust belt. The cluster of seismicity in the lower portion of the figure ($37^{\circ}45'N$, $69^{\circ}45'E$, approximately) occurs near the salt domes mapped in Figure 1, and well away from the front of the fold-and-thrust belt. A detail of this area is shown in Figure 4.



[Figure 2]. In contrast, the seismicity that marks the Kulyab area stands out as a cluster of epicenters distinct from the main trend of the Vakhsh fold-and-thrust belt. They also occur well back from the deformation front, in a area that is relatively aseismic elsewhere along strike.

Epicenters of earthquakes in the Kulyab area from 1964-1980, from the yearly catalogs, *Zemletracenniye v SSSR* (hereafter, 'ZSSSR catalogs'), are shown in Figure 4, along with shaded digital topography. There are 352 earthquakes listed, all with magnitudes greater than about 2.5. All earthquakes in this area are shallow (< 20 km), and there is a clear association of some events with the mapped salt domes. The large cluster of activity in the lower right corner of the figure occurred following the $M=5$ earthquake on 02 April 1973 (hereafter, "1973 earthquake"). This sequence is associated with a diapir at depth, discussed below.

For the region of Figure 4, the b -value is approximately 1.1-1.2. This is comparable to the induced seismicity at Nurek reservoir [Simpson and Negmatullaev, 1981]; that is, with the high proportion of smaller earthquakes in comparison with regions outside of the reservoir area. Higher b -values are typical of induced seismic activity [Gupta and Rastogi, 1976], wherein induced events are triggered by effective stress changes resulting from changes in the subsurface pore pressure regime. We suggest that the high b -value we have determined may be "normal" for this area, because of the existence of the naturally high formation pressures noted above. The high b -values may thus be a fluid pressure effect that distinguishes this region from other areas in Tadzhikistan.

The Kulyab area has produced several earthquakes of magnitude ~ 5 in this century [Gubin, 1960], including large shocks in 1937, 1952, 1959, 1972, 1973 and 1978. The April 2nd, 1973 earthquake ($M=5.3$) is the largest and perhaps the best studied to date: it was documented and studied by Kon'kov [1974], who combined data from the Kulyab seismic station with macroseismic data to relocate the epicenter of the main shock. The relocated event lies ~ 20 km NNW of the epicenter reported in ZSSSR, at a depth of ~ 12 km, at the northern edge of the buried Sari-Chashma diapir, 10 km SE of Kulyab. Assuming that all ZSSSR epicenters from April 1973 have an equal horizontal mislocation, the sequence is replotted with geologic and geographic data in Figure 5.

The sequence apparently occurred along the northern margin of the Sari-Chashma diapir, at depths from 0 to 10 km. The main event (April 2, 00h02m43s) was included in a spectral study of Central Asian earthquakes by Zapol'skiy and Loginova [1984] which suggests that this event produced lower frequency seismic waves than other earthquakes of comparable size. We have recorded low frequency microearthquakes at Nurek which may be associated with salt deposits, but more work needs to be done to determine the cause of the anomaly. For the April 1973 earthquake and its aftershocks, the b -value was ~ 0.8 , considerably lower than the regional value.

Figure 3. Landsat image of the southeastern Tadjik Depression (the grid lines are approximately 10 km apart). The two surface salt domes are conspicuous features of the geology of this area.



Figure 4. Earthquake epicenters from the Soviet Catalogs for the Kulyab region, mapped on shaded digital topography from the Defense Mapping Agency. There is a close spatial correlation between some groups of earthquakes and the mapped salt domes. The cluster of earthquakes in the lower right are associated with a buried salt diapir (see Figure 5).

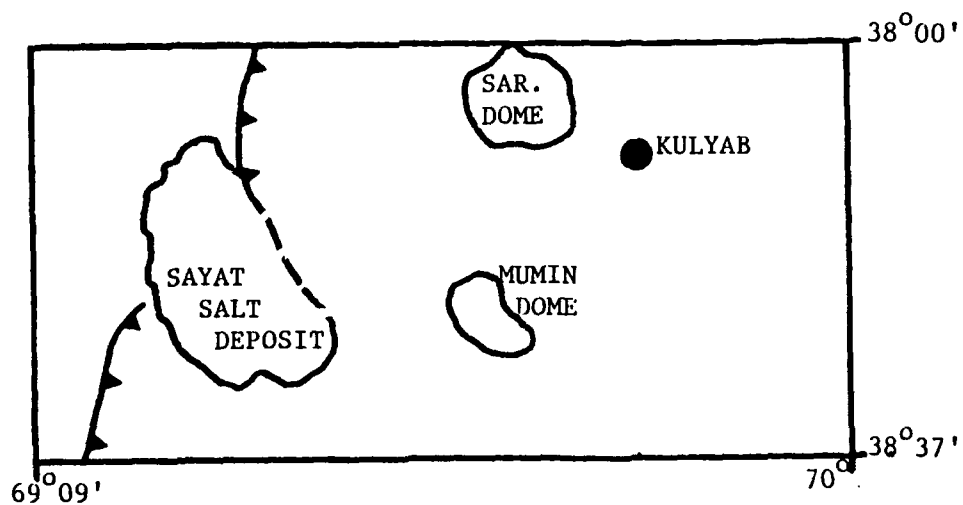
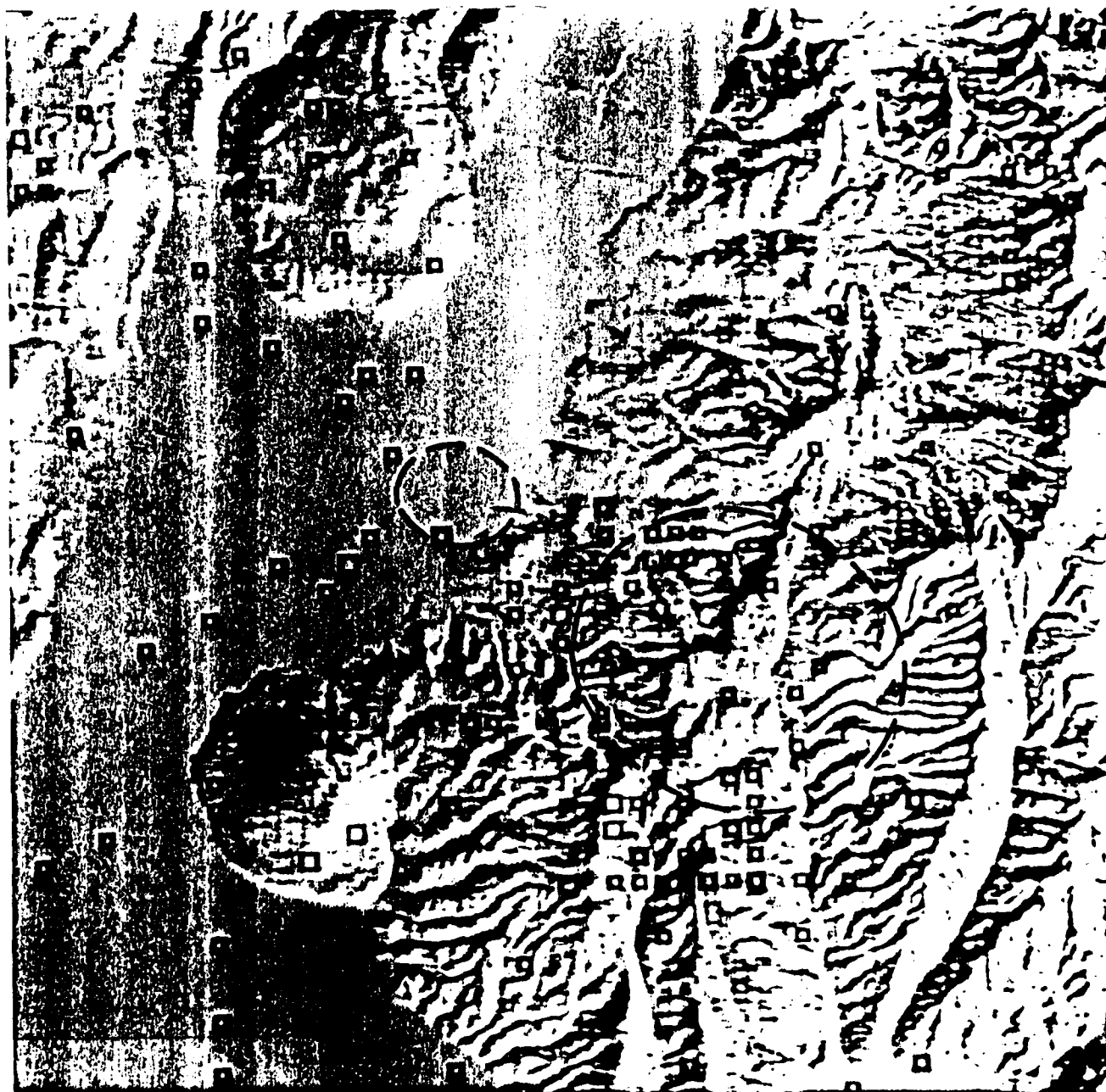


Figure 5. Detail of the Kulyab area. Digital topography and epicenters from the April 1973 earthquake and its aftershocks. The locations of mapped subsurface diapirs are from Kon'kov [1974].



Discussion

Unfortunately, data on the deep structure of the diapir or surface strains in the local area are unavailable. Thus, we are not currently able to determine the amount or character of the deformation that is associated with the Sari-Chashina diapir. Nevertheless, because of the very active nature of the tectonics of Tadjikistan, it is appropriate to compare the dynamics of the Kulyab salt domes with the domes in the active area of southern Iran, where some detailed studies of salt dynamics have been made. From these accounts [Talbot and Jarvis, 1984; and references cited earlier], it seems that *active* salt diapirism can be associated with very high rates of deformation. The highest natural rate of salt extrusion is from the Kuh-e-Namak intrusion in Iran [Ala, 1974], which rises at 170 mm/yr. The Mumin dome (see Fig. 4) is of the same scale as the Kuh-e-Namak, being more than 2.5 km thick and rising more than 1500 m above the adjacent alluvial plain. We therefore suspect that the diapirs near Kulyab reflect the same high degree of activity as the Iranian intrusions.

Depths and focal mechanisms of earthquakes in the Kulyab area are not well constrained. Elsewhere in the Tadjik Depression, the seismicity is largely confined to the sedimentary section above the salt-layer decollement [Leith and Simpson, 1986]. Thus, we suspect that the 1974 earthquake sequence reflects fracturing of the country rock above or adjacent to the diapir. This may account for the relatively higher b-value calculated for this sequence.

Our studies in this active tectonic area provide a sharp contrast to studies of the seismicity of salt dome areas in the U.S. More work needs to be done to answer the critical question of the mechanics of the deformation.

Acknowledgements. We thank J. Lewkowicz and DARPA for providing the Digital Terrain data for this region and J. Rachlin for providing numerous useful references. This work was supported by DARPA/AFGL under contract F19628-85-K-0022 and by USGS contract G14080001-1168.

References

- Ala, M. H., 1978, Salt diapirism in southern Iran, *Am. Assoc. Petrol. Geol. Bull.*, v. 58, p. 1758-1770.
- Azimov, P. K., Ye. V. Lebzi and Yu. M. Ovchinnikov, 1982, Deep structure and problems of completion of the sub-salt sediments of southwest Tadjikistan, *Neftegazovaya Geol. i Geofiz.*, n. 3, p. 23-27.
- Baar, C. A., 1977, *Applied Salt Rock Mechanics 1: The in situ Behavior of Salt Rocks*, Elsevier, Amsterdam, 294 pp.
- Braunstein, J. and G. D. O'Brien, eds., *Diapirs and Diapirism*, Am. Assoc. Petrol. Geol., Tulsa, 420 pp.
- Carter, N. L. and F. D. Hansen, 1983, Creep of rocksalt, *Tectonophysics*, v. 92, p. 275-333.
- Cohen, B. L., 1977, The disposal of radioactive wastes from fission reactors, *Science*, v. 263, p. 21.

Simpson and Leith: Salt Dome Earthquakes

- Dorman, J., G. V. Worzel, J. L. Warzel and D. Dumas, 1975, Geophysical investigations of salt at the University of Texas geophysics laboratory, *Geotech Tech. Rept.*, p. 333-342.
 - Gubin, I. Ye., 1960, *Patterns of Seismic Activity in Tadzhikistan*, Acad. Sci. Tadzhikistan, Dushanbe, 450 pp.
 - Gupta, H. K. and B. K. Rastogi, 1976, *Dams and Earthquakes*, Elsevier, Amsterdam, 229p.
 - Hannon, W. J., 1985, Seismic verification of a comprehensive test ban, *Science*, v. 227, p. 251.
 - Jackson, M. P. A. and C. J. Talbot, 1986, External shapes, strain rates and dynamics of salt structures, *Bull. Geol. Soc. Am.*, v. 97, p. 305-323.
 - Kalomazov, R. U. and M. A. Vakhtikov, 1975, Appearance and Nature of anomalously high formation pressures in the Kulyab megasyncline of the Tadzhik Depression, *Neftegazovaya Geologiya i Geofizika*, n. 10, p. 3-6.
 - Kent, P. E., 1966, Temperature conditions of salt dome intrusions, *Nature*, v. 211, p. 1387.
 - Kent, P. E., 1979, The emergent salt plugs of southern Iran, *J. Petrol. Geol.*, v. 2, p. 117-144.
 - Kon'kov, A. A., 1976, The Kulyab earthquake of 2 April, 1973, p. ___-___ in *Zemletryacennii v SSSR v 1973 Godu*, I.V. Gorbunova and others, eds., Nauka, Moscow.
 - Leith, W., 1985, A Mid-Mesozoic extension across Central Asia?, *Nature*, v. 313, p. 567-570.
 - Leith, W. and W. Alvarez, 1986, Structure of the Vakhsh fold-and-thrust belt, Tadzhik SSR (Reply), *Bull. Geol. Soc. Am.* (in press).
 - Leith, W. and D. W. Simpson, 1986, Seismic domains within the Gissar Kokshal seismic zone, Soviet central Asia, *J. Geophys. Res.*, v. 91, p. 689-699.
 - Lerche, I., ed., 1986, Review of Salt Domes and Salt Tectonics, in press.
 - Luchinkov, V. S., 1982, Upper Jurassic halogen deposits of southeast Central Asia, *Trudy Inst. Geol. i Geofiz.*, n. 535, p. 19-33.
 - Racine, D. and P. Klouda, 1979, Seismicity of the salt areas of Texas, Louisiana, Oklahoma and Kansas, *Tech. Report AL-79-3*, Teledyne Geotech, Alexandria, 27 pp.
 - Sadikov, T. S., 1982, Halogenic formation of southwest Tadzhikistan, in *Structure and Condition of Formation of Salt Formations*, A. L. Yanshin, ed., Nauka, Novosibirsk, 1981.
 - Simpson, D. W. and S. K. Negmatullaev, 1981, Induced seismicity at Nurek reservoir, Tadzhikistan, USSR, *Bull. Seis. Soc. Am.*, v. 71, p. 1561-1586.
 - Talbot, C. J. and R. J. Jarvis, 1984, Age, budget and dynamics of an active salt extrusion in Iran, *J. Struct. Geol.*, v. 6, p. 521-533.
 - Zapol'skiy, K. K., and G. M. Loginova, 1984, Features of strong, shallow-focused earthquakes in Tadzhikistan, *Izvestiya Fiz. Zem.*, v. 20, n. 4 (trans. AGU).
- Zemletryacenniiye v SSSR, 1964-1980*, Nauka, Moscow.

**FOCAL DEPTHS OF SHALLOW LOCAL EARTHQUAKES
FROM COMPARISON OF POLARIZATION FILTERED DATA WITH SYNTHETICS**

N.L. Barstow, J.A. Carter, and A. Suteau-Henson*
Rondout Associates, Inc.
Stone Ridge, New York 12484

* Now at Science Applications International Corp.

INTRODUCTION

The research reported here concerns an effort to refine our ability to discriminate between local and/or regional nuclear explosions and earthquakes based on the depth of an event. If the depths of seismic events can be determined accurately, many events can be eliminated as potential nuclear explosions based on the practical limit of nuclear explosion burial depth. This discriminant has been used for many years at teleseismic distances.

Our approach to this problem has been to improve phase identification and picking abilities of depth phases pP and sP through filtering and three-component polarization methods and to compare the waveform data to synthetic seismograms. The synthetic seismograms are computed using the locked mode method (Harvey, 1981). Frequencies from zero to 5 Hz are computed. For a given source we are calculating a suite of source depths in an attempt to match depth phase arrivals to those in the pre-processed data.

The success of determining focal depth using depth phases and comparing them to synthetics depends largely on:

1. good approximations of crustal velocity structure
2. recovery and correct identification of the phases in the data.

ANALYSIS OF JANUARY 19, 1982 NEW HAMPSHIRE EARTHQUAKE

In this report we discuss one earthquake to illustrate the sensitivity of synthetic seismograms to different input velocity models and focal mechanisms as well as to illustrate our approach to identifying depth phases. The earthquake chosen is the Gaza, N.H., magnitude 4.5 event of January 19, 1982. Since the source is in the Appalachian Province and the receiver (RSNY) is in the Grenville Province we calculated separate synthetics using the two velocity models (Figure 1) to test which is more appropriate.

Figure 1 shows radial and vertical components for the initial 15 seconds of the synthetic seismograms calculated for two velocity models. RSNY is the theoretical receiver, a distance of 267 km and an azimuth of 295° from the New Hampshire source. The velocity models and Moho reflections are shown schematically for comparison. The focal mechanism is given by: strike = 280° , dip = 75° and rake = -11° . The input focal depths are comparable.

As expected, the prominent phases and their arrival times are different for the two different velocity models. The Pn phase is nodal for the radiation pattern, despite small differences in take-off angles for the two models. It is simply indicated at the appropriate arrival time. For the New England model, PmP is small relative to sPmP. They both arrive before the intra-crustal reflections PiP and sPiP. For depths greater than 10 km, however, PiP arrives before sPmP (see figure 4). PiP and sPiP are sharp arrivals because of the large velocity contrast at 15 km in the crustal model. Vp increases from 6.1 km/sec to 7.0 km/sec at this boundary.

For the Grenville model, Pg preceeds the Moho reflections (for a source depth of 7 km). The amplitude of sPmP relative to PmP is smaller for the Grenville model than for the New England model because the

upgoing sPmP is crossing a fairly sharp internal discontinuity near the source while the downgoing PmP only crosses this boundary once, near the receiver. In the case of New England structure, the sharp discontinuity is below the source, instead of above it. In addition, PmP is close to a nodal plane and small differences in take-off angle, resulting from differences in the velocity structures, may be contributing to the difference in the amplitudes of PmP.

Even though the two velocity models produce strikingly different synthetic seismograms, it is important to note that, in this example, the time between the arrivals of the downgoing and upgoing Moho reflections is the same. Thus, if one can independently identify these two phases in the actual data, a match (ignoring absolute travel times) to the Grenville synthetic would suggest a depth of 7 km and a match to the New England synthetic would suggest a depth of 6 km. Here, there would be only a small effect of velocity model on depth determination. If, however, one uses the computed phase travel times to help identify depth phases in the real data, the variation in travel time with velocity model could lead to misinterpretations of the real data.

Figure 2 shows 15 seconds of synthetics calculated for 2 different focal mechanisms. The mechanism shown at the bottom was determined from P-wave first motion data, mainly from the Northeast United States Seismic Network (Pulli et al., 1983). The mechanism at the top of the figure differs mainly in the quadrants of dilatation and compression. The azimuth to station RSNY is very close to a nodal plane in both instances, so there is not a great difference in radiation pattern. Thus, the same initial phases appear on both sets of seismograms, but the amplitudes of these phases are different. If theoretical radiation patterns can be used to predict actual phases in the data, then it will be helpful to have independently determined fault plane solutions.

Comparison of Data to Synthetics

It would be very difficult to compare the raw data recorded at RSNY to the synthetic seismogram. With polarization filtering, however, we have been able to recover polarized phases (see Figure 3) that were obscured by the p-coda of the unfiltered seismograms. After polarization filtering, we low-pass filter the data to remove frequencies greater than 5 Hz, which are not modeled by the synthetics.

Figure 4 shows comparisons of the vertical-component RSNY processed data to the vertical-component synthetic depth section calculated for the New England model. Twenty seconds are shown. We began by positioning the data at a depth of about 9 km (Figure 4A). There are several arrivals in the data that match predicted arrivals. These are, in order, PmP, sPmP, the dual arrivals PiP and Pg, and finally an upgoing phase arriving toward the end of this time window. Clearly, the match is not perfect. Signal arrives in the data later than the appropriate time for sPiP, and, subsequently until the late phase (in the data, about 14 seconds after the initial P), there is not a good correlation between data and synthetics. A comparison of travel times for the first arriving phase in the data and synthetics suggests that they may not be the same phase. The travel time of synthetic PmP at a source depth of 9 km (with the given input velocity model) is 40.40 seconds, whereas the travel time of the first phase in the data is 38.59 seconds. Allowing for uncertainties in the actual origin time of the earthquake and for uncertainties in crustal structure, they could be the same phase. If, however, we assume that the origin time and velocity model are appropriate, we can match several early p-phases by aligning the data at a depth of approximately 4 1/2 km as illustrated in Figure 4B. Since the real-data travel time is more appropriate for Pn, the first arrival is now aligned with the predicted Pn arrival time. For this shallower depth, the data match predicted arrival times for Pn, PmP, sPmP and for the late up-going phase. Again, the correlation is not perfect.

It is clear that the interpretations depend on the correct identification of the arrivals in the data. In addition to travel times, the azimuth and apparent angles of incidence can be used to help identify phases. Figure 5A shows the results of an adaptive polarization analysis of the first 20 seconds of the same state-filtered seismograms that we have been comparing to the synthetics. The first three traces in the figure are

the vertical, and the adaptive radial and transverse horizontal components. The direction of maximum signal strength as a function of time represented by the azimuth and apparent angle of incidence, is indicated (with error estimates) below the RZ product trace. The positive values for the product of the radial and vertical components indicate that all the phases are arriving at the receiver as p-waves. Since adaptive polarization analysis of the synthetic seismograms indicated the same thing, we know that the last conversions were to p-waves for both the real and synthetic data.

Interestingly, we noted that the last arrival, which had matched a predicted phase in the synthetics at both the 4.5 and 9 km depth positions, is probably not even modelled by the synthetics. Though highly polarized and hence a prominent phase, it is fourteen degrees off the correct azimuth from the source. Unlike the two other out-of-line azimuths (see Figure 5A), the error estimate does not allow enough uncertainty to put it in line. Furthermore, this late phase is approaching the receiver at a shallower angle than any other arrival (see the apparent angles of incidence), yet the late phase in the synthetic seismograms was approaching the receiver at the steepest angle in the same 20 second time window. A steep, late arrival would be consistent with a multiply-reflected phase.

The phase immediately proceeding the last phase (by almost 1 second) is more consistent with the synthetics because that phase is approaching at a steeper angle. Using that approach, a good match is obtained by inserting the data at a depth of 6 km (Figure 5B). Here, the first arrival is a predicted PmP and there are phases matching the predicted sPmP and the dual arrival of Pg and PiP, as well as the late multiply-reflected phase. In addition, the relative amplitudes match the synthetics fairly well.

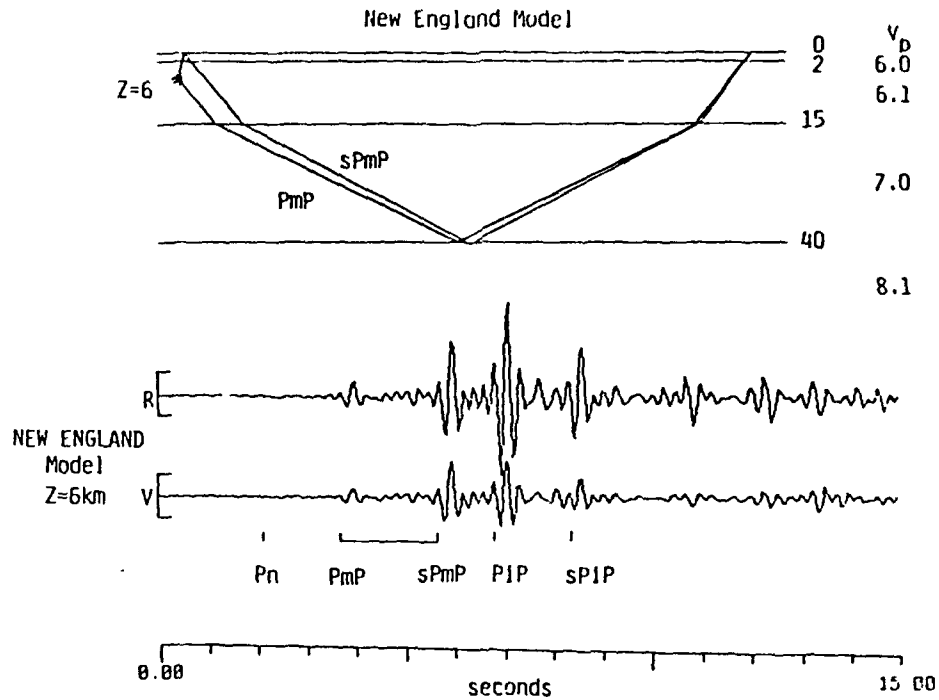
FUTURE WORK

Eight additional events in the northeast U.S. and adjacent Canada have been synthesized and we are currently processing the data to compare with them. The results of this study will enable us to assess the effectiveness of these approaches for depth determination. We will evaluate the recovery and identification of regional phases as well as the theoretical modelling of regional phases.

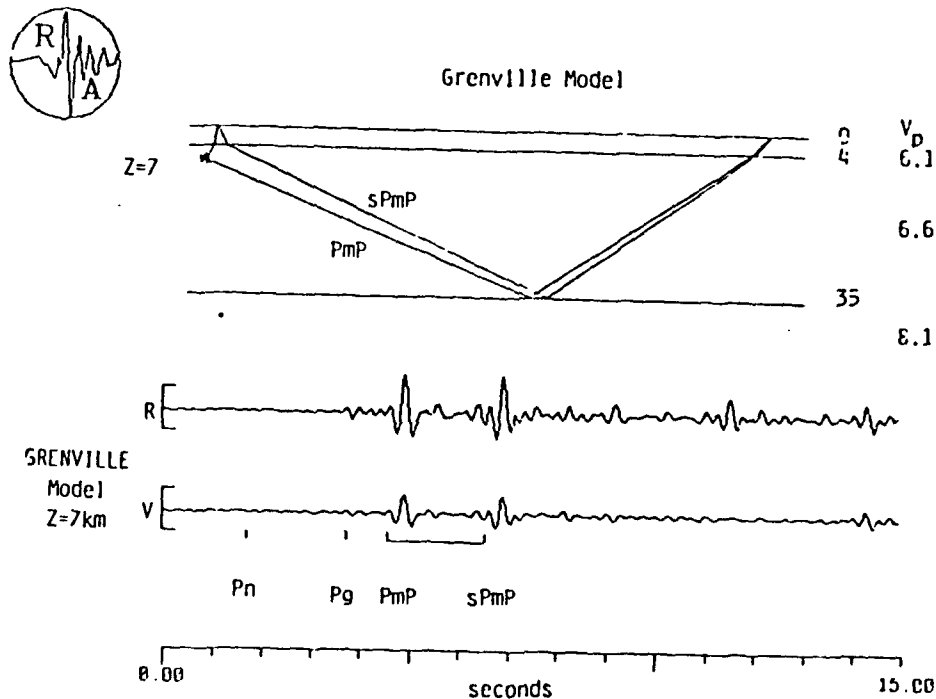
REFERENCES

- Harvey, D., 1981, Seismogram Synthetics Using Normal Mode Superposition: the Locked Mode Approximation Method, *Geophys. J. Roy. Astr. Soc.*, 66, 37-69.
- Pulli, J.J., J.C. Nabelek, J.M. Sauber, 1983, Source Parameters of the January 19, 1982 Gaza, New Hampshire earthquake, *abst. Earthquake Notes* vol. 54, No. 3, p.28-29.

A



B



January 19, 1982, $\Delta = 267$ Km, Azimuth= 295.

Figure 1. Two velocity models and resulting synthetic seismograms.

A= New England Model, source depth= 6 Km. Source-to-receiver Moho, reflections shown schematically. 15 seconds of radial and vertical component synthetics, with phases identified. PiP and sPiP are internal reflections at the 15 Km boundary.

B= Grenville model, source depth= 7 Km. Source-to-receiver Moho reflections shown schematically. 15 seconds of radial and vertical component synthetics with phases identified.

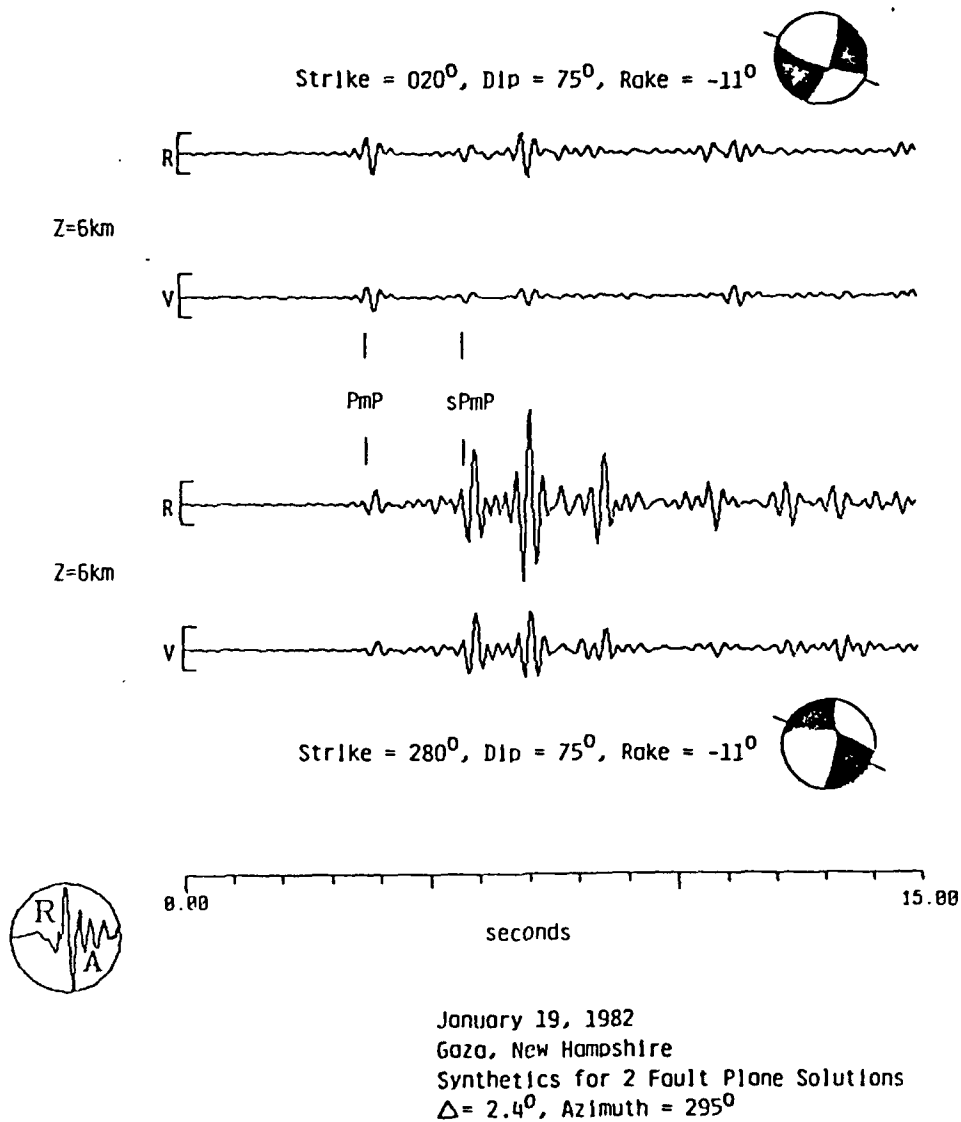


Figure 2. Two fault plane solutions and resulting synthetic seismograms. Fifteen seconds of the radial and vertical components are shown for each of the two different input solutions. The azimuth to RSNY is indicated by a line on the fault plane solution, a lower hemisphere projection with compressional quadrants filled in.

RSNY

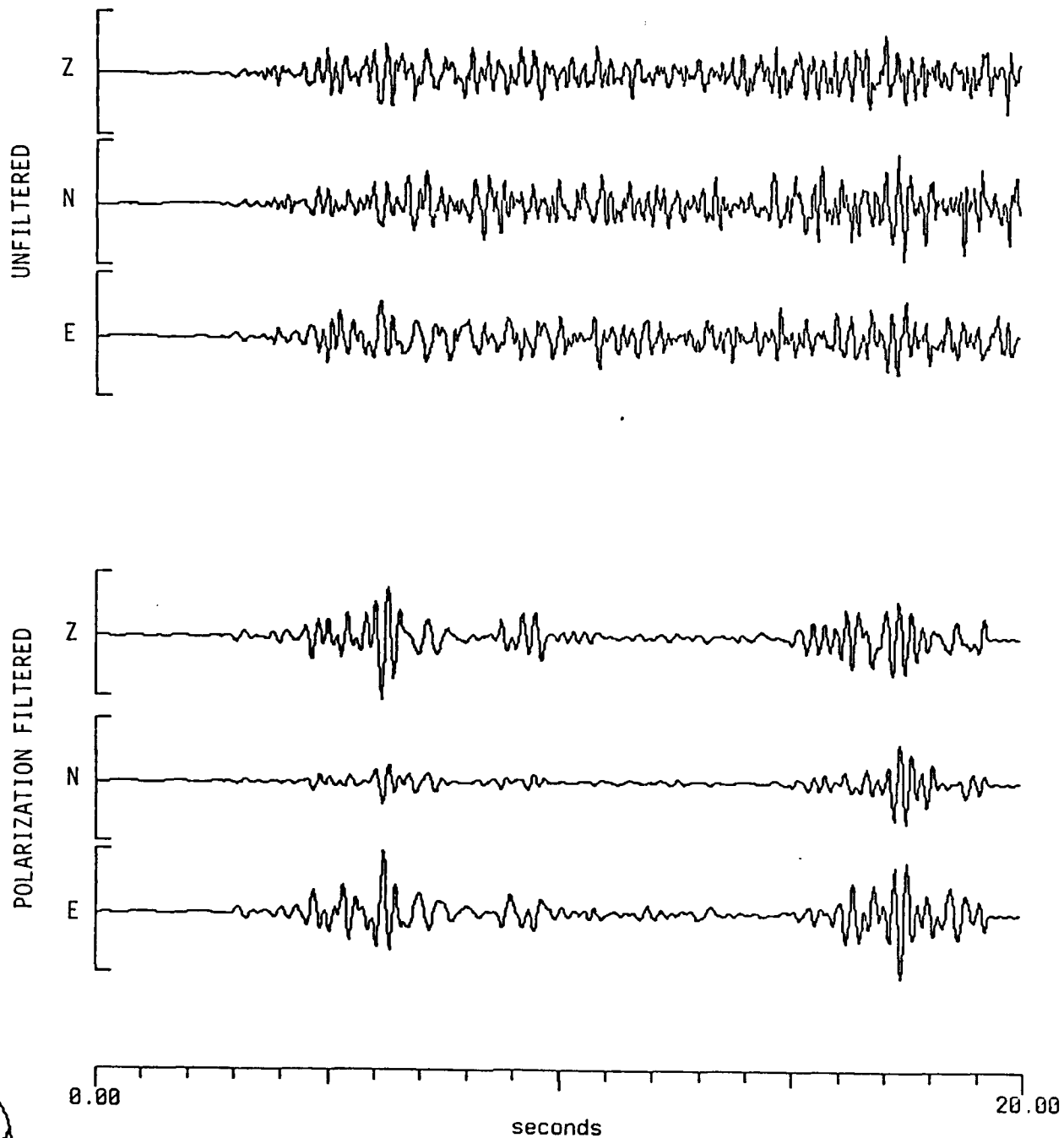


Figure 3. Comparison of unfiltered data (top 3 traces) with polarization filtered data (bottom 3 traces). The seismograms record the January 19, 1982 New Hampshire earthquake at station RSNY in New York. The filtered data pass only rectilinearly polarized frequencies as a function of time.

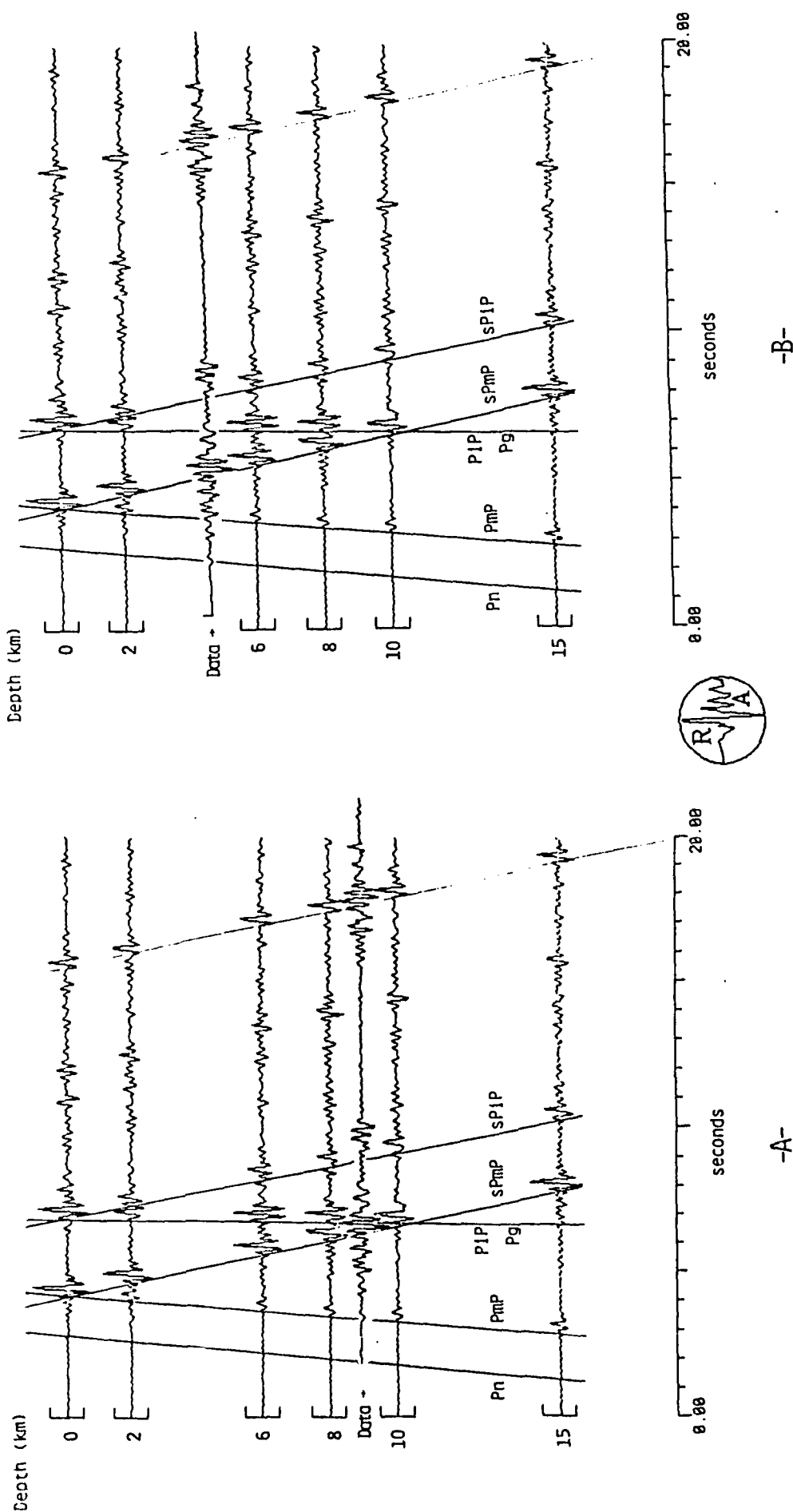
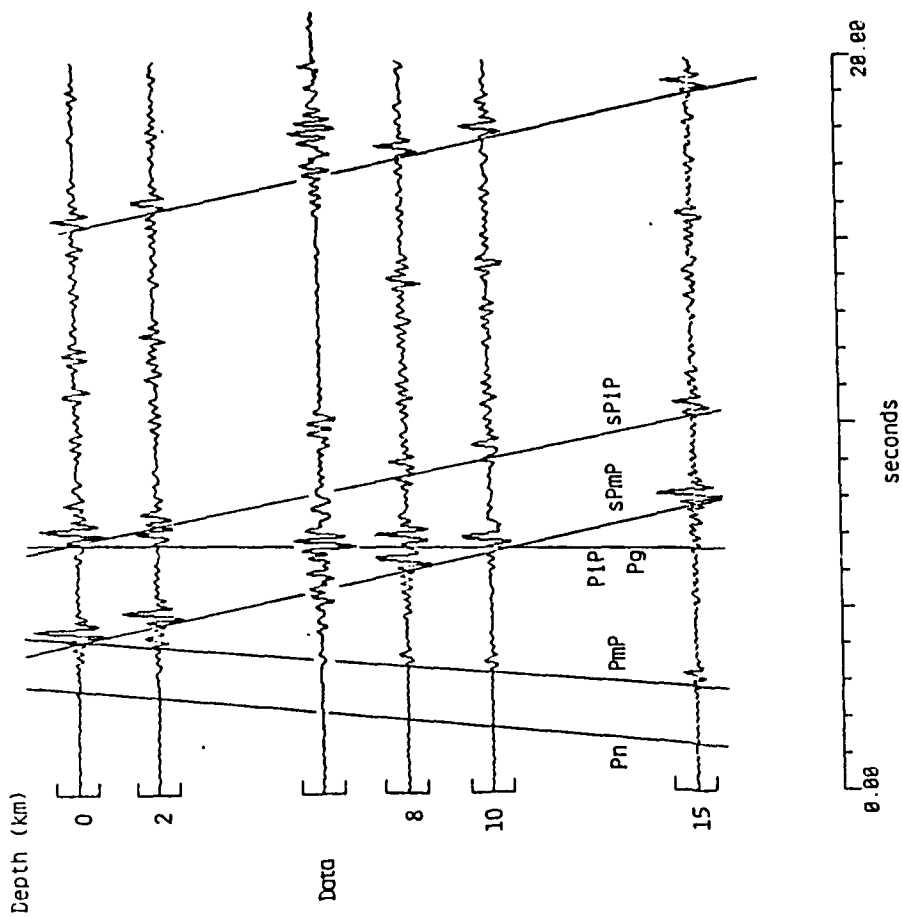


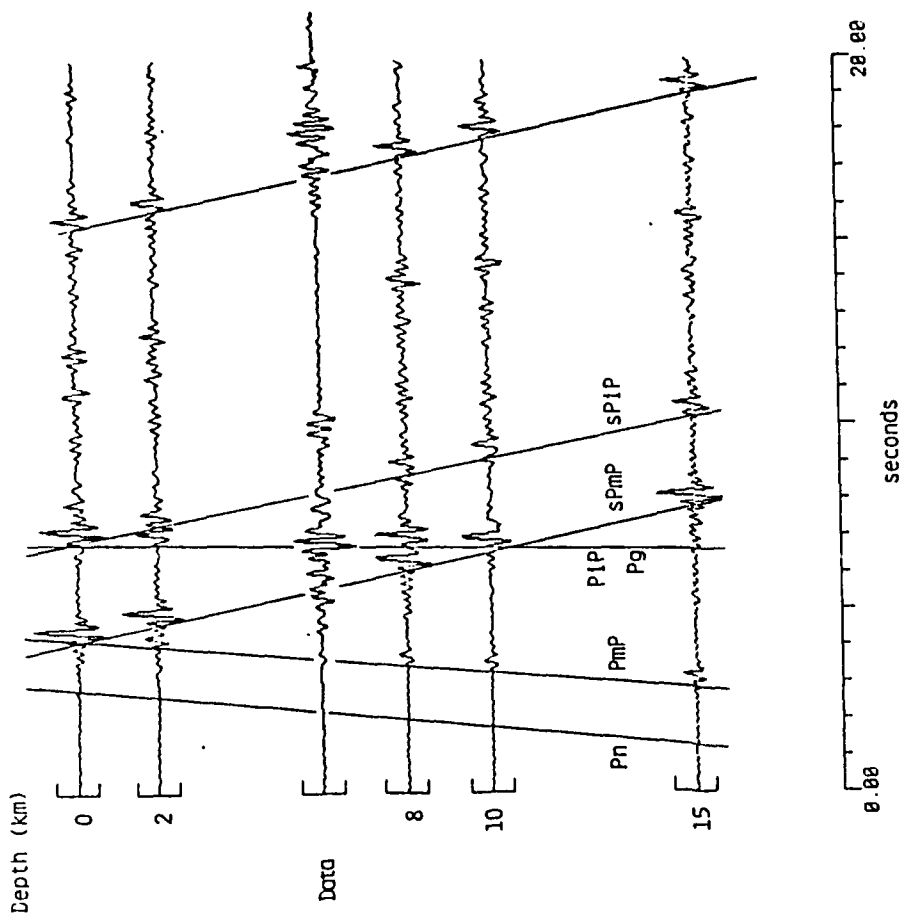
Figure 4. Comparison of synthetic seismograms calculated for a suite of depths with data for the January 19, 1982 earthquake. The synthetics are the same for both A. and B. above, but the position of the data trace in the depth section is at 9 km depth in A. and at 4½ km depth in B. The vertical components of both data and synthetics are shown.



ADAPTIVE POLARIZATION
January 19, 1982
Gaza, New Hampshire

-A-

Figure 5A. Adaptive polarization of state filtered seismogram recorded at RSNY. The values of azimuth and apparent angle of incidence are given with estimated errors.



-B-

Figure 5B. Like Figure 4 except that the real data are plotted at a depth of 6km in the depth section. See text for discussion.

Observations of First-Order Mantle Reverberations

JUSTIN S. REVENAUGH AND THOMAS H. JORDAN

*Department of Earth, Atmospheric and Planetary Science
Massachusetts Institute of Technology, Cambridge, MA 02139*

INTRODUCTION

The reverberative interval of the seismogram, defined as that portion between the surface-wave train propagating along the minor arc and the first body wave arrivals from the major arc, is dominated by core-reflected phases such as ScS_n and other reverberations from internal discontinuities. On a SH -polarized seismogram these reverberations can be conveniently classified by the number of internal mantle reflections they experience; ScS_n and $sScS_n$ phases suffer no such reflections and are therefore termed zeroth-order reverberations, those experiencing one reflection are first-order reverberations, and so forth.

We have observed first-order reverberations--specifically SH -polarized ScS_n and $sScS_n$ phases reflected at near normal incidence from upper mantle discontinuities--on long period, digital seismograms of the HGLP and SRO networks. Such arrivals correspond to a dynamic ray family denoted by $\{ScS_n, Sd^{\pm}S\}$, where n is the multiple of the parent (zeroth-order) phase, ' d^+ ' signifies a reflection from the top of an internal discontinuity at depth d , and ' d^- ' signifies a reflection from the bottom. Each $\{ScS_n, Sd^{\pm}S\}$ arrival is comprised of either n or $n+1$ dynamic analogs, depending on the depths of the source and reflector and on whether the reflection is topside or bottomside. This increasing multiplicity offsets the amplitude decay owing to attenuation and helps maintain the amplitude of the ray family as the ScS reflection number n increases. Figure 1 illustrates the ray paths for the family $\{ScS_n, S400^+S\}$, the topside reflections from the 400-km discontinuity.

In this paper we employ observations of first-order mantle reverberations in frequency band 10-30 mHz to constrain the average shear attenuation of the upper and lower mantle as well as the reflection coefficient of the 650-km discontinuity.

OBSERVATIONS

The data set discussed here comprises SH -polarized seismograms of 11 Tonga events with focal depths ranging from 229 km to 604 km recorded at the HGLP station KIP on the island of Oahu. We have identified both topside and bottomside reflections from the 650-km discontinuity,

$\{ScS_n, S650^\pm S\}$, for $2 \leq n \leq 4$. Similar reflections from the 400-km discontinuity have also been observed, although their signal-to-noise ratios are typically lower. Employing the *PA2* model of western-Pacific upper-mantle structure [Lerner-Lam and Jordan, 1986], we have generated synthetic seismograms of the reverberative interval by both normal-mode summation and geometrical-optics ray theory. Results from the two methods indicate that the geometrical-optics approximation provides an excellent description of reflections from sharp discontinuities at center frequencies on the order of 30 mHz. Synthetics have been used to model the energy in the reverberative interval in the band 5-50 mHz and to match both the phase and amplitude of the zeroth- and first-order reverberations.

Figure 2 compares the reverberative interval observed for the 03 Mar 1974 event ($h = 515$ km, $\Delta = 49.9^\circ$) with the ray-theory synthetic. To facilitate the identification of individual phases, the synthetic has been decomposed into individual families of dynamic analogs. Figure 3 is a similar comparison for a shallower event ($h = 229$ km, $\Delta = 45.4^\circ$). Figure 4 shows observed and theoretical seismograms of the reverberative interval for a suite of focal depths.

Particularly prominent in both the data and synthetics are the topside reflections $\{sScS_n, S650^+ S\}$ and the bottomside reflections $\{ScS_n, S650^- S\}$. The phases $\{ScS_n, S650^+ S\}$ and $\{sScS_n, S650^- S\}$ are obscured by zeroth-order phases except for the shallowest events. On the synthetics the first-order reverberations for the 400-km discontinuity have roughly 40% of the amplitude of the 650-km reflections. On the observed seismograms the amplitude ratios are more variable, but good examples of 400-km reverberations include the $\{sScS_n, S400^+ S\}$, $\{ScS_n, S400^- S\}$ arrivals in Figure 2 and the $\{ScS_n, S400^+ S\}$ and $\{sScS_n, S400^- S\}$ arrivals in Figure 3 for $n = 2, 3$.

RESULTS

A detailed inspection of Figure 4 reveals that the time interval between $\{sScS_n, S400^+ S\}$ and $\{sScS_n, S650^+ S\}$ on the observed seismograms is less than that predicted by model *PA2*. Using waveform cross-correlation to measure travel time residuals of first-order reverberations relative to the zeroth-order phase, denoted by ΔT_{400} and ΔT_{650} respectively, we find a differential transition-zone residual $\Delta T_{TZ} = \Delta T_{650} - \Delta T_{400}$ of -11.0 ± 2.0 s for 9 phase pairs. Visually, $\{sScS_n, S400^+ S\}$ appears to arrive at the time predicted by *PA2*, and this observation is corroborated by small values obtained for ΔT_{400} . Evidently, the vertical shear-wave travel time from the surface to the 400-km discontinuity predicted by *PA2* is approximately correct, but either *PA2*'s average transition-zone shear velocity is too slow and/or the discontinuity at the base of the

transition zone, which is located at 670 km in *PA2*, is too deep. Positive residuals observed for the differential travel time of $\{ScS_n, S650^-S\} - ScS_n$ are consistent with the latter hypothesis. Raising the discontinuity by 20 km would bring the theoretical times in line with the data, so that the 650-km depth used to identify this discontinuity is more correct.

We have applied the phase-equalization and stacking algorithm of *Jordan and Sipkin* [1977], modified to account for reflection from discontinuities, to 20 $\{sScS_n, S650^+S\}$ and $sScS_n$ phase pairs. Members of the $\{sScS_n, S650^+S\}$ family have propagation paths very similar to $sScS_n$ with the exception of an additional 'pegleg' path element in the upper mantle. Attributing all the differential attenuation to the upper mantle and using *PA2* to calculate all propagation corrections, our best estimate of Q_{UM} , defined by the depth integral

$$Q_{UM}^{-1} = \frac{2}{T_{UM}} \int_0^{650} v_s^{-1}(z) Q_\mu^{-1}(z) dz,$$

is 94 ± 20 over the frequency band 10-30 mHz. This result is consistent with *Nakanishi's* [1980] estimate of 70 for the Sea of Japan above 552 km depth, derived from $sScS_n/ScS_n$ spectral ratios, and with *Sipkin and Jordan's* [1980, Table 4] Oceanic Model B, which has $Q_{UM} = 84$. By a similar procedure, we obtained an estimate of average lower mantle Q_{LM} of 190 ± 60 from 18 $\{ScS_n, S650^-S\}$ and ScS_n phase pairs, which when combined with the Q_{UM} estimate, predicts a whole-mantle Q_{ScS} of 145 ± 35 . The whole-mantle Q measured in this indirect way is in agreement with a value of $Q_{ScS} = 150 \pm 10$ computed by phase-equalizing and stacking ScS_n phases. *Sipkin and Jordan* [1980] found $Q_{ScS} = 155 \pm 11$ for the same source-receiver geometry.

There is, however, a strong dependence of our values of Q_{UM} and Q_{LM} on the reflection coefficient R_{650} assumed for the 650-km discontinuity. After linearizing the relation between Q and R_{650} about a single frequency, we inverted for perturbations to *Sipkin and Jordan's* [1980] Oceanic B Q structure and R_{650} calculated from *PA2*. At 20 mHz this resulted in values of $Q_{UM} = 115 \pm 31$, $Q_{LM} = 175 \pm 30$ and $R_{650} = -0.084 \pm 0.003$ (normalized to a constant angle of incidence of 10°).

The low Q_{LM} estimate obtained in this experiment corroborates *Sipkin and Jordan's* [1979, 1980] hypothesis that the attenuation structure of the lower mantle is frequency dependent at very low frequencies. Recent free-oscillation solutions give lower-mantle Q_μ values of 350 (model QMU of *Sailor and Dziewonski* [1980]) and 360 (model SL8 of *Anderson and Hart* [1978]) in the mode band 3-10 mHz. These are significantly greater than our estimate of 175 ± 30 , suggesting Q_μ decreases with frequency in the lower mantle between 10 and 30 mHz.

We note that our estimate of the reflection coefficient R_{650} is relatively insensitive to errors in the Q estimates, which allows us to measure R_{650} very stably. The result, $R_{650} = -0.084 \pm 0.003$ is in consistent with velocity models derived from both body waves and normal modes; e.g., $R_{650} = -0.081$ (model ATL of *Grand and Helmberger* [1984]) and -0.078 (model PREM of *Dziewonski and Anderson* [1981]).

DISCUSSION

In this brief report, we have documented (evidently for the first time) that first-order mantle reverberations can be observed as discrete phases on the seismogram. Moreover, we have demonstrated that these reflected phases can be used to estimate the average properties of the major mantle layers over relatively short path lengths. The agreement obtained between data and ray-theory seismograms implies that the most of the low-frequency energy arriving within the reverberative interval can be parameterized by eight quantities; namely, the travel times and average Q 's for the upper mantle, transition zone and lower mantle, and the reflection coefficients of the 400-km and 650-km discontinuities. Further refinement of the methodology, specifically the use of full waveform inversion, should allow the estimation of these eight parameters from a single seismogram. It may then be possible to recover from large sets of seismograms the lateral variations in these eight quantities by tomographic techniques.

REFERENCES

- Anderson, D. L. and R. S. Hart, Attenuation models of the earth, *Phys. Earth Planet. Inter.*, **16**, 289-306, 1978.
- Dziewonski, A. M. and D. L. Anderson, Preliminary reference earth model, *Phys. Earth Planet. Inter.*, **25**, 297-356, 1981.
- Grand, S. P. and D. V. Helmberger, Upper mantle shear structure beneath the northwest Atlantic ocean, *J. Geophys. Res.*, **89**, 11465-11475, 1984.
- Jordan, T. H. and S. A. Sipkin, Estimation of the attenuation operator for multiple ScS waves, *Geophys. Res. Lett.*, **4**, 167-170, 1977.
- Lerner-Lam, A. L. and T. H. Jordan, How thick are the continents?, *J. Geophys. Res.*, submitted, 1986.
- Nakanishi, I., Attenuation of shear waves in the upper mantle beneath the Sea of Japan, *J. Phys. Earth*, **28**, 261-272, 1980.

Sailor, R. V. and A. M. Dzieworski, Measurements and interpretation of normal mode attenuation, *Geophys. J. R. astr. Soc.*, **53**, 559-581, 1978.

Sipkin, S. A. and T. H. Jordan, Frequency dependence of Q_{scs} , *Bull. Seism. Soc. Am.*, **69**, 1055-1079, 1979.

Sipkin, S. A. and T. H. Jordan, Regional variation of Q_{scs} , *Bull. Seism. Soc. Am.*, **70**, 1071-1102, 1980.

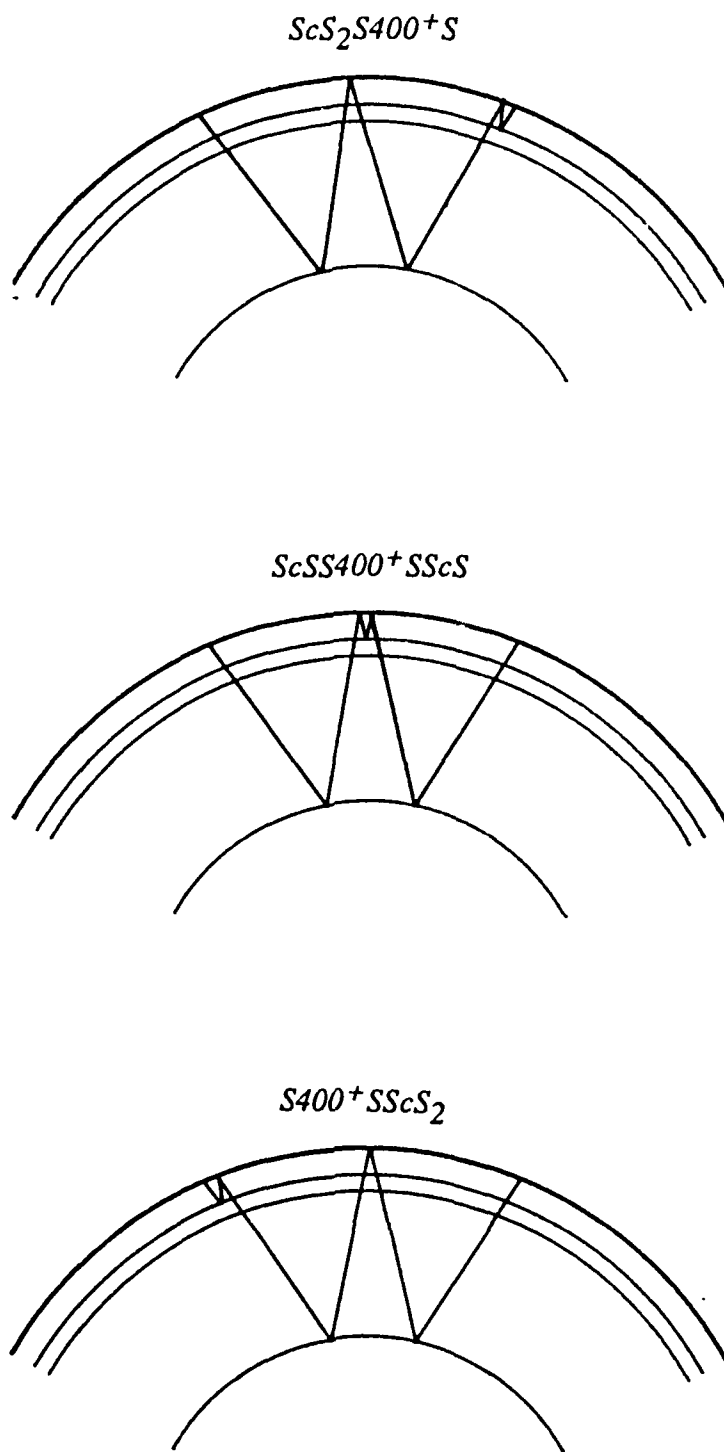


Figure 1. Ray paths for the three members of the family $\{ScS_2, S400^+S\}$, the first-order reverberation from the topside of the 400-km discontinuity, for a surface-focus source. The three phases shown here are dynamic analogs; i.e., they have the same travel time, amplitude and phase at the receiver and thus constructively interfere to produce an observable arrival. The phase $S400^+SScS_2$ would not exist for a source below the 400-km discontinuity, reducing the multiplicity of the family to two.

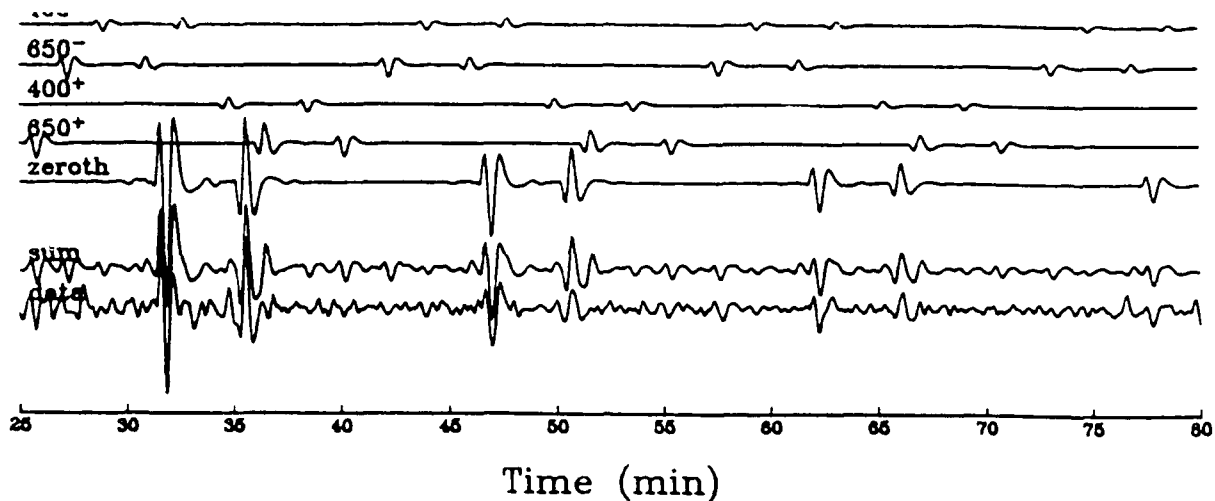


Figure 2. Portion of *SH*-polarized data (bottom) and ray-theoretical (above) seismograms showing the reverberative interval for an event with focal depth $h = 515$ km. The first major arrivals are ScS_2 and $sScS_2$. The notation of any first-order reverberation can be deduced by appending the specific reflection (e.g., $S650^+S$) to the appropriate zeroth-order phase. Note the slow decay with increasing multiple number n of the first-order reverberations.

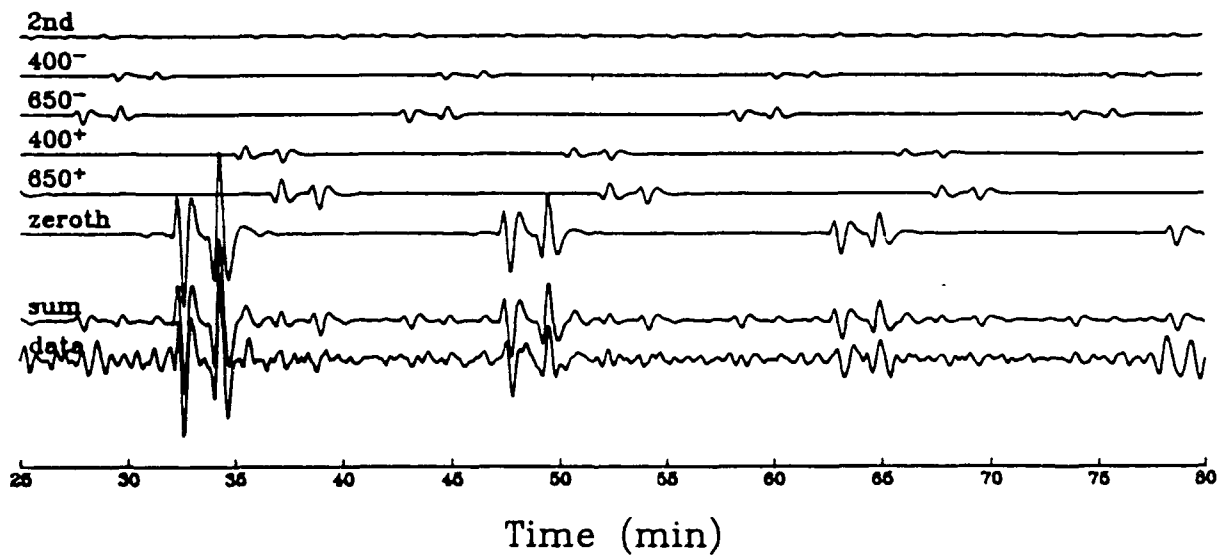


Figure 3. Portion of *SH*-polarized data (bottom) and ray-theoretical (above) seismograms showing the reverberative interval for an event with focal depth $h = 229$ km.

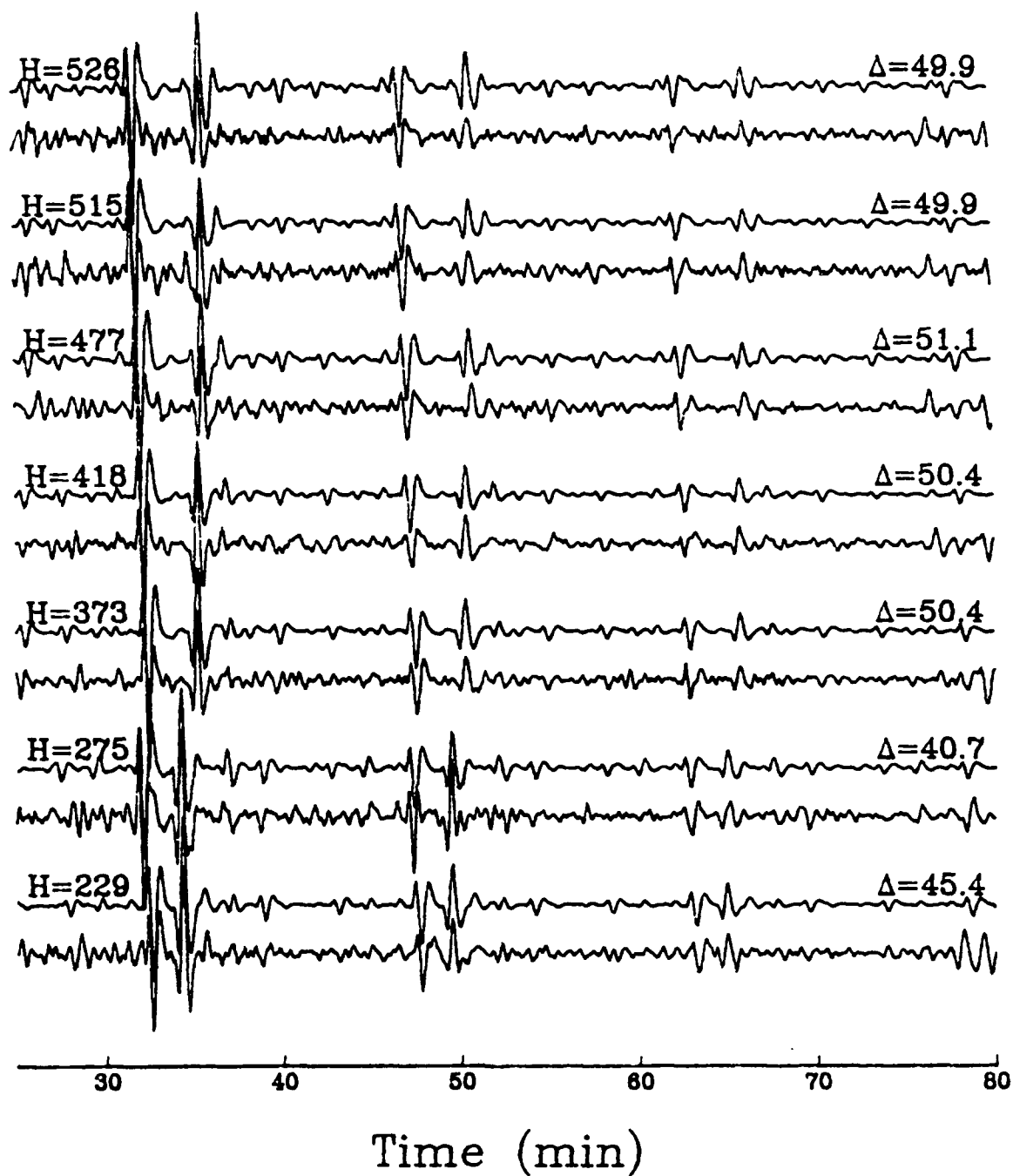


Figure 4. Seismograms of the reverberative interval from seven earthquakes in the Tonga seismic zone recorded on the HGLP instruments at station KIP. The top trace for each event is a synthetic, the bottom trace is data.

YIELD ESTIMATES FROM VERTICAL- AND TRANSVERSE-COMPONENT L_g SPECTRA AND
POLARIZATION FILTERING TO ENHANCE REGIONAL PHASES*

Shelton S. Alexander
The Pennsylvania State University

ABSTRACT

Transverse component L_g appears to give equally good or better spectral estimates of yield than vertical-component L_g for both Semipalatinsk and NTS. For relatively long propagation paths ($>20^\circ$) from Semipalatinsk to Europe and Iran the frequency band from .6-1.2 Hz appears to give the best estimates of source strength. Path attenuation is accounted for by using Q estimates derived from average spectral slopes for a suite of events of different magnitude in the source area. Yield estimates are made by comparing attenuation-corrected source spectra with theoretical source spectra for explosions of different yield. Direct estimates from $m_b L_g$, assuming and partially confirming transportability of empirical relationships developed in North America, provide an alternative means of estimating Soviet yields that agrees well with Nuttli's coda-Q results using L_g .

To enhance desired regional arrivals, a frequency-domain phase-difference polarization filter, PHADIF (O'Neill, 1983), has been applied to a set of regional events recorded at the RSTN station RSNY and at other 3-component stations, including LRSM, in the northeastern U.S. The length of the time segment used for adaptive processing is varied in order to optimize filter effectiveness. The efficiency of the filtering process is significantly reduced by a choice of a window either too small or too large with respect to the dominant period of the desired phase. Pre-filtering with appropriate band-pass filters improves signal to noise and assures that suitable window lengths can be chosen for effective polarization filtering. Crustal P, SV, SH, and L_g phases are enhanced separately.

* Contract No. F19628-85-K-0009

INTRODUCTION

For yield estimation the use of Lg has advanced to the point where it is clear that it provides a robust measure of the relative yield among explosions that is comparable to that provided by P-waves. As in all methods to estimate absolute strength (yield) the question of systematic biases must be addressed. In the case of Lg Nuttli has argued that Lg vs yield experience at NTS can be transported to Semipalatinsk provided that path effects can be properly taken into account. His approach has been to use the coda Q method which relies on period vs time measurements in the coda of Lg at each observing station. For large propagation distances the concern is the reliability of the Q correction obtained by that approach. We have taken a different approach in accounting for Q effects which does not depend on the assumptions inherent in the coda Q method. Specifically we use the noise-corrected Lg spectra from a suite of explosions from the same source area (Semipalatinsk) recorded at particular stations to obtain by least-squares fitting the best estimate of the attenuation parameter $1/QU$ for each station. This average attenuation parameter is then used to obtain noise- and attenuation-corrected source spectra for individual events. The theoretical relationship relating source excitation spectra to yield is then used to estimate yield. Alternatively we could use empirical source spectra for events of known yield elsewhere and compare with observed values to obtain an event's yield, on the assumption that coupling is identical or that appropriate corrections for coupling differences can be made. This approach is applicable to single station measurements just as is the coda Q method. However, if there are sufficient observing stations spanning a range of azimuths from the source, it is preferable to use a source-path-receiver decomposition to obtain direct estimates of source excitation, average Q, and station terms for each frequency; then the yield estimation is made from the source spectrum using the

same theoretical relationship or empirical calibration as in the single station case. In this presentation the results from matching observations to theoretical curves for individual stations are emphasized.

An alternative approach to yield estimation using Lg was devised that assumes transportability of Nuttli's Lg magnitude relationship developed for earthquakes in the eastern United States. The differential excitation for an earthquake and explosion of comparable body-wave magnitude as a function of frequency was used to obtain the correction term needed to obtain an Lg magnitude equivalent to the body wave magnitude for explosions at Semipalatinsk; this procedure is a value of m_{bLg} that can be compared to Nuttli's m_{bLg} values obtained from the coda Q approach.

The emphasis has been on using Lg spectra so that more information is used to estimate source strength than a single time-domain amplitude measurement provides. This strategy also permits one to use the best signal to noise frequency bands for making yield estimates. We have found that tectonic release effects at Semipalatinsk start to become important for frequencies below about .3 Hz and that at large distances such as Grafenberg noise becomes a problem above about 1.2 Hz. Ideally we would like to include higher frequencies, hence broader signal bandwidth, to provide additional degrees of freedom in estimating source strength.

The following brief presentation highlights these approaches and gives examples of our results.

The work on polarization filtering is currently in its relatively early stages, so it will not be emphasized in this report. However, an example is given together with the results of cepstral stacking over a regional array to enhance depth phases for the Lancaster PA earthquake of April 23, 1984.

By taking the average spectral slopes from the noise-corrected Lg spectra for a suite of Semipalatinsk events recorded at Grafenberg, we obtained an average value of $1/QU$ of 2968 for the frequency range .3 - 1.2 Hz. The following equation gives the expression for the observed spectrum at distance r .

$$U_{ex} = 4\pi\mu\bar{\psi}(\omega) \cdot Ie^{i\phi I} \cdot e^{-\frac{\pi f}{QU} r} \cdot e^{-\frac{\omega r}{ic(\omega)}} \cdot S \cdot K_R(h)$$

where $\bar{\psi}(\omega)$ is reduced displacement potential.

$$S = -e^{i\frac{3\pi}{4}} [k_R \frac{A_R}{\pi K_R \gamma} (\frac{2}{\pi K_R \gamma})^{1/2}]$$

$$K_R(h) = \left[\frac{\dot{u}^*(h)}{\dot{\omega}_o} \right] - \frac{1}{2u} \left[\frac{\sigma^*(h)}{\dot{\omega}_o/c_R} \right]$$

By correcting for $1/QU$ and calculating S , μ , and K_R for the source medium (granite) and crustal structure, we obtain values of the "observed" reduced displacement potential that can be compared with theoretical curves for different yields. Figure 1 shows a suite of these curves for a von Seggern-Blandford source with the Grafenberg observations for the 12/07/76 $m_b = 5.9$ event superimposed. By least-squares fitting we obtain an estimated yield of 58 KT. The preliminary results of applying the same procedure to other Semipalatinsk events gives the following results:

TABLE 1. Preliminary yield estimates of Semipalatinsk events from spectral matching after Q correction.

<u>Date</u>	<u>m_b</u>	<u>Yield Estimate</u>
12/07/76	5.9	58
05/29/77	5.8	38
11/30/77	6.0	58
08/29/78	5.9	78
09/15/78	6.0	98
11/04/78	5.6	37
11/29/78	6.0	89
06/23/79	6.2	115
07/07/79	5.8	98
08/04/79	6.1	153
08/18/79	6.1	164

TABLE 2. Comparison of $m_b L_g$ estimates at Grafenberg for Semipalatinsk events using a different method than Nuttli used in his coda Q calculations for the same events at different stations.

<u>Date</u>	<u>m_b(ISC)</u>	<u>$m_b L_g$</u>	<u>$m_b L_g$ (Nuttli)</u>
12/07/76	5.9	5.752	5.71
09/15/78	6.0	5.790	5.87
11/04/78	5.6	5.596	5.57
11/29/78	6.0	5.822	6.01
06/23/79	6.2	5.929	5.92
07/07/79	5.8	5.823	5.87
08/04/79	6.1	5.941	6.01
08/18/79	6.1	5.940	6.03
12/02/79	6.0	5.782	6.05
12/23/79	6.2	5.950	6.12
06/12/80	5.6	5.513	5.74
12/14/80	5.9	5.749	5.92
03/29/81	5.6	5.429	5.45
04/22/81	6.0	5.779	5.97
09/13/81	6.1	5.966	6.10
08/29/78	5.9	5.836	5.80
10/18/81	6.1	5.797	6.09
04/25/82	6.1	5.991	6.13
12/05/82	6.1	5.828	6.21
12/26/82	5.7	5.468	
10/06/83	6.0	5.726	5.93
10/26/83	6.1	5.903	6.10
03/29/84	5.9	5.830	5.97
04/25/84	5.9	5.727	5.86
05/26/84	6.0	5.980	6.07

It should be emphasized that these are preliminary values and we must explore further the assumptions involved. Ideally, we would also like to average the estimates from several stations. However, the fact that our spectra conform to the slope of the theoretical curves suggests that the Q correction is appropriate and that our source model is also very reasonable. We are exploring these sources of uncertainty to attempt to characterize the accuracy of such estimates. It would be highly desirable to avoid assumptions about source structure and uncertainties in Q by having calibration events of known yield so that estimates of other events can be obtained empirically. To that end we are attempting to obtain LRSM data at Grafenberg for the cratering event at Shagan River whose yield has been estimated independently as 125 KT (Marshall et al., 1979); this event predates the installation of the broad-band stations at Grafenberg, precluding a direct comparison using common instruments.

The values given above are obtained from estimates of vertical-component Lg spectra. We have found that transverse-component data give equally good or better spectral estimates of source strength than vertical-component recordings. This is shown in Figure 2 which compares the Lg vertical, transverse, and combined vertical and transverse component Lg vs ISC magnitude at .7 Hz; the regressions have the smallest standard deviation at this frequency although .6 and .8 Hz results are comparable. Note that the transverse component gives a very good fit both for the narrow-band filter maximum value (top) and the RMS value (bottom). This suggests that the transverse component spectra should also be used to estimate yield for individual events, after making a correction for the average transverse to vertical ratio at each station.

An alternative approach to coda-Q was used to obtain estimates of Lg magnitudes for Soviet explosions that consists of using the measured relative levels of excitation of Lg for the explosion of 1/15/76 and the nearby

earthquake of 3/20/76 both of which had nearly identical body-wave magnitudes (about 5.2) and assuming that the Nuttli Lg magnitude formula developed for earthquakes in the eastern United States remains valid for the USSR. The station MAIO was used to obtain the relative Lg excitation vs frequency for these two events as Grafenberg data were not suitable because of poor signal to noise, but for other events GRF was used to calculate Lg magnitudes, assuming that the eastern U.S. formula developed by Nuttli can be used. (The average Q obtained using the spectral approach discussed above was approximately 900 and this corresponds closely with the attenuation embodied in Nuttli's formula.) The results of this calculation at .7 Hz after applying the correction factor of .81 magnitude units to equalize bodywave and Lg magnitudes at that frequency are given in Table 2 for a suite of Soviet events. As seen in this table the values agree well with those obtained by Nuttli using the coda Q approach at totally different observing stations. Thus we conclude that the Lg magnitude relationship that applies in the eastern U.S. can be transported without modification to western USSR at least for the path from Semipalatinsk to Grafenberg. His formula also gives an m_{bLg} value for the earthquake of 3/20/76 observed at MAIO that agrees closely with the m_b value, implying that Nuttli's m_{bLg} formula applies to that path as well. Ideally we would like to use several single station estimates to obtain a better Lg magnitude, but the Grafenberg results are very consistent, as might be expected from examining the data in Figure 2. The spectral slope approach can be used at any station to obtain the appropriate distance correction term to use in Nuttli's formula, if it is found not to be transportable directly.

REGIONAL PHASE ENHANCEMENTS

In order to take advantage of source information contained in regional recordings of earthquakes and explosions it is important to isolate, enhance, and characterize various body wave and surface wave arrivals. Among the techniques for such decomposition and enhancement are polarization filtering and cepstral analysis. We are currently exploring the applicability of these techniques for regional recordings in settings that are analogs to USSR areas of interest. An example from eastern north America is shown in Figures 3,4, and 5 depicting respectively the source-receiver geometry, observed seismograms at the 3-component station at Oswego, New York, and the polarization-filtered seismograms for a magnitude 4.2 earthquake located at Lancaster, Pennsylvania. It is clear that the P, SV, and Rayleigh filters selectively enhance those phases. In turn, these records can be used to isolate and further analyze given phases. If a local array is available (e.g. NORESS) then combined wavenumber-polarization filtering will provide further enhancement. Work in progress will explore this combined approach.

For the array shown in Figure 3 we also have attempted to enhance depth phases by stacking of individual cepstra obtained from rather long (up to 20 sec) body-wave time windows. The rationale is that the pP-P and sP-P delay times will be nearly common at all regional stations where crustal refractions are first arrivals whereas other relative delay times (e.g. mode-conversions and other phase arrivals) will vary leading to non-coincident peaks in the cepstra. For the regional array shown in Figure 3 we have stacked the individual spectra both by summing and taking their product. These results are shown in Figure 6 where it is clear that in both stacks a strong peak exists with a delay time of 1.9 sec. This corresponds to the depth phase sP-P delay time which matches the expected delay time for the independently-known depth of 4.8-5.0 km (based on

near-source aftershock studies) and the radiation-pattern expected for the source geometry obtained from fault-plane solutions for which these stations are on or near a pP mode). These results suggest that this approach would be very useful to apply to any regional array of stations at distances where pP-P and sP-P delay times should be nearly constant. It also appears that the stack obtained from the product of individual cepstra gives the best resolution of the depth-phase delay time; it also has the further advantage that it will enhance even when relative polarities of the phases change with azimuth, whereas the simple sum may suffer some cancellation. This cepstral stacking approach should work for very shallow events provided sufficient signal bandwidth is available to define the cepstral peaks for small delay times. Efficient High frequency transmission have been observed for crustal settings analogous to the USSR areas of interest, so regional networks may be capable of resolving typical explosion depths.

REFERENCES

Marshall, P. D., D.L. Springer, and H. C. Rodean, 1979, Magnitude Corrections for Attenuation in the Upper Mantle, Geophys. J. R. Astron. Soc., Vol.57, 609-638.

VON SEGGERN-BLANDFORD SOURCE

12/07/76. A1(Z). MB=5.9

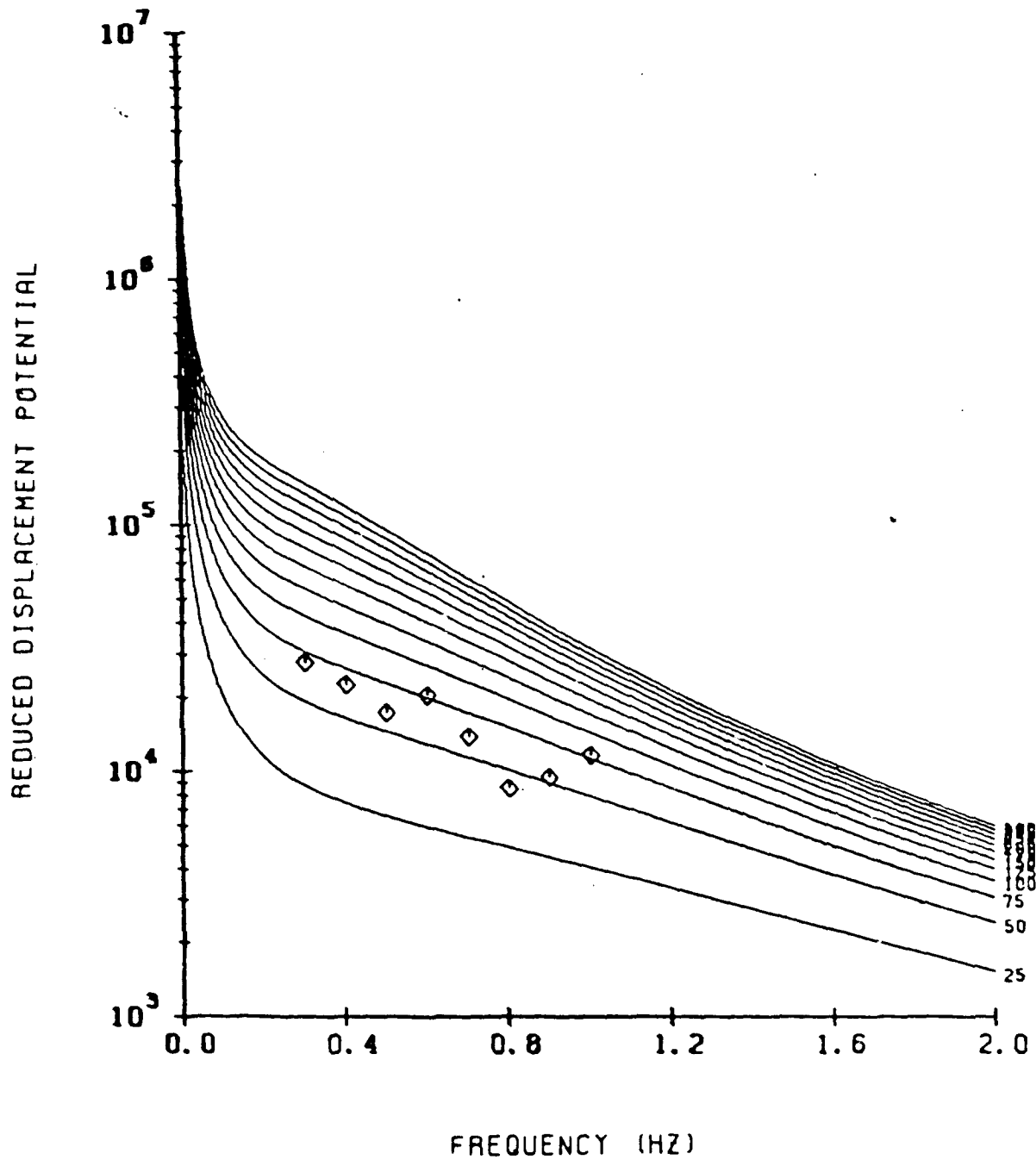


Figure 1

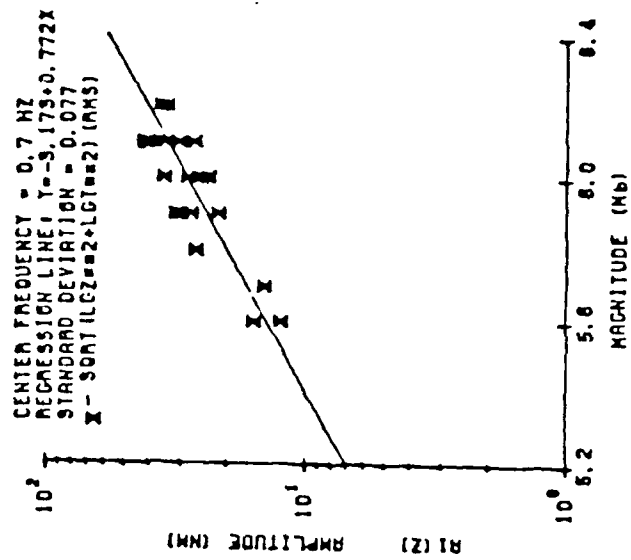
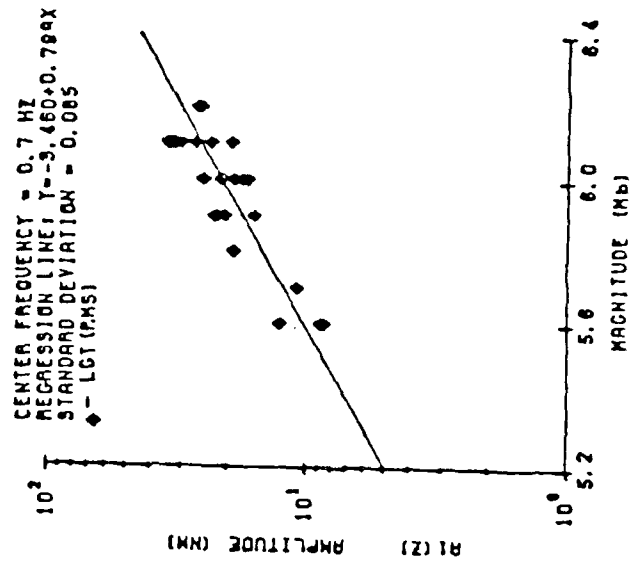
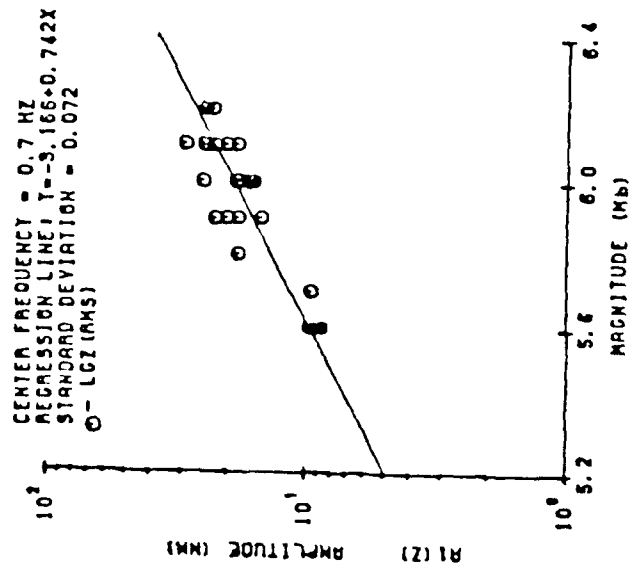
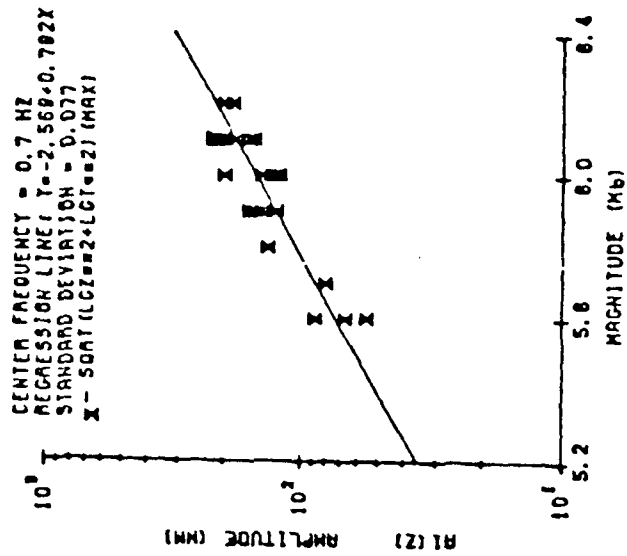
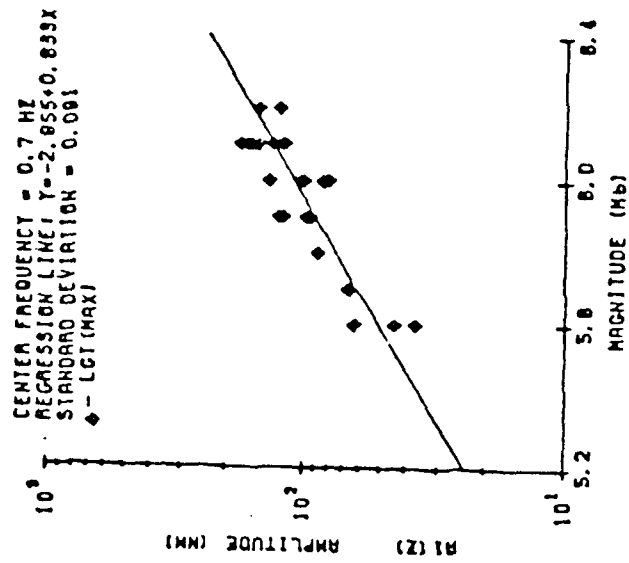
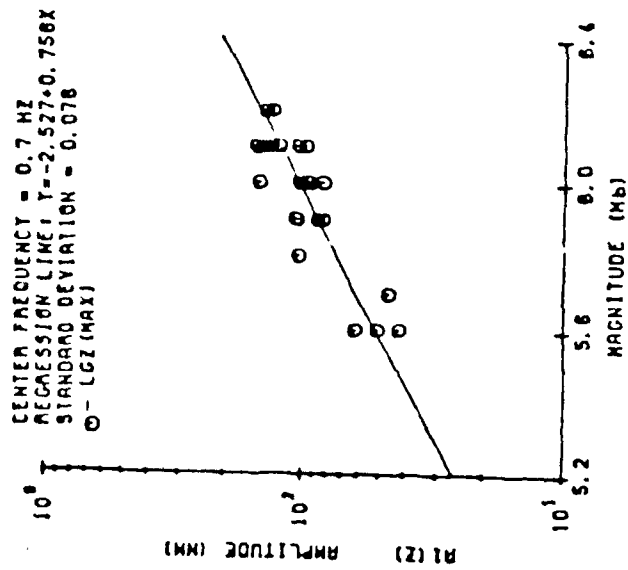


Figure 2

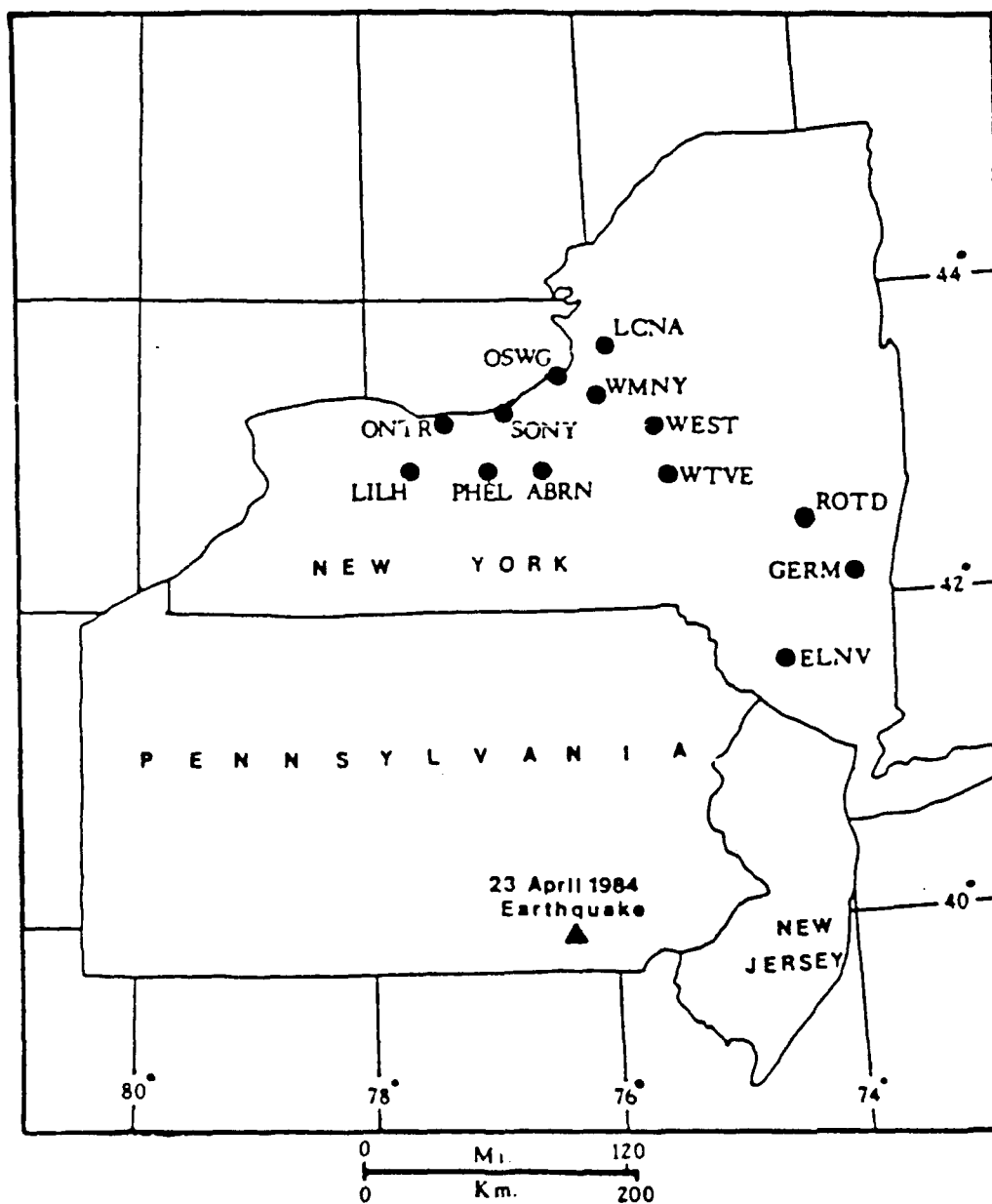


Figure 3. Location of the N.E. U.S. Seismic Network stations used in the cepstral analysis of the April 23, 1984 earthquake. These stations are operated by Woodward-Clyde Consultants, of Wayne, N.J. (modified after Woodward-Clyde Consultants, 1985)

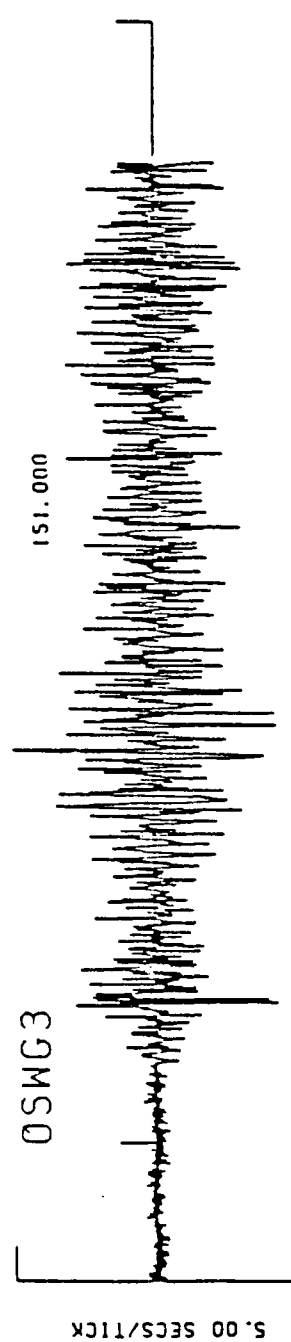
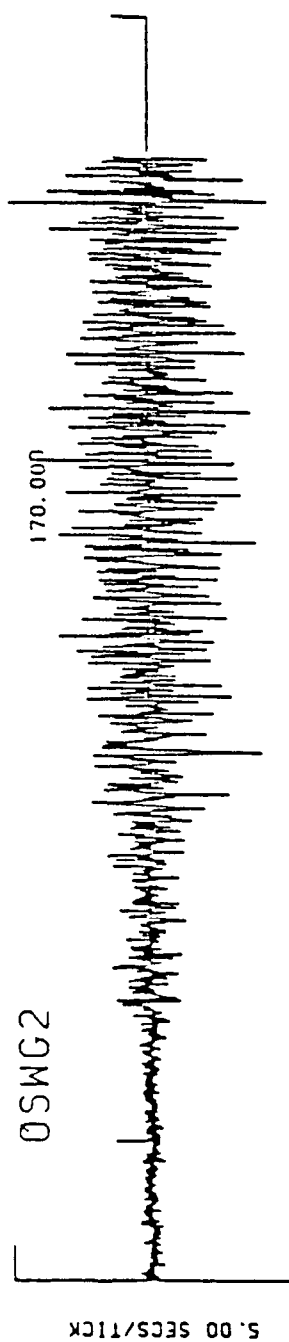
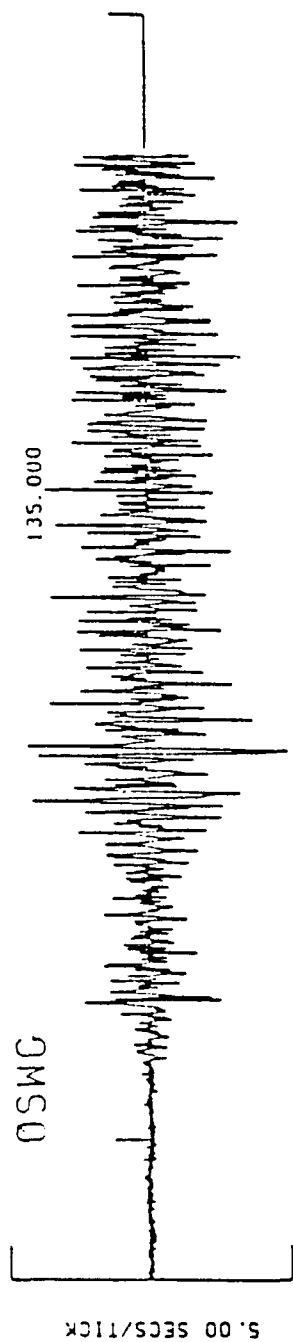


Figure 4

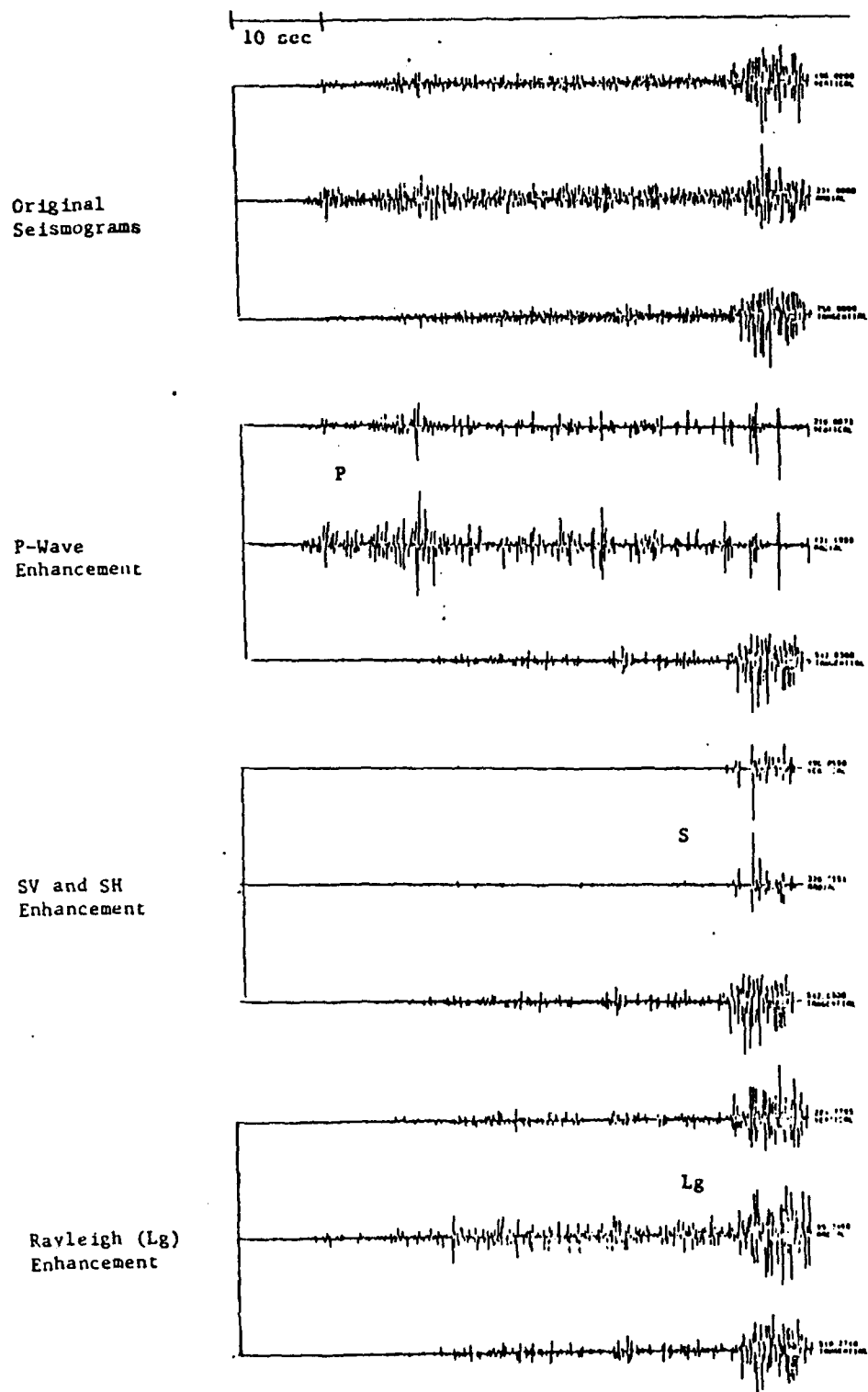


Figure 5. Results of polarization filtering of the Oswego, NY recording of the Lancaster, PA $M_b L_g$ 4.2 mainshock.

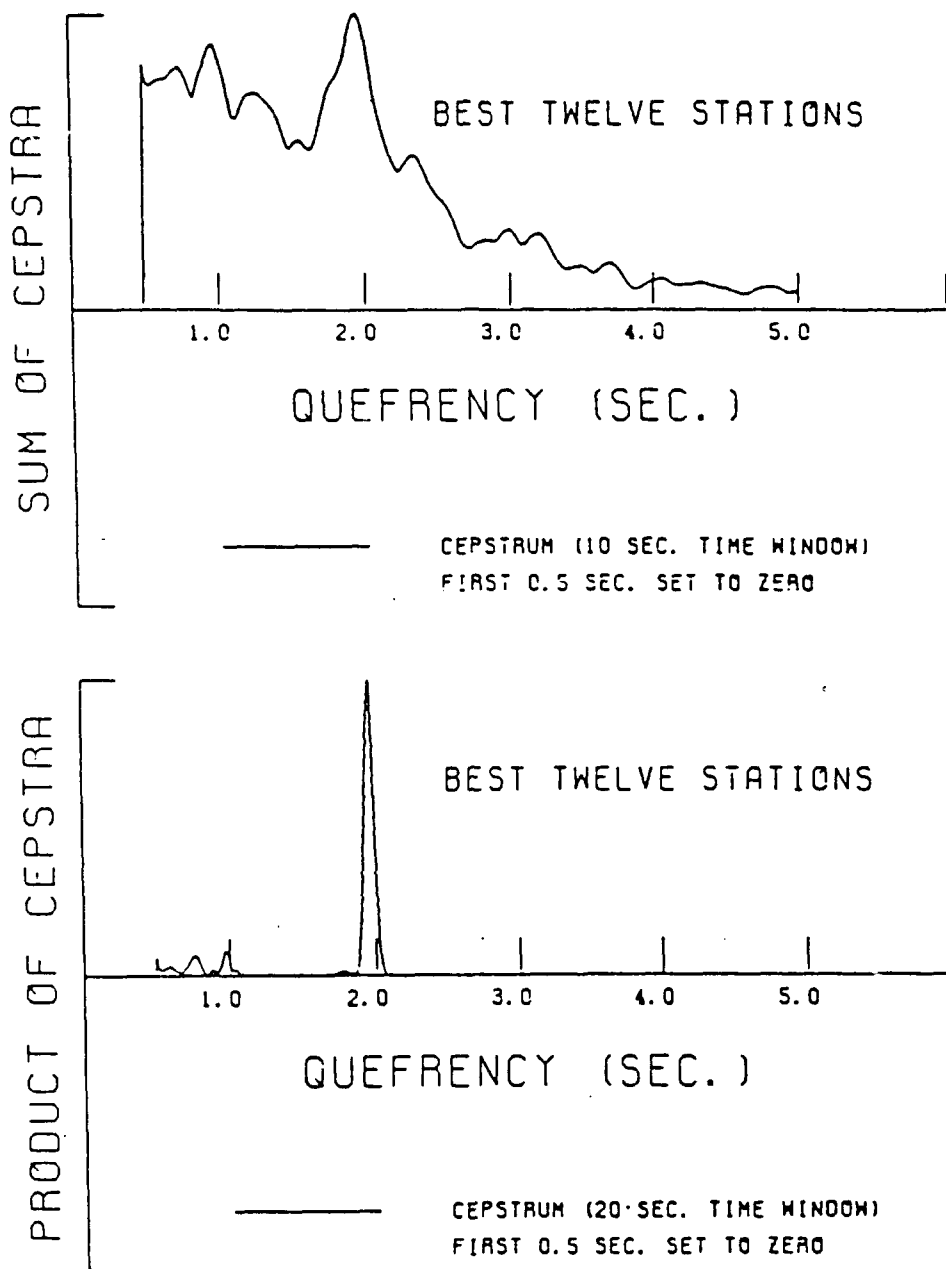


Figure 6. The sum and the product of the cepstra for the "Best Twelve" stations which recorded the April 23, 1984 earthquake.

A Numerical Investigation of Topographic Effects on 2-D Explosive Line Sources

K. L. McLaughlin, R. S. Jih, and Z. A. Der
Teledyne Geotech Alexandria Labs

INTRODUCTION

Jih et al (1986) propose methods for introduction of free surface topography in heterogeneous elastodynamic two dimensional (2-D) linear finite difference (LFD) calculations. We have applied these methods to explosive line sources for simulation of far field "teleseismic" P waves. The motivation for these numerical experiments are to examine the extent of scattering from near source topography. Several important test sites have substantial topography within a few (1 Hz P wave) wavelengths of the source. These test sites include the French southern Sahara test site, the Soviet Novaya Zemlya test site, and the Soviet Degelen Mtn test site.

To explore the variability that may be introduced by near source topography, several simple test cases have been investigated. These test cases indicate that the $\log(\max)$ measure of the far-field teleseismic P waveform may experience 0.3 magnitude unit fluctuations due to the interference effects of a linear P+pP combination when the significant topography is extreme. The results can change rapidly with takeoff angle and location of the 2-D line source under the topography. As a worst case, the southern Algeria test site located within Taourirt Tan Afella Massif will serve as a model for some more specific calculations. This granite mountain rises from the (1100 meter elevation) Ahaggar plateau to a peak of 2100 meters in less than 1 km. The mountain is only 16 km^2 and has slopes that locally exceed 45° . Several tests were conducted at this site in southern Algeria from 1962 to 1966. A topographic map from Duclaud and Michaud (1970) is shown in Figure 1, with locations from Faure (1972). Contours are at 100 meter intervals and the granite outcrop is indicated by the dashed line. In recent years Blandford and Shumway (1982), Blandford et al (1984) and McLaughlin et al (1986a) have conducted investigations of the m_b observed from these explosions at WWSSN stations. Furthermore, available LRSM data and the EKA and YKA arrays have been analyzed (see McLaughlin et al 1986b) for estimates of the explosion spectra and time functions.

TAOURIRT TAN AFELLA MASSIF

A north-to-south cross section of Taourirt Tan Afella Massif (P wave velocity of 5.2 km/s) is shown in Figure 2A with a 15° incident planar P wave. A planar, band-limited P wave is incident upon the medium from below and the dilatational strain is measured at the source locations. The far-field displacement P waveform due to an explosion line source at these locations is then inferred from this transfer function by reciprocity. Figures 2B through 2E illustrate the dilatational field at intervals of 0.2 second as the P wave reflects from the free surface. Note that at time interval 0.4 second, the strong constructive and destructive interference that results from the reflections directly beneath the peaks of the ridge (2-D mountain). The linear pP contribution from this location would be large and variable for a receivers at a takeoff angles near 15° . At time intervals 0.6 and 0.8 seconds we see what appear to be Rayleigh waves trapped at the surface as well as dilatational coda behind the specularly reflected P wave.

Source locations indicated by triangles in Figure 2A were used to infer far-field P waveforms from 2-D explosive line sources shown in Figure 3A and 3B. The waveforms have been convolved with von Seggern and Blandford (1972) explosive source time functions (50 and 120 KT), an attenuation operator ($t^* = 0.45 \text{ sec}$), and an LRSM instrument response.

Waveforms are shown for takeoff angles of 0, 5, 10, 15, and 20 degrees. These two source locations are labeled "RUBIS" and "SAPHIR" analogous to the two locations (R and S) of Figure 1. Several interesting features are evident in these 2-D numerical simulations.

For the location "SAPHIR", the maximum amplitude decreases with increasing takeoff angle (see Figure 3A). The elastic pP contribution increases in such a way as to reduce the "b-c" amplitude with increasing takeoff angle. The coda amplitude increases with increasing takeoff angle as the free-surface interaction becomes more complicated and the conversions of P-SV energy increase at the free surface. The "SAPHIR" location is roughly coincident with the focal point of the topographic profile and the pP reflection may be amplified at this source location.

The "RUBIS" location also shows an increase of coda amplitude with increasing takeoff angle (See Figure 3B). For the shallowest takeoff angle of 20°, there is a reflection, larger than the main P wave. The "RUBIS" "b-c" amplitude does not show as strong a variation with takeoff angle. The topography directly above the "RUBIS" location is less steep and the pP free surface interaction is distorted. However, the topography to the north of the "RUBIS" location introduces scattered arrivals responsible for the strong coda. The "RUBIS" location is above the "focal point" of the topographic profile and the pP reflection may be de-focused at this source location.

Spectral ratios of the "RUBIS"-to-"SAPHIR" 2-D synthetics showed that as the takeoff angle increases, "RUBIS" becomes enriched in high frequencies with respect to "SAPHIR". The modulation of the spectra makes this comparison difficult if the bandwidth is limited as it is in real data to frequencies below 4.0 Hz. However, the spectral ratio of the two events at a common station may give clues as to which event received the largest contribution of scattered energy in the coda due to the topography above the source.

Six sites recorded both RUBIS and SAPHIR for which spectral ratios could be computed (YKA, EKA, KN-UT, HN-ME, BL-WV, and LC-NM). The results from the spectral ratios indicate that the "average" slope between the two events over the stations is near zero, and that some of the stations show positive slopes while others show negative slopes. The bandwidths are in most cases limited to between 0.5 and 3.0 Hz. The azimuths of these stations span about 45°, from due north (EKA) to northwest (BL-WV). Except for YKA, the data indicate that RUBIS and SAPHIR have similar average frequency content and that the effect of scattering may vary rapidly with azimuth in the real 3-D world.

Four events EMERAUDE, GRENAT, RUBIS, and SAPHIR were deconvolved at the EKA and YKA arrays using the method of Shumway and Der (1985). The results are shown in Figure 4. The equivalent seismic sources for the events are shown side-by-side for the two arrays and a comparison can be made for EMERAUDE, GRENAT, and SAPHIR (RUBIS was poorly recorded at YKA). The initial waveform is similar for each event at the two arrays while the differences are greatest beginning about 0.5 sec after the main P wave. SAPHIR shows the clearest differences between the two arrays in that the negative pulse following the positive pulse is strong at EKA but absent at YKA. EMERAUDE and GRENAT show differences in timing of the negative (and small positive) pulses following the initial P wave. These differences argue in favor of a scattering model for the variations in the free surface interaction for these events.

CONCLUSIONS

We have made qualitative comparisons of 2-D LFD calculations for line sources under a topographic feature with observations of explosions at the French southern Sahara Test Site. The 2-D models would suggest that the linear free surface (pP) reflections would be strongly

affected by topography for RUBIS and SAPHIR. The topography could produce variations of 0.3 magnitude units in the P-wave teleseismic magnitude. The topographic scattering is expected to be strongly dependent on the azimuth and takeoff angle. Additional topographic profiles are being studied to gain an understanding of this variability.

Although simple spectral ratio measures do not show convincing evidence for scattering from the topography, the seismic source deconvolutions at EKA and YKA exhibit significant variation in the free surface interaction. Further work along these lines will concentrate on the analysis of the LRSM waveform data available for RUBIS and SAPHIR, as well as the amplitude patterns of teleseismic P-wave $\log(a)$, $\log(ab)$, and $\log(\max)$ at WWSSN stations.

REFERENCES

- Blandford, R. R. and R. H. Shumway (1982), Magnitude-yield for nuclear explosions in granite at the Nevada test site and Algeria: joint determination with station effects with data containing clipped and low-amplitude signals, *VSC-TR-82-12*, Teledyne Geotech, Alexandria, Va.
- Blandford, R. R., R. H. Shumway, R. Wagner, and K. L. McLaughlin (1984) Magnitude yield for nuclear explosions at several test sites with allowance for station effects, truncated data, amplitude correlation between events within test sites, absorption, and pP, *TGAL-TR-83-6*, Teledyne Geotech, Alexandria, Va.
- Jih, R. S., K. L. McLaughlin, and Z. A. Der (1986), Boundary conditions of arbitrary polygonal topography in elastic finite difference scheme for seismogram generation, *TGAL-TR-86-03*, (in preparation) Teledyne Geotech, Alexandria, Va.
- McLaughlin, K. L., R. H. Shumway, R. O. Ahner, M. Marshall, T. W. McEfresh, and R. Wagner (1986a) Determination of event magnitudes with correlated data and censoring: a maximum likelihood approach, *TGAL-86-01*, Teledyne Geotech, Alexandria, Va.
- McLaughlin, K. L., A. C. Lees, and Z. A. Der (1986), Teleseismic spectral estimates of M_0 and Ψ_∞ estimates for four French Explosions in southern Sahara, *TGAL-86-03*, (in preparation) Teledyne Geotech, Alexandria, Va.
- Crough, S. T., (1981), Free-air gravity over the Hoggar massif, northwest africa: evidence for alteration of the lithosphere, *Tectonophysics*, 77, 189-202.
- Duclaux, F. and M. L. Michaud (1970), Conditions experimentales des tirs nucleaires souterrains francais au Sahara, R. Acad. Sc. Paris, t. 270 (12 Janvier 1970) Serie B 189-192.
- Faure, J. (1972) Recherches sur les effets geologiques d'explosions nucleaires southeraines dans un massif de granite saharien, Centre d'Etudes de Bruyeres-le-Chatel, Commissariat a l'Energie Atomic Report CEA-R-4257 Service de Documentation CEN-SACLAY B.P. no. 2, 91-GIF-sur-Yvette, France.
- Marshall, P. D., D. L. Springer, and H. C. Rodean (1979), Magnitude corrections for attenuation in the upper mantle, *Geophys. J. R. astr. Soc.* 57, 609-638.
- von Seggern D. H. and R. R. Blandford (1972), Source time functions and spectra for underground explosions, *Geophys. J. Roy. astr. Soc.*, 31, 83-87.

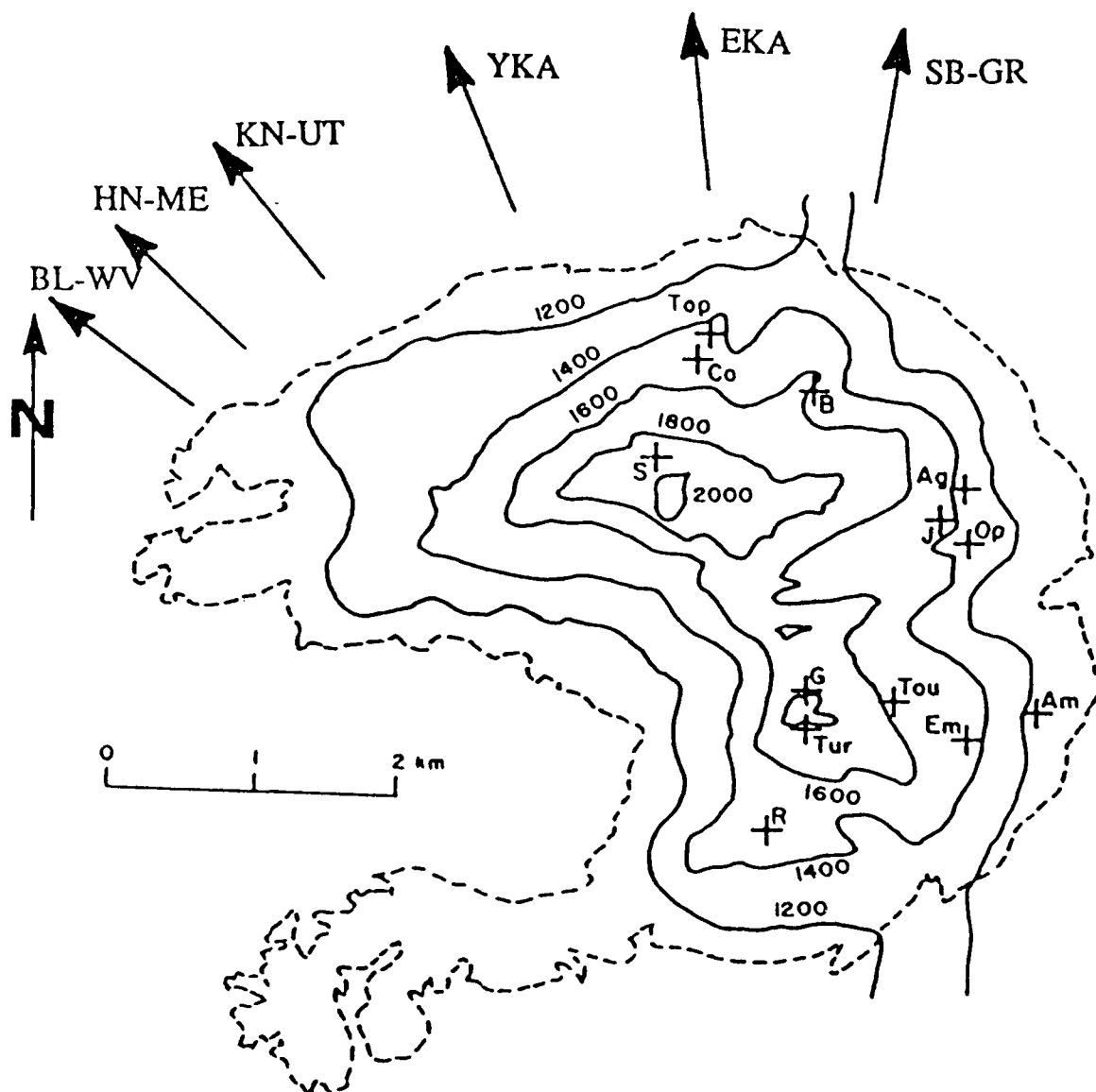


FIGURE 1. Topographic map from Duclaux and Michaud (1970) with locations from Faure (1972) for SAPHIR (S), RUBIS (R), EMERAUDE (E), and GRENAT (G). Contours are 100 meters. The dashed line is the outcrop of the Taourirt Tan Afella Massif granite.

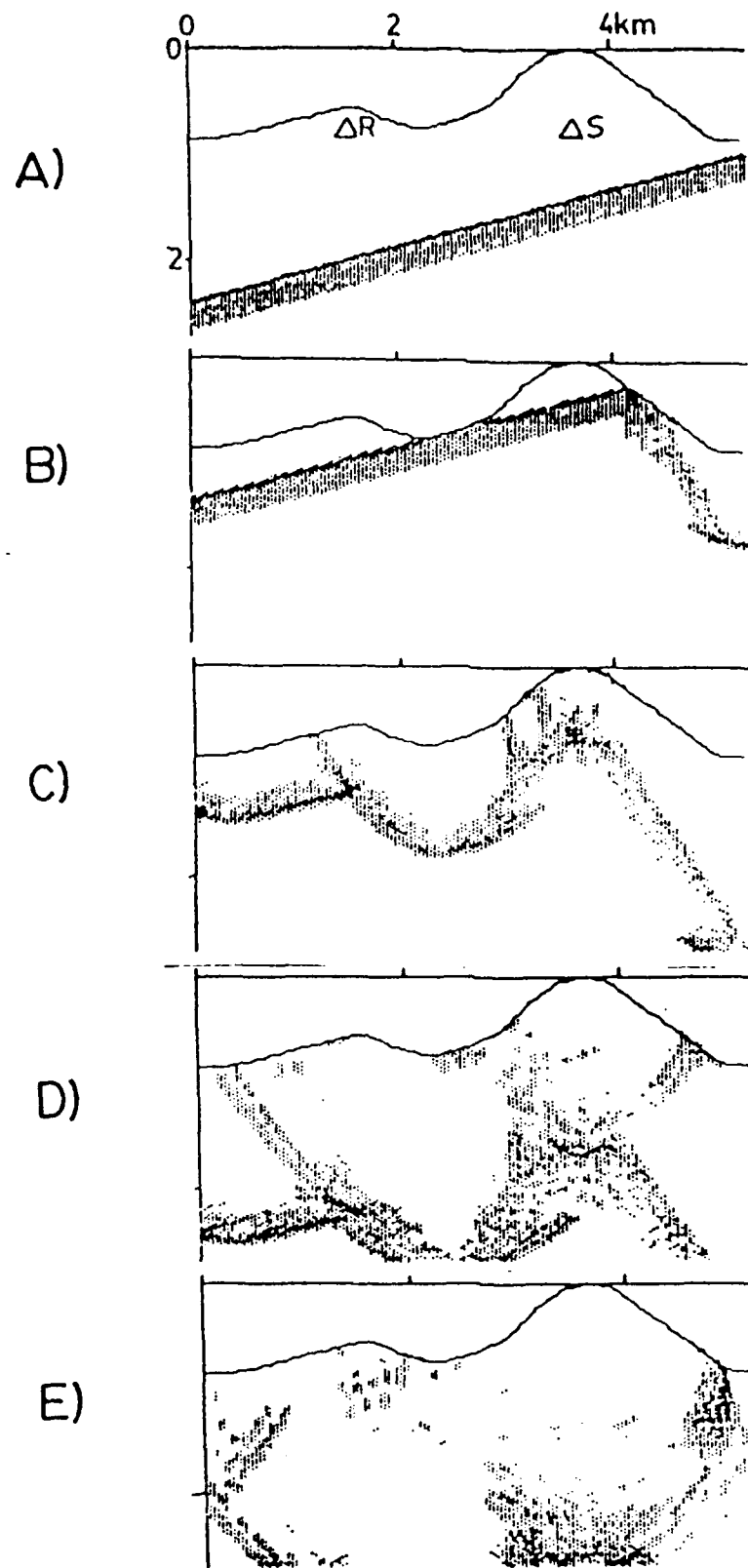


FIGURE 2A. North-to-south topographic profile for Taourirt Tan Afella with and incident 15° plane dilatational wave, time = 0.0 sec. Line source locations are indicated by "S" and "R". 4B, C, D, and E show the dilatational strain (P-wave) field at time = 0.2, 0.4, 0.6 and 0.8 sec.

Figure 1 displays five stacked waveforms, likely ECGs, showing the effect of increasing thoracic angle on the R wave. The waveforms are labeled from top to bottom: 20 DEG, 15 DEG, 10 DEG, 5 DEG, and NORMAL. The x-axis is labeled 'SECONDS' with a '0' at the start. As the angle increases, the R wave becomes taller and more peaked, and the S wave becomes deeper.

87

SAPHIR

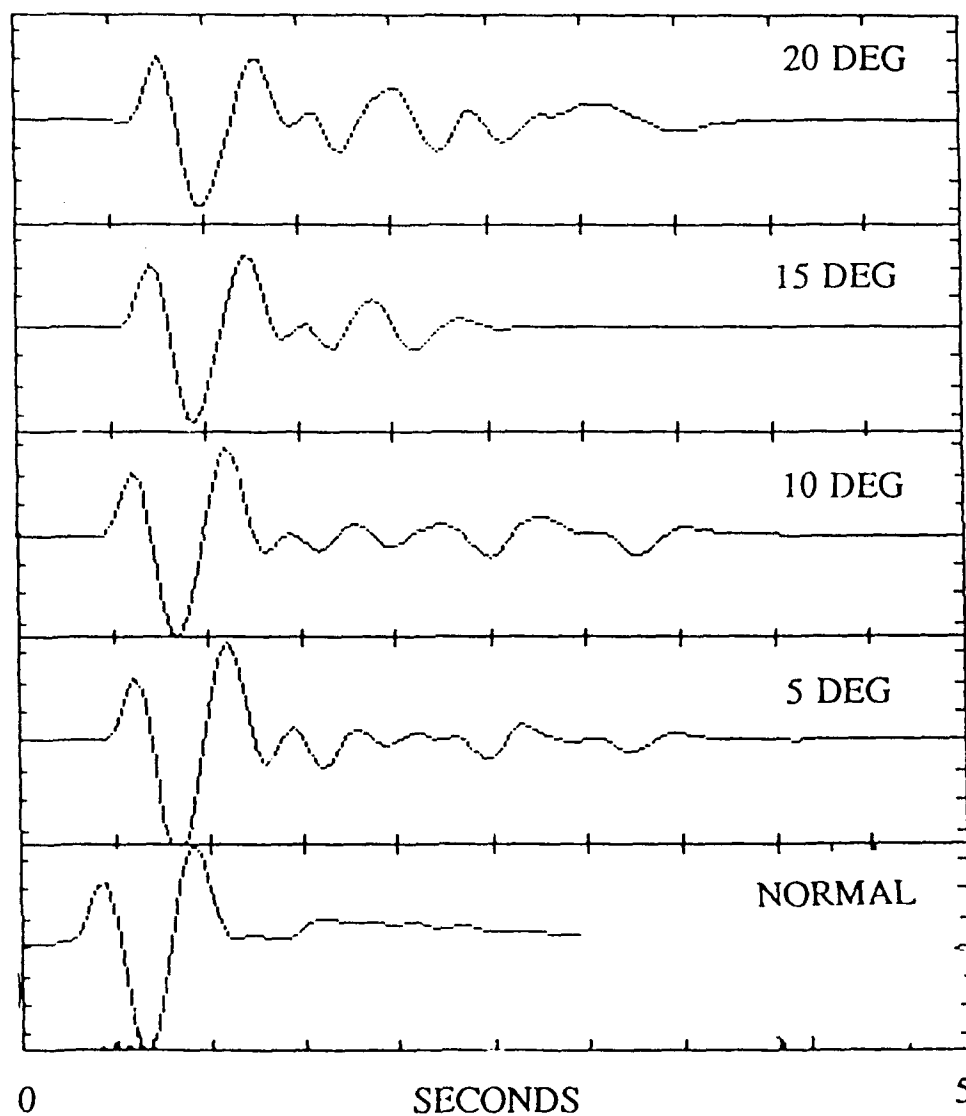


FIGURE 3A(LEFT). Synthetic far-field P-wave seismograms for takeoff angles of 0, 5, 10, 15, and 20 degrees for the line source location indicated by "S" in Figure 4A. 100 KT source with $t^* = 0.45$ sec, and LRSM instrument response. FIGURE 3B(RIGHT). Synthetic far-field P-wave seismograms for takeoff angles of 0, 5, 10, 15, and 20 degrees for the line source location indicated by "R" in Figure 4A. 100 KT source with $t^* = 0.45$ sec, and LRSM instrument response.

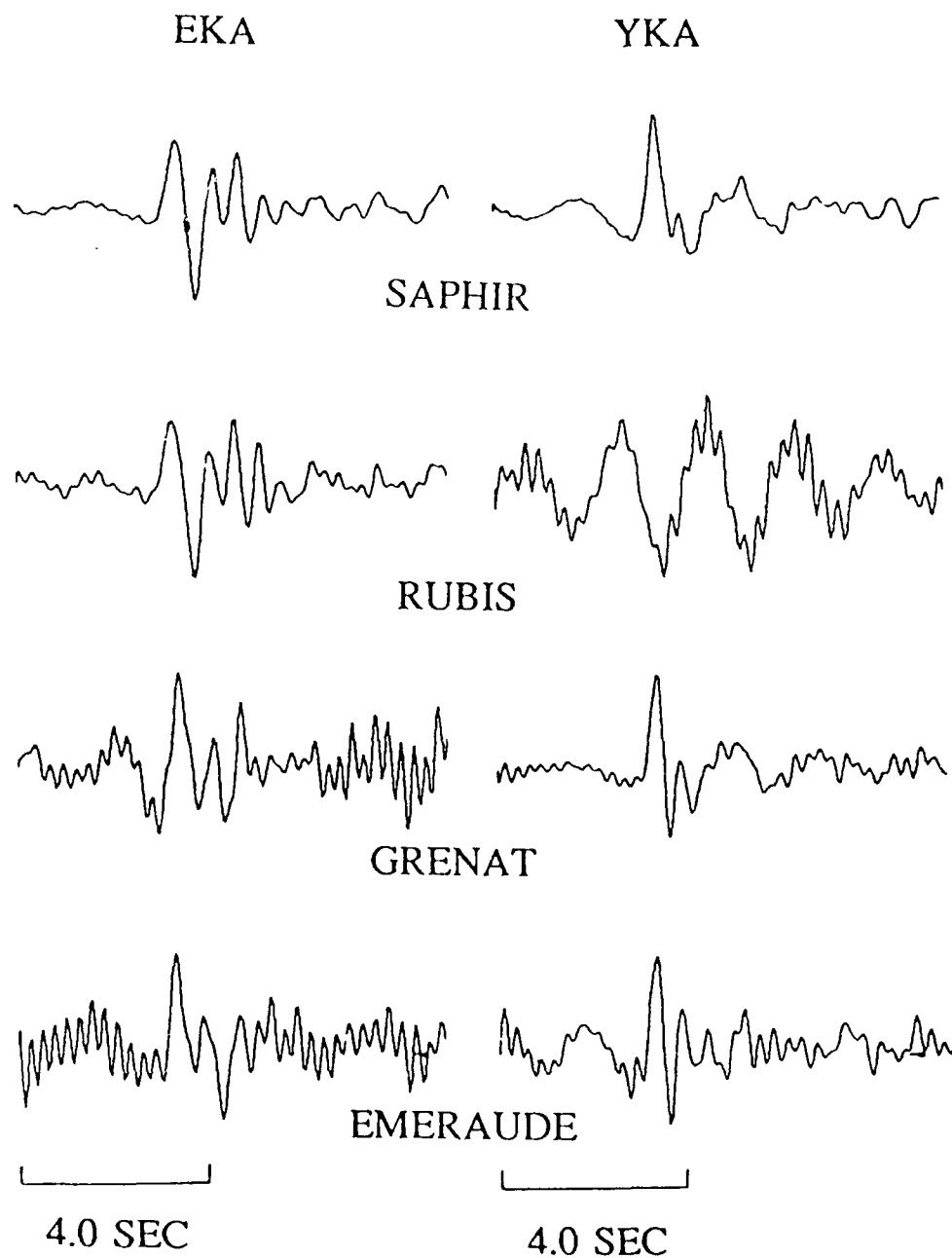


FIGURE 4. Equivalent seismic sources from the deconvolution of RUBIS and SAPHIR data at the arrays EKA and YKA using the method of Shumway and Der (1985). RUBIS was poorly recorded at YKA. Note the variation between EKA and YKA for the events EMERAUDE, GRENAT, and SAPHIR. The variation is the greatest for SAPHIR where a negative pulse that follows the positive pulse at EKA is absent at YKA.

ESTIMATES OF SEISMIC COUPLING AND NUCLEAR EXPLOSION YIELDS USING SEISMIC MAGNITUDE AND MOMENT DATA

By

Charles B. Archambeau

SUMMARY

Observations of the spectral character of direct compressional waves from underground nuclear explosions, both in the near and far field distance ranges, suggest that the purely explosive produced P wave has a form that can be represented by a simple step function pressure equivalent. Here, however, the "elastic radius" for the equivalent is significantly larger than the radius at which high strain flow and fracture effects cease, and corresponds to the (mean) radius where strain dependent losses, at relatively low strain levels in the range 10^{-4} to 10^{-6} , cease.

Using this simple equivalent source representation and the assumption that the (reversible) work done on the medium outside the elastic radius is proportional to yield, it follows that m_b values depend directly on yield and upon two source dependent coupling parameters K_c and K_E , which are termed the non-linear and elastic coupling parameters, respectively.

On the other hand, M_s is dependent only on yield and the non-linear coupling parameter K_c , while the moment M_0 is simply related to M_s , and is dependent only on K_c , and the Poisson ratio at the source elastic radius, as well as yield. The coupling parameter K_E may be expressed in terms of the elastic velocities at the elastic radius of the source, while K_c is strongly dependent on a variety of local material properties, including porosity, water content, pressure and the fracture density within the material surrounding the explosion.

It is found that the available magnitude-yield data for US nuclear explosions, in a wide variety of media, require four sets of the coupling constants, K_c and K_E , for a simultaneous description of both m_b and the M_s observations. The resulting empirical magnitude-yield curves correspond to a high coupling set for m_b and M_s , two intermediate coupling sets and a low coupling set.

These magnitude-yield curve sets provide a means of estimating yield using both m_b and M_s together, provided tectonic release effects and differences in test site absorption, relative to NTS, are taken into account. On the other hand, if the range of coupling at some other test site is assumed to be within the range sampled by the U.S. data, then it is possible to estimate the (combined) difference in near site absorption and tectonic effects between NTS and any other test site.

This inference method is applied to USSR explosion data, with the objective of first estimating absorption and tectonic release differences. Both (m_b , M_s) and (m_b , M_0) data indicate a difference in absorption between NTS and the Kazakh test site which is such that observed m_b values from Kazakh will be larger, by from .3 to .35 magnitude units, than those from NTS for explosions of the same yield. Next, using a most probable value of .32 for "m_b bias" between the sites, the yields of the largest Kazakh explosions were estimated using the appropriate sets of (corrected) coupling curves, where it is required that the tectonic release corrected M_s (or M_0), as well as the m_b observations, give the same estimate of yield. This

procedure results in estimates of USSR test yields, with the largest values all very near 150 kt. In particular, two events since 1978 have values somewhat larger than the 150 kt. value (i.e. near 170 and 180 kt), with the remaining large events having most probable yield values at, or slightly below, 150 kt.

Explosion Spectra

The spectral character of the compression wave radiated by explosions seems, quite remarkably, to be well described by the simple Sharpe solution, which corresponds to a step pressure pulse applied to the boundary of a spherical "cavity" within an elastic solid. Specifically, this simple solution has the form:

$$\tilde{u}_p(r, \omega) = \frac{P_0 R_0^3}{4\mu} \left[\frac{v_p}{v_p^2 - \left(\frac{v_p}{2v_s} \right)^2 R_0^2 \omega^2 + i v_p R_0 \omega} \right] \frac{e^{-ik_p r}}{r} \quad (1.)$$

in the spectral domain, where R_0 is the effective cavity radius and P_0 the magnitude of the pressure step at R_0 . Here v_p and v_s are the compression and shear velocities in the surrounding elastic medium and μ is the rigidity of the material, while ω and $k_p = \omega/v_p$ are the angular frequency and wave number respectively.

Since an actual explosion involves the production of a vapor filled cavity and a surrounding zone of crushed and heavily fractured material that behaves plastically in response to the shock wave generated by the explosion, as indicated by Figure 1, it is necessary to interpret the empirical fit provided by equation (1.) in terms of an "effective cavity radius, R_0 ", and an "effective pressure", P_0 , at this radius. Thus R_0 must be interpreted as a radial distance near the elastic zone boundary shown in Figure 1; in particular R_0 must be like the radius R_e (an "elastic radius") shown in this figure. Similarly, P_0 is the magnitude of the pressure at R_e and must be simply related to the yield strength of the (cracked) material.

The fact that this very simple equivalent applies to both tamped (coupled) and to decoupled explosions in cavities is surprising, in view of the very complicated non-linear physical phenomena that actually occurs as a consequence of an explosion. However, it appears that this simple spectral structure is, in part, a consequence of the non-linear strain dependent losses in the outer, initially microfractured, zone surrounding the shock fractured zone produced by the explosion.

In this regard, the non-linear process in the initially fractured rock appears to function in such a way as to attenuate the spectral peaking that is often predicted by complex finite difference calculations and to "smooth out" the spectrum so that it is quite flat up to a corner frequency, at which point it begins to decay as $1/\Gamma^2$ with increasing frequency. In particular, this strain dependent mechanism produces attenuation characterized (approximately) by an inelastic quality factor Q_1 , such that:

$$Q_1^{-1} \approx \begin{cases} c_1/f & ; \quad f > f_c^{(P)} \\ c_1 f & ; \quad f < f_c^{(P)} \end{cases} \quad (2.)$$

where $f_c(p)$ is the P wave corner frequency and c_1 is independent of frequency, but is a function of the explosion yield and the physical properties of the medium. But, since the attenuation of the wave field is controlled by a transfer function of the form:

$$T_Q(l) = \exp \left[\frac{-\pi f \Delta}{Q_1 v_p} \right]$$

where Δ represents distance, then at high frequencies, that is for f greater than the $f_c(p)$, the attenuation is independent of frequency. Therefore, the attenuation by this process reduces the high frequency part of the explosion spectrum uniformly for frequencies $f > f_c(p)$, and exponentially with frequency for frequencies lower than $f_c(p)$.

This then accounts for the selective attenuation of the spectral peak of the wave entering this non-linear zone (i.e. the wave field at R_e^* in Figure 1.) However it also shows that the spectral slope at high frequencies ($f > f_c(p)$) is not altered by the loss mechanism, but that the corner frequency of the wave spectrum after passing through this region will be significantly less than the spectrum of the wave field entering this zone.

These characteristics, of little or no peaking in the spectra of most explosions and lower corner frequencies than those predicted using finite difference modeling, are observed in explosion P wave spectra at regional and teleseismic distances. These effects are therefore those that appear to be chiefly responsible for the simple spectral structure of observed P waves from explosions and help explain why the Sharpe spectrum fits these observations with rather large values of R_0 and low values of P_0 .

The direct P wave spectrum in equation (1.) has asymptotic properties that are easily seen to have the form:

$$\tilde{u}^P(r, \omega) = \frac{P_0 R_0^3}{4\mu v_p} S_e(\omega) \left(\frac{e^{-ik_p r}}{r} \right)$$

$$S_e(\omega) = \left[1 - \left(\frac{R_0 \omega}{2v_s} \right)^2 + i \left(\frac{R_0 \omega}{v_p} \right) \right]^{-1} \sim \begin{cases} 1 & : \omega \ll 1 \\ \left(\frac{2v_s}{R_0 \omega} \right)^2 & : \omega \gg 1 \end{cases}$$

Based on these asymptotic limits for $S_e(\omega)$ one can define a corner frequency as the point of intersection of high and low frequency asymptotes. This characteristic frequency is therefore:

$$\omega_e(p) = 2\pi f_c(p) = \frac{2v_s}{R_0} \quad (3.)$$

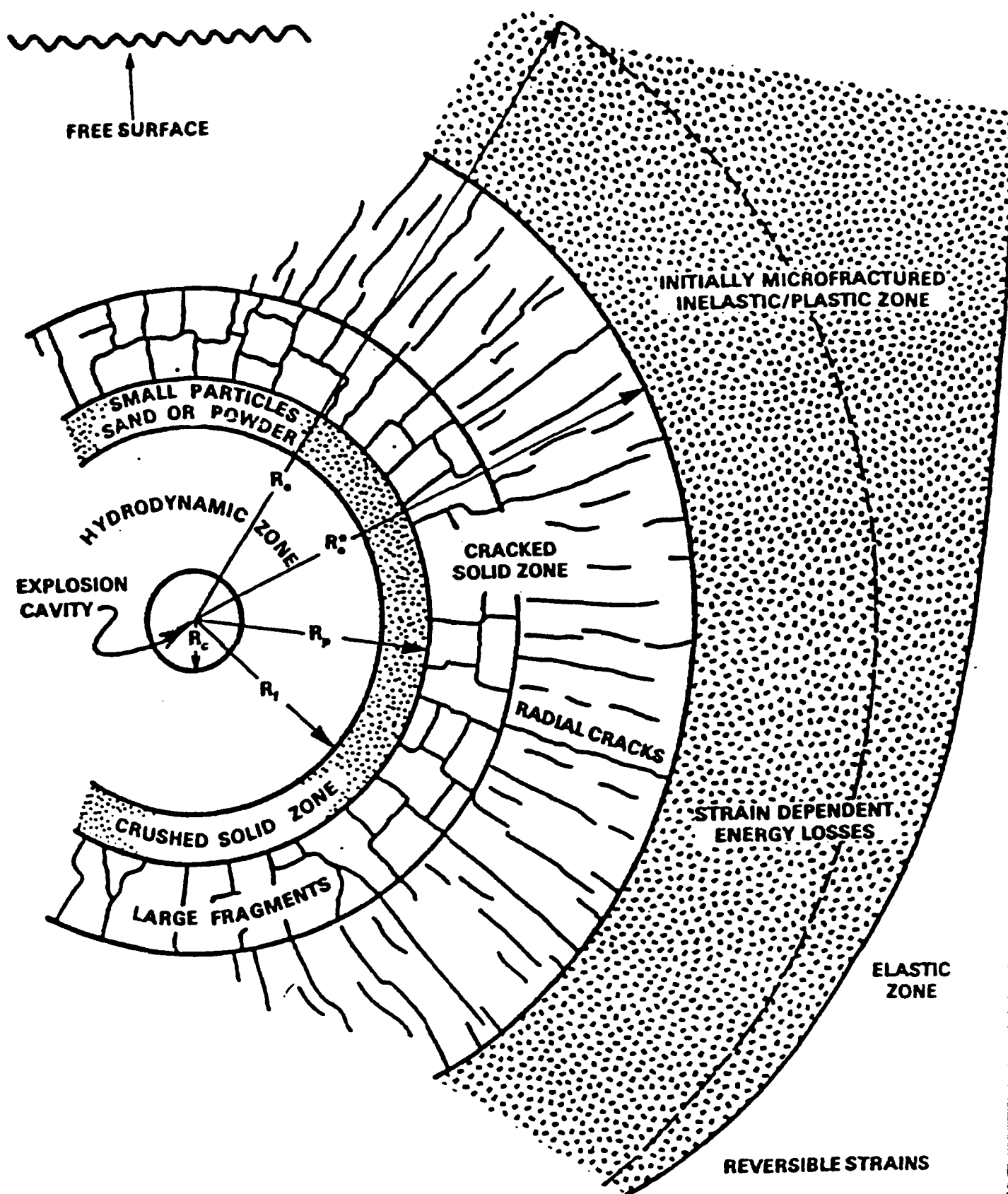


Figure (1.) - Schematic representation of zones of non-linear behavior around a tamped nuclear explosion

It is also easy to show that the fundamental mode Rayleigh wave will have the vertical displacement spectrum given by:

$$\tilde{w}_R(r, \omega) = \left(\frac{2v_s^2}{v_p^2} \right) M_O S_e(\omega) \left[\tilde{A}_R \epsilon_n \left(\frac{k_R}{2\pi} \right)^{1/2} \right] e^{-ik_R r} \quad (4.)$$

where \tilde{A}_R and ϵ_n are frequency dependent excitation factors, and $k_R = \omega/c_R$ is the Rayleigh wave number. Here:

$$M_O = \pi \left(\frac{v_p^2}{v_s^2} \right) P_O R_O^3$$

is the "moment" of the explosion.

Scaling Relations for P_O and R_O

Some very elementary considerations lead to scaling relations for the two parameters characterizing the explosion source. To obtain such relations we only need to make one assumption, and that is that the change in energy of the elastic medium is proportional to the yield, W , of the explosion. In this case:

$$\Delta U = CW$$

where ΔU is the change in internal elastic energy of the medium and C is a constant dependent on material properties.

Noting that ΔU must also be equal to the reversible work done on the medium by the explosion, so that it is equal to ΔW_R , then:

$$\Delta U = \Delta W_R \simeq \int_{R_O}^{R_O + \Delta R} [4\pi r^2 P] dr \simeq 4\pi \bar{P}_O R_O^3 \left(\frac{\Delta R}{R_O} \right),$$

where \bar{P}_O is the mean (equivalent) pressure acting during elastic deformation of the medium outside the elastic radius R_O . Here ΔR is the displacement of the elastic boundary, due to the explosive pressure at R_O . (Both R_O and P_O are "equivalent" quantities arising from the replacement of the actual explosion, which involves melting and creation of a large shock wave, among other things, by an equivalent "pressurized cavity" source with pressure P_O and radius R_O .)

Now if Y is the (compressive) stress value equal to the intrinsic strength of the material at the radius R_O , then by definition of an "elastic radius" the stress induced in the material by the deformation at R_O will be just equal to Y . That is

$$Y = k_s \left(\frac{\Delta R}{R_O} \right),$$

where k_s is the adiabatic bulk modulus and $\Delta R/R$ is the radial strain. Consequently:

$$\Delta W_R \simeq \left(\frac{4\pi Y}{k_s} \right) \bar{P}_O R_O^3$$

Now, if we also use the relation $\Delta W_R = CW$, with W the explosion yield, and let \bar{P}_O be denoted as the parameter P_O , appearing in the original equation for the Sharpe solution, then we have:

$$\left. \begin{aligned} P_O R_O^3 &= K_C W \\ K_C &= \frac{C k_s}{4\pi Y} \end{aligned} \right\} \quad (5-a.)$$

The constant K_C will be called the (nonlinear) coupling constant for the explosion.

It is worth noting, for decoupled explosions, that Latter *et. al.* (1959) obtained:

$$\left. \begin{aligned} P'_O R'^3_O &= K_C^{(DEC)} W \\ K_C^{(DEC)} &= \left(\frac{\gamma-1}{4\pi/3} \right) \end{aligned} \right\} \quad (5-b.)$$

where P'_O is the pressure at the cavity wall, and R'_O is the radius of the decoupling cavity. Here γ is about 1.2 for an air filled cavity, so $K_C^{(DEC)} \simeq .048$. (Because decoupling efficiencies are theoretically about a factor of 200, then we should expect to obtain K_C values for tamped explosions with maximum values near 10. It turns out that observations imply that observed K_C values range from about 10 to about 1, with the range dependent on material properties. For example granites and salt have K_C values near 10, while weak, porous dry rocks have values near unity.)

Teleseismic Spectral Amplitudes and Magnitudes

As a consequence of these relations, we can obtain simple analytical expressions for teleseismic (or regional) spectral amplitudes. In particular, the teleseismic P wave amplitude spectrum is approximated by:

$$\tilde{u}_P^T = \left(\frac{K_C W}{K_E} \right) \left[\frac{T_R(\Delta)}{\sqrt{\rho_R v_P^R}} e^{-\pi f t_P^*} \right] |S_e| \quad (6.)$$

where $T_R(\Delta)$ is the ray theoretic spreading factor, $t_P^* = \Delta/(v_P Q_P)$ is the attenuation factor, and $\rho^{(R)}$ and $v_P^{(R)}$ denote the density and P wave velocity at the receiver. Here,

$$K_E = K_E(\rho^{(s)}, v_P^{(s)}, v_S^{(s)})$$

is the elastic coupling constant, and is only a function of the elastic velocities and density at the

source.

Given that the seismic body wave magnitude is defined by

$$m_b = \overline{\log[|\bar{u}_P^T|/T]} + b(\Delta) \quad ; \quad T \sim 1 \text{ sec.}$$

where $b(\Delta)$ is the distance correction factor, T the period of the P wave amplitude and with the bar indicating an average over different station observations, then (7.) produces the result:

$$m_b = \log \left[|S_e| W \right] + \log K_c - \log K_E + b'(\Delta) - (\pi \log e) t_P^*$$

Using the scaling relations applied to the spectral factor $|S_e|$, where the amplitude spectrum scales directly with W , while the corner frequency scales inversely as the one third power of the yield; then we have:

$$m_b = \begin{cases} \log W + \log K_c - \log K_E + b'(\Delta) - (\pi \log e) t_P^* & ; \quad \text{for } f_c^{(P)} \gtrsim 1 \text{ Hz} \\ 1/3 \log W + \log K_c - \log K_E + b'(\Delta) - (\pi \log e) t_P^* & ; \quad \text{for } f_c^{(P)} \lesssim 1 \text{ Hz} \end{cases} \quad (7.)$$

Thus the body wave magnitude is predicted to have unit slope as a function of $\log W$ for explosions of lower yield, such that $f_c^{(P)} \gtrsim 1 \text{ Hz}$, and a lower slope of $1/3$ at higher yields.

It turns out, for explosions in strong, high coupling materials, that the point at which the slope in the m_b versus yield curve changes is near 150 kt. For weaker, lower coupling, media this "break point" is at somewhat lower yields, closer to 100 kt. In any case, the reason for this change in slope is because the body wave magnitude measurement is always made near 1 Hz. For larger explosions this frequency will be above the corner frequency and therefore on the part of the source spectrum that is decreasing as f^{-2} with increasing frequency. Thus, rather than the measurement being made on the flat part of the spectrum, as it is for the smaller explosions, it is made on a sloping part of the spectrum above the corner frequency and this part of the spectrum does not increase as rapidly with increasing yield as does the flat portion of the spectrum.

The spectrum for the regional or teleseismic Rayleigh wave is given in equation (4.), and using this relation in the definition,

$$M_s = \log \left[\frac{|\bar{W}_R|}{T} \right] + B(\Delta) \quad ; \quad T \sim 20 \text{ sec.}$$

now gives the simple result:

$$M_s = \log W + \log K_c + B'(\Delta) \quad ; \quad f_c^{(P)} \gtrsim .05 \text{ Hz} \quad (8.)$$

Here the magnitude-yield curve will have unit slope for all explosions in the yield range of interest since the measurement is made below the corner frequency of the source spectrum.

Since the moment, from previous equations, can be expressed as

$$M_O = \pi \left(\frac{v_P^2}{v_s^2} \right) K_c W$$

then

$$\log M_O = \log W + \log K_c + \log \left[\pi \left(\frac{v_P}{v_s} \right)^2 \right] = M_s + \log \left[\pi \left(\frac{v_P}{v_s} \right)^2 \right] - B'(\Delta)$$

and the moment is linearly related to the yield and simply related to M_s .

Observed Magnitude-Yield Results

If we adopt these analytical relations as a basis of interpretation for the observed data, then we can look for evidence of systematic variations of magnitude versus yield that are in conformance with the predictions. In this regard Figure 2 shows data, from NTS and other (non-Soviet) test sites, plotted against predicted magnitude-yield curves with the coupling constants, in the relation (8.) and (9.), adjusted to provide a reasonable fit to the data. All the explosions shown are expected to produce high coupling, inasmuch as they are in salt, granite, volcanic rocks or saturated tuff and rhyolite. The coupling constant K_c required to provide a fit turns out to be 9.35, and so is close to the expected maximum value of around 10.

It is worth noting that the Aleutian events are expected to have higher m_b values than NTS events, because of the difference in upper mantle low velocity - low Q zones under the sites. In this regard, the correction to be applied to the Aleutian data, to make it comparable to NTS data, is indicated by the vertical bars on the appropriate data points. Similarly, the Salmon explosion, in Mississippi, is expected to have a somewhat higher m_b value than the NTS events for the same reasons, and this correction is similarly indicated.

The high coupling data fits the theoretically predicted curves quite well. However some events do not exhibit high coupling for both m_b and M_s , with some showing "intermediate coupling" for M_s and high coupling for m_b . This can be attributed to the fact that m_b depends on both K_c and K_E , while M_s depends only on K_c . Thus changes in the "elastic coupling" constant K_E , from event to event, can produce higher coupling for m_b than for M_s , and vice-versa.

It is evident that the event Scotch and Rex appear somewhat anomalous, in that they both show very high M_s coupling but rather low m_b coupling. This can be attributed to high levels of tectonic release that may have biased the M_s measurements, to produce high M_s values, and/or lower than normal m_b values. (An equivalent tectonic double couple, oriented in a manner corresponding to a dip slip fault, would produce increases in M_s and decreases in m_b . See Murphy and Archambeau, 1986, for a study of the evidence for similar effects associated with the Rulison explosion, among others.) The M_s "correction" needed to bring the m_b and M_s values in line with "normal" values for K_c and K_E is indicated for the Rex and Scotch events in Figure (2). The correction is about .3 magnitude units and is certainly within the range to be expected, based on the magnitudes of tectonic effects observed for other explosions. However, in reality, we would expect both the m_b and M_s values to be affected, rather than just one of them. The relative size of these changes would be dependent on the nature (ie. the orientation) of the equivalent source for the tectonic release. Lacking detailed data for these particular events makes such an inference impossible, however it is certainly of some importance that events like these be studied in more detail.

In spite of one or two anomalous events that may be linked to "unusual" tectonic effects, the data shown in Figure (2.) certainly can be fit by the theory, and this data is compatible with the predicted change in slope for the m_b curve. Further, the values of K_c and K_E needed

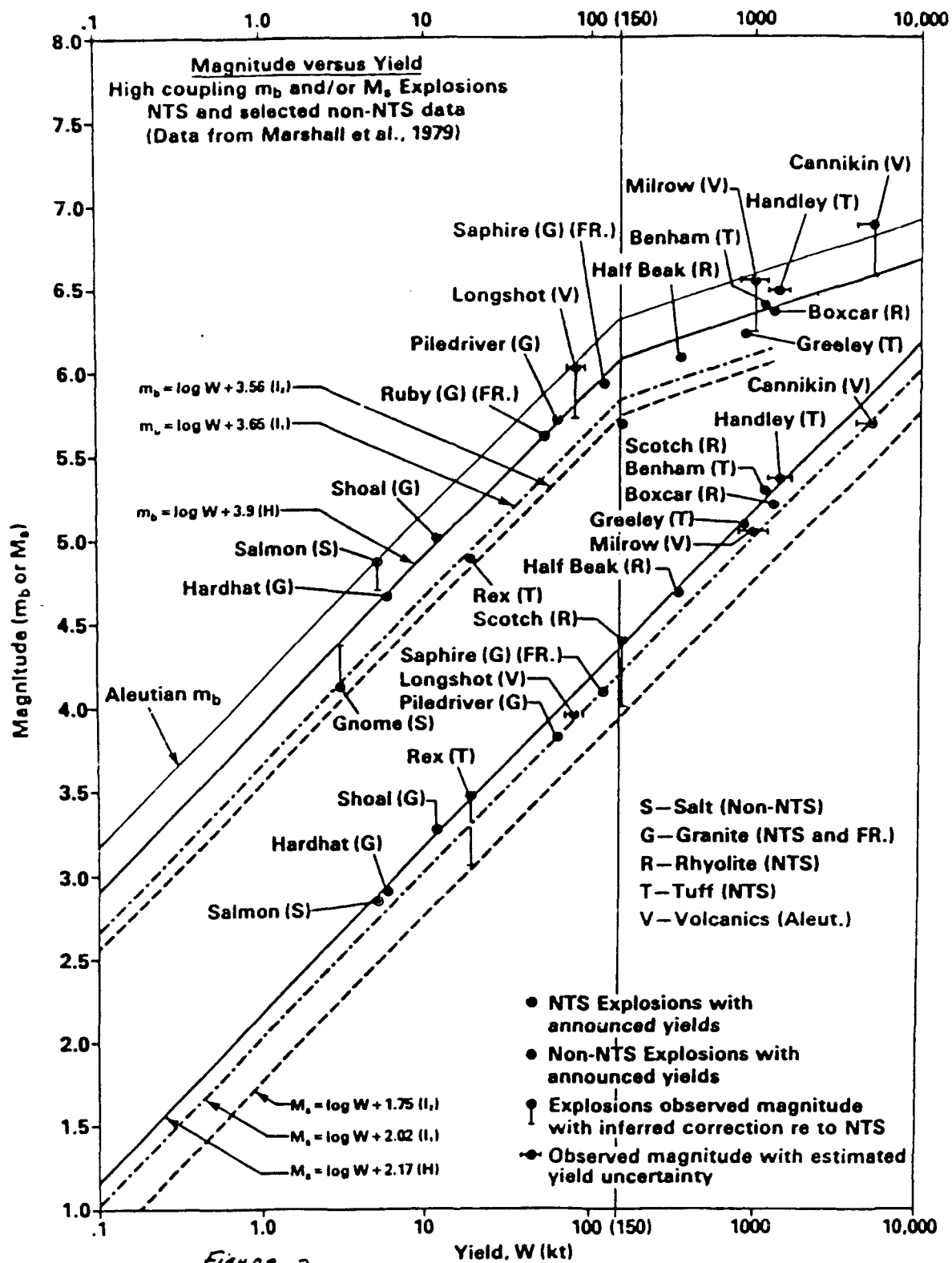
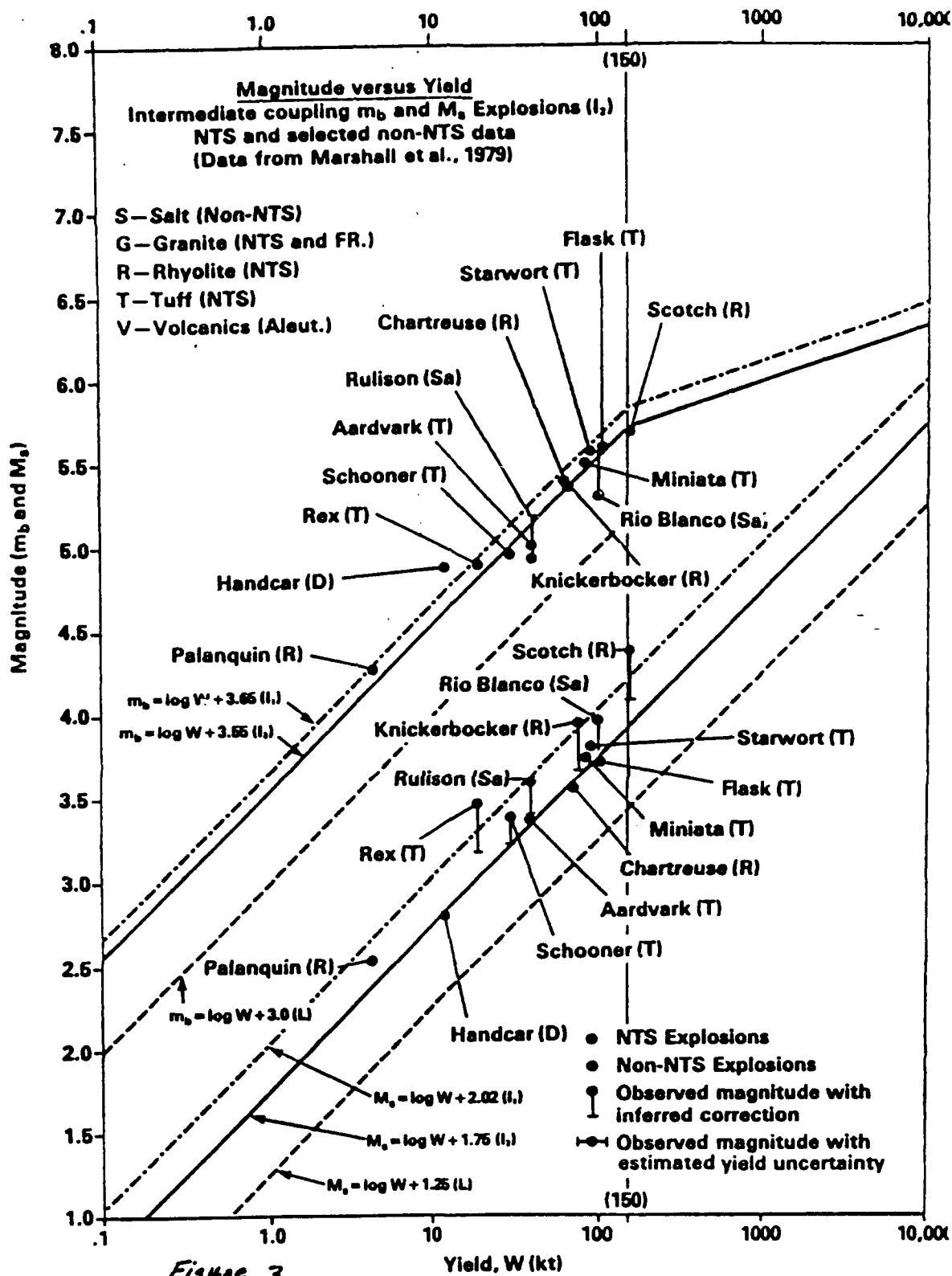


Figure 2.



to obtain the fit prove to be in the range expected on the basis of physical considerations.

As expected, explosions in weaker materials and/or partially saturated rocks display similar fits to the theoretical curves, but with lower values of K_C . Figure (3.) shows data for what are termed intermediate coupling explosions. In this figure the Rulison explosion is shown, with the correction factors for tectonic release indicated for both m_b and M_s values. Again the fit to the theoretical curves is quite good and encompasses all the explosions in known weak and/or partially saturated rocks. The K_c value for these events is about half that for the high coupling explosions.

Figure (4) shows the appropriate best fit curves for low coupling explosions in dry alluvium or tuff-rhyolite. The K_c value used to obtain this fit was near unity, and so only about 10% of the high coupling value needed to fit the data from explosions in granite and other strong, or fully saturated rocks. Thus, the explosion coupling ranges over an order of magnitude, for rocks in which one might conduct underground tests, and accounts for much of the scatter observed in magnitude values from explosions of the same yield in different geologic materials.

Clearly it is necessary to account for coupling variability in order to obtain meaningful estimates of explosion yield. Further, it seems clear that if we are to infer proper bias estimates from statistical samples of explosion data from different test sites then it is necessary to account for variability of near source coupling that can exist between test site material, as well as the variability that can be produced within the data set from a given site.

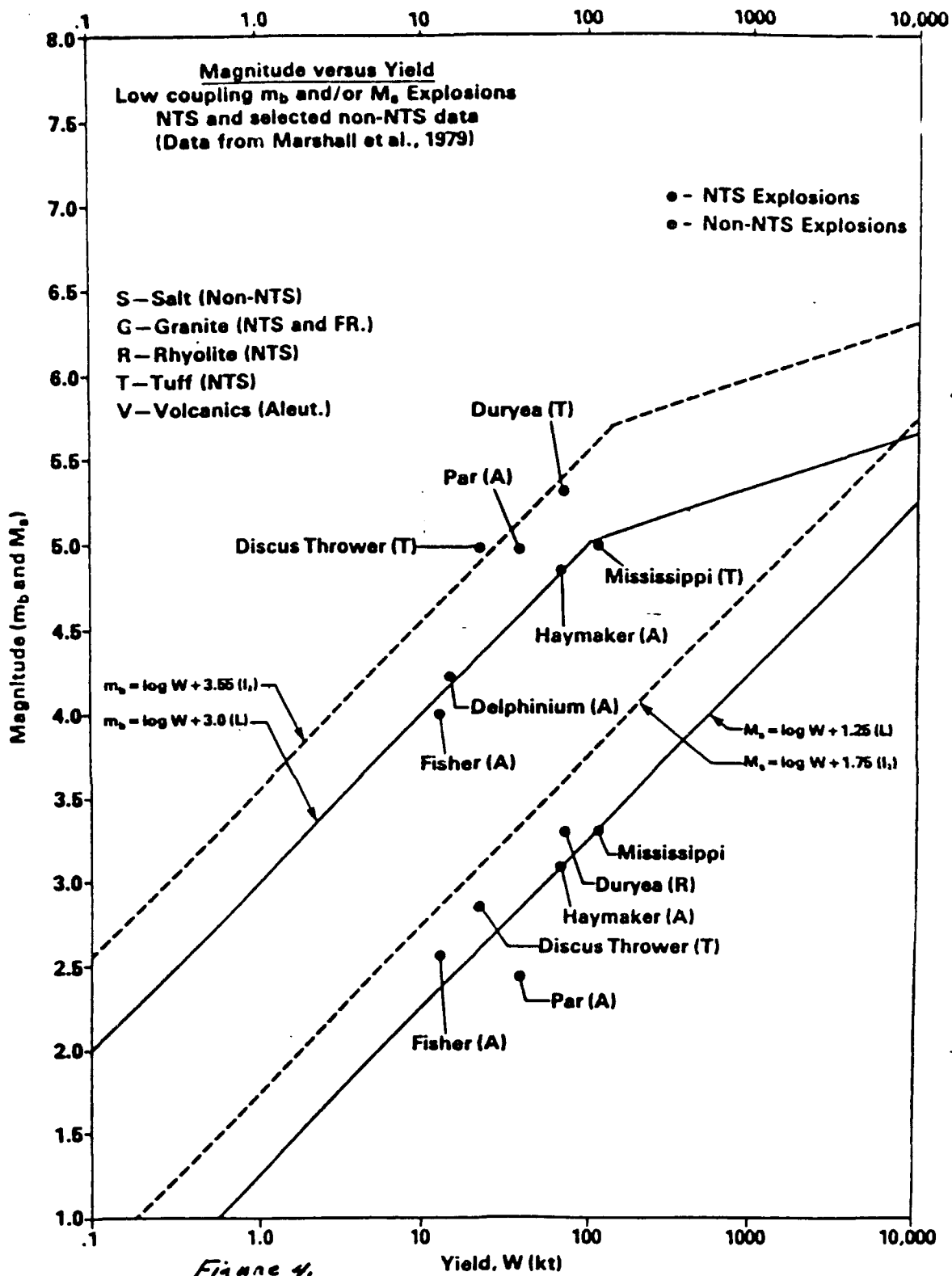
Finally, it is equally clear that anomalous m_b and M_s values will occur and be caused by highly variable tectonic effects. These anomalous events will often involve both m_b and M_s perturbations, and such "perturbations" can be large. Therefore use of any yield estimation method, say m_b versus yield, can produce a fictitiously large (or small) yield estimate because of the fluctuating tectonic effects. To guard against this possibility it is obvious that one must check such events for evidence of high tectonic release, and correct both m_b and M_s for any such effect. (Current practice does not include corrections to m_b , under the assumption that tectonic perturbations of m_b are small. That this need not be the case is obvious from the study of the Rulison and Rio Blanco events in Colorado. It is also quite clear that Soviet explosions at Kazakh involve thrust type tectonic source equivalents and that this tectonic component will similarly affect m_b values quite strongly.)

An alternate way of showing the fit of the theoretical curves to the data is shown in Figure (5). Here the $m_b - M_s$ magnitude difference has been plotted against yield and more clearly shows a change in slope of the magnitude curve near 150 kt. The curves shown are consistent with those given earlier in Figures (2) through (4).

Another way of displaying the data, without the necessity of knowing the yield, is shown in Figure (6). Clearly the data plots in a manner similar to the $m_b - M_s$ magnitude versus yield curves, and suggests a way of classifying the coupling for a given explosion of unknown yield.

In this regard, Figure (7) shows $m_b - M_s$ versus M_s data for both NTS and Kazakh explosions. Several theoretical curves are plotted for each site, representing high and intermediate coupling curves. (The symbols I/H, for example, denotes the M_s / m_b coupling and, in this case, corresponds to intermediate, (I) coupling for M_s and high (H) coupling for m_b .) Clearly the NTS data is roughly contained within the bounds of the different coupling curves shown.

On the other hand, the Kazakh data shown is displaced upward, indicating a bias in the $m_b - M_s$ values, which is likely to be due to a different transfer function for the Kazakh site, or



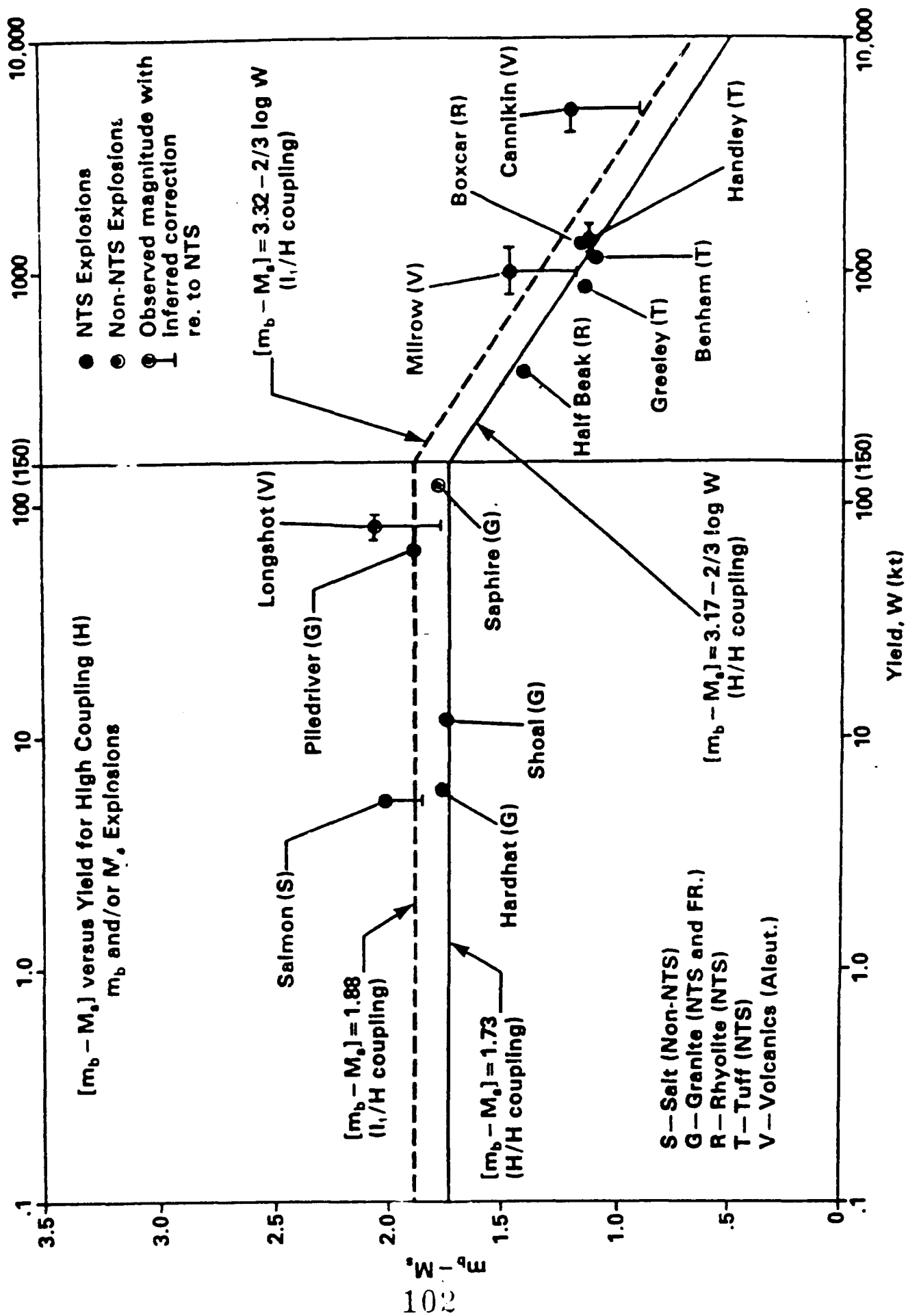


Figure 5.

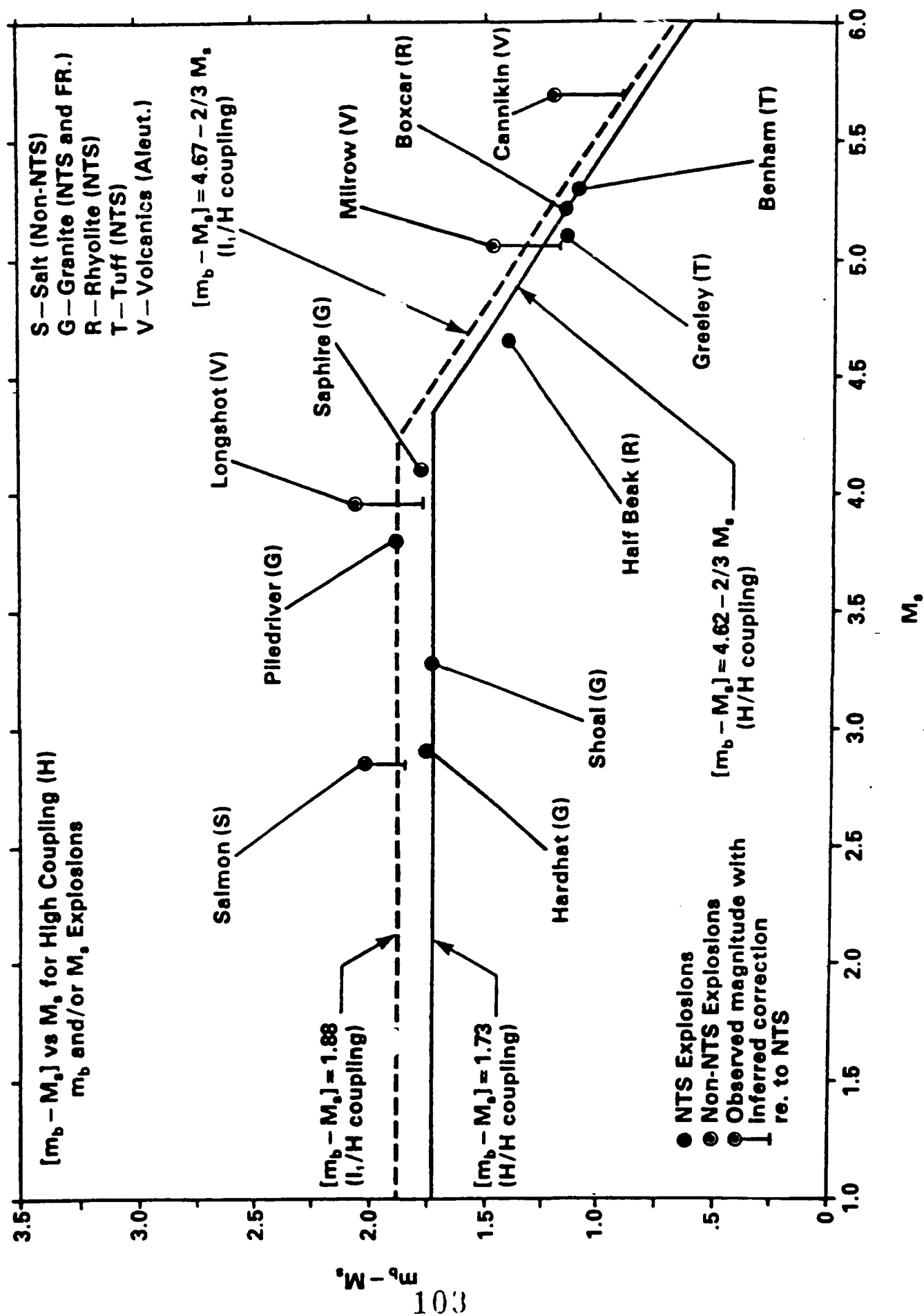


Figure 6.

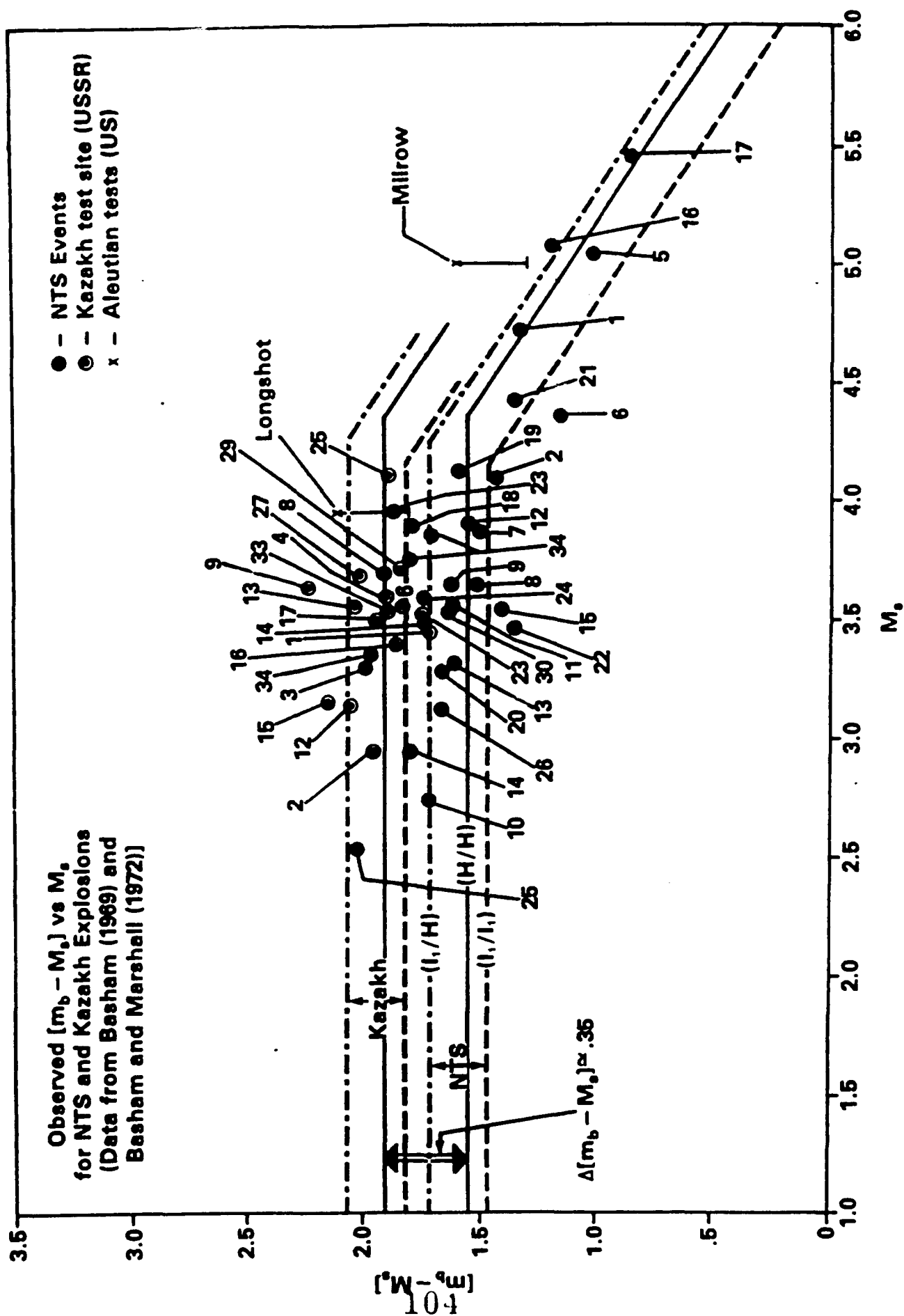


Figure 7.

be due to different tectonic release, or both. In any case, if the NTS coupling curves are simply shifted upward, until they bound the Kazakh data, one finds an $m_b - M_s$ bias factor of .35 magnitude units. However, we still don't know how this bias is distributed between the m_b and M_s values, nor can we be sure of its cause. Nevertheless there can be no doubt that a significant bias exists.

In order to obtain a determination of the origins of the bias, the data can be corrected for tectonic release effects. The residual bias observed could reasonably be associated with a "Q-bias" effect.

In this regard, Figure (8) shows NTS and Kazakh m_b and moment data, with tectonic release corrections applied to the moment estimates. Here the log of the moment simply replaces M_s , which was used previously. The shift in the Kazakh data is only slightly smaller than that obtained from uncorrected m_b / M_s data. However, since tectonic corrections have not been applied to m_b values, we can only say that the bias indicated is due to a bias in m_b , rather than any bias in M_s , between the sites. (It is assumed, consistent with other observations, that M_s average values are not affected by bias due to propagation and that the only bias effect that arises for M_s is that associated with different tectonic release mechanisms.)

Thus a value for the m_b bias between Kazakh and NTS can be obtained by this approach, and the value obtained accounts for coupling variability. This value is, however, a composite of both Q-bias effects and tectonic bias effects on m_b . Further, the variability and scatter in the data can be interpreted in terms of coupling variability of the media at the sites. (Here we have implicitly assumed that the range of coupling observed at NTS is also to be expected at Kazakh.)

For a given event, of unknown yield, we can also estimate the nature of the coupling appropriate to the event by associating the event with one or the other of the coupling curves shown. Finally, the change in slope of the theoretical curves shown always occurs at a yield near 150 kt, so that a rough estimate as to whether an explosion is above or below the 150 kt threshold can easily be obtained from such a simple plot.

Yield Estimation

To obtain well constrained yield estimates it is evident that the best approach is to use both m_b and M_s data simultaneously. This also gives, as a by-product, the appropriate coupling constants, K_c and K_E , for each explosion. It is also evident that both m_b and M_s must be corrected for any tectonic release effects. By use of the combined m_b and M_s (or moment) data, employing plots like those in Figures (6) through (8), one can obtain an estimate of any bias correction in m_b that might exist. In addition, a rough determination of the coupling appropriate to a particular event can be obtained from such a plot and the NTS magnitude-yield curves can then be adjusted to apply to any other site. At this point, observations of m_b and M_s which have both been corrected for tectonic effects can be used to obtain yield estimates consistent with both types of magnitude observation.

Figure (9) shows data corresponding to the largest Kazakh events since 1978. In this case the NTS based m_b versus yield curves, of Figures (2) through (4), have been shifted upward by .32 units in order to account for the NTS-Kazakh bias. The data are plotted so as to give the same yield estimate from both the m_b and M_s values observed. (This forces the observations onto one or the other of the different magnitude-yield curves, each of which corresponds to different coupling.)

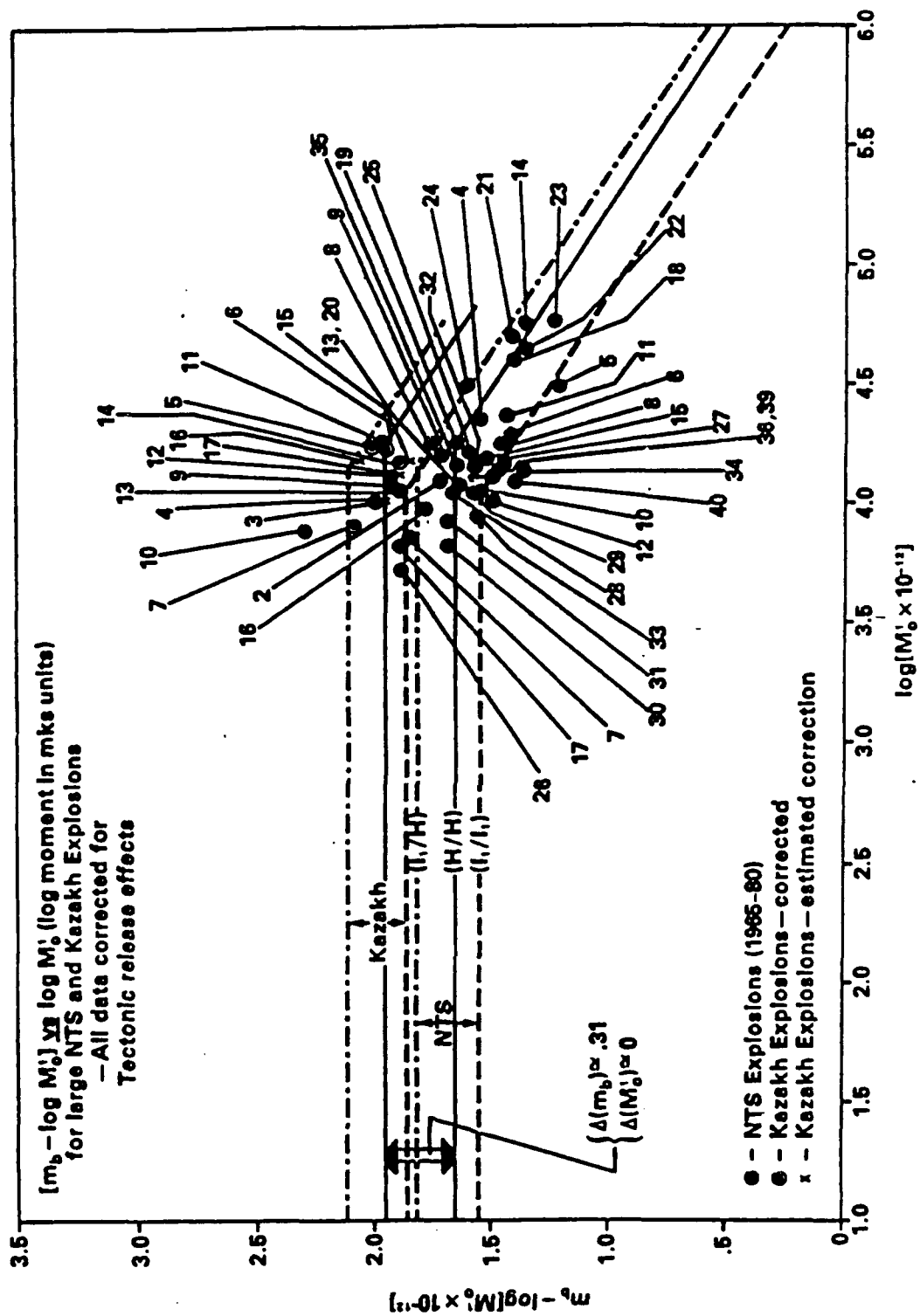
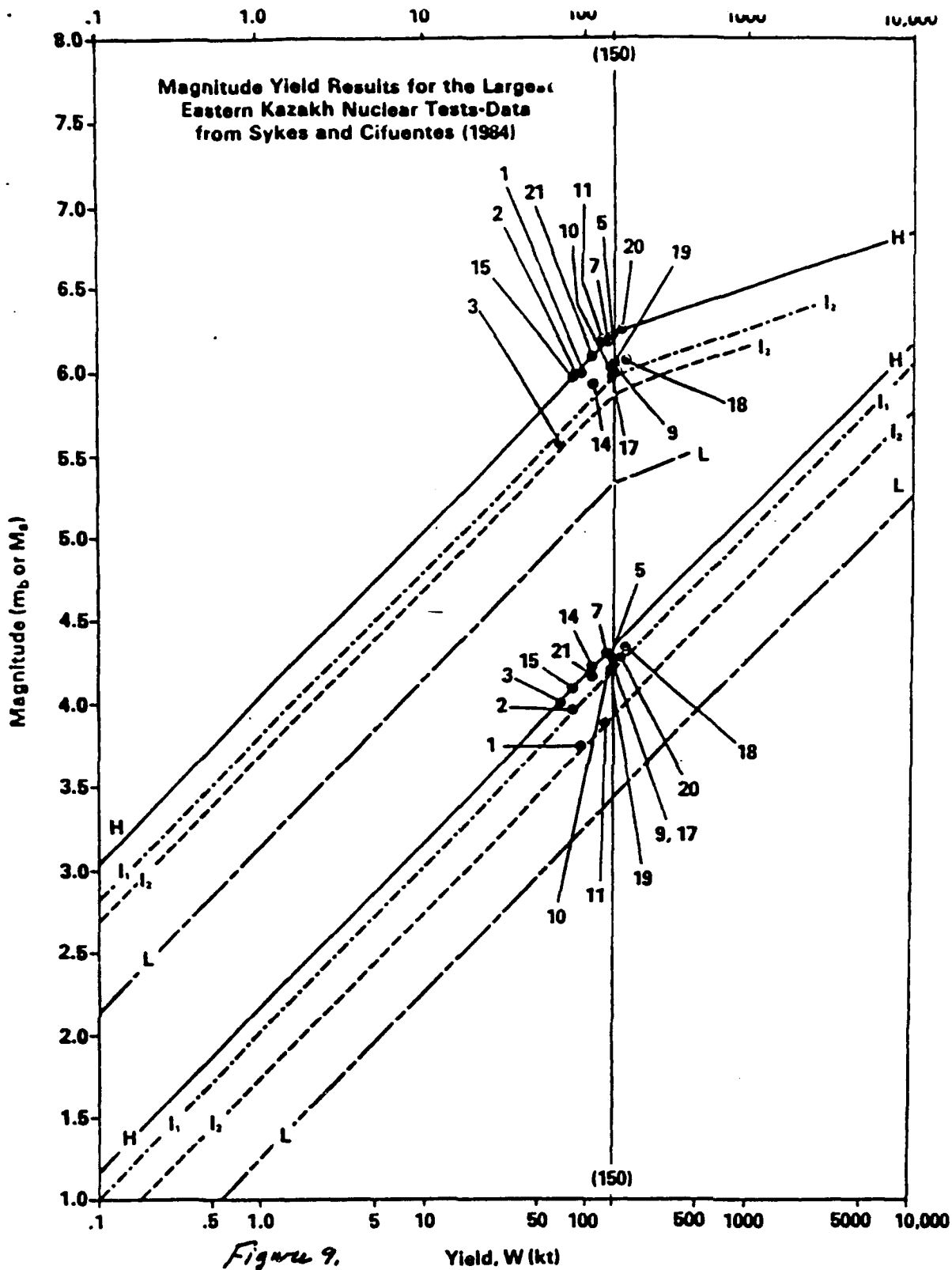


Figure 8.



As can be seen from the distribution of the data, two Soviet explosions are slightly over the 150 kt threshold; in particular two events give yields at 168 and 180 kt. These values have an uncertainty of about ± 30 kt associated with them, and so still could be below, or at, the 150 kt limit.

Since these m_b data have not been corrected for tectonic bias effects, it is also possible that some of the events have larger tectonic component effects associated with them than is accounted for through use of a "composite" bias which incorporates both propagation bias and an average "tectonic bias". Therefore, we might expect more scatter in the results than would be the case if careful corrections were also applied to the observed m_b values, as well as to the M_s values. Nevertheless, the data indicates that no systematic testing above 150 kt has occurred at Kazakh, at least as evidenced by this data set. Further, since these events represent some of the largest observed from Kazakh, this result implies that this conclusion applies to all Soviet tests.

July 16, 1986



James F. Lewkowicz
AFGL/LWH
Hanscom AFB, MA 01731-5000

Dear Jim,

Following Bill Best's suggestion, I have attempted to summarize my impressions of the AFGL/DARPA Seismic Research Symposium, 5 - 8 May 1986. The organization and operation of the meeting was very professional. The facilities at the Academy were excellent. The only problem within this area was the lack of discussion during the presentations. There have been few meetings I have attended that resulted in good interchange among investigators. The size of the group may preclude such interchange.

Within the technical presentations there were three areas that I felt significant advances were illustrated.

1. Techniques for quantifying two and three dimensional wave propagation effects were demonstrated. Initial attempts to investigate the effects of topography and structure were reported (Helmberger, McLaughlin). This work needs to be coupled with careful data analysis such as that reported by T. Lay at teleseismic distances if it is to be utilized. If two and three dimensional effects are shown to be important then we must address the question of doing geological characterization in multiple dimensions. I do not believe this question is being addressed.

2. Attempts to quantify more complex source effects was apparent. Utilizing a variety of data sets researchers reported on both forward (Day, Burdick) and inverse studies (Wallace, Johnson) to delineate such physical properties as coupling, spall, and deviatoric strain release. Problems seem to exist in the uniqueness of these models. There was little discussion of trade-offs among different models. Few presentations discussed the role material properties play in these models.

James F. Lewkowicz
July 16, 1986
Page 2.

3. A number of workers showed attempts to study data sets from very close to the source out to teleseismic distances with the purpose of constraining wave propagation effects more completely. Baumgardt with his analysis of the Soviet events is an example. Work such as this type illustrates the utility of broadband data extending to high frequencies. It also highlights the complexity of such wave propagation and tying multiple data sets together.

I was pleased to be included in this years program review.

Sincerely,

A handwritten signature in cursive script, appearing to read "Brian".

Brian W. Stump